

Multi-Temperature Blackbody Spectrum of a Thin Accretion Disk around a Kerr Black Hole: Model Computations and Comparison with Observations

Li-Xin Li^{1,2}, Erik R. Zimmerman, Ramesh Narayan, Jeffrey E. McClintock

Harvard-Smithsonian Center for Astrophysics, 60 Garden Street, Cambridge, MA 02138

lli, ezimmerman, rnarayan, jmccclintock@cfa.harvard.edu

ABSTRACT

We use a ray-tracing technique to compute the observed spectrum of a thin accretion disk around a Kerr black hole. We include all relativistic effects such as frame-dragging, Doppler boost, gravitational redshift, and bending of light by the gravity of the black hole. We also include self-irradiation of the disk as a result of light deflection. Assuming that the disk emission is locally blackbody, we show how the observed spectrum depends on the spin of the black hole, the inclination of the disk, and the torque at the inner edge of the disk. We find that the effect of a nonzero torque on the spectrum can, to a good approximation, be absorbed into a zero-torque model by adjusting the mass accretion rate and the normalization. We describe a computer model, called KERRBB, which we have developed for fitting the spectra of black hole X-ray binaries. Using KERRBB within the X-ray data reduction package XSPEC, and assuming a spectral hardening factor $f_{\text{col}} = 1.7$, we analyze the spectra of three black hole X-ray binaries: 4U1543-47, XTE J1550-564, and GRO J1655-40. We estimate the spin parameters of the black holes in 4U1543-47 and GRO J1655-40 to be $a/M \sim 0.6$ and $\sim 0.6 - 0.7$, respectively. If $f_{\text{col}} \sim 1.5 - 1.6$, as in a recent study, then we find $a/M \sim 0.7 - 0.8$ and $\sim 0.8 - 0.9$, respectively. These estimates are subject to additional uncertainties in the assumed black hole masses, distances and disk inclinations.

Subject headings: black hole physics — accretion, accretion disks — radiation mechanisms: thermal — X-rays: binaries

¹Chandra Fellow

²Present address: Max-Planck-Institut für Astrophysik, Karl-Schwarzschild-Str. 1, Postfach 1317, 85741 Garching, Germany

1. Introduction

Although the standard theory of thin accretion disks around black holes was developed over thirty years ago (Pringle & Rees 1972; Shakura & Sunyaev 1973; Novikov & Thorne 1973; Lynden-Bell & Pringle 1974), a straightforward confrontation of the model with observations is still not possible because of the challenging task of computing the observed spectrum of an accretion disk around a Kerr black hole. When fitting the soft X-ray spectra of black hole binaries, the multi-temperature disk model DISKBB is often used, which describes an approximate Newtonian model of a thin disk (Mitsuda et al. 1984; Makishima et al. 1986). This model has been criticized by Gierliński et al. (2001) for not applying the proper boundary condition at the inner edge of the disk. More seriously, the model does not include relativistic effects.

Various efforts have been made to include relativistic effects and the appropriate boundary condition in calculating the spectra of black hole accretion disks (Cunningham 1975, 1976; Hanawa 1989; Ebisawa et al. 1991; Zhang et al. 1997; Agol & Krolik 2000; Gierliński et al. 2001; Ebisawa et al. 2003; Davis et al. 2004). However, accurate quantitative analysis of observational data, e.g., trying to determine the radius of the disk inner edge from spectral data with a view to estimating the spin of the black hole, requires a sophisticated model that treats all relativistic effects including the self-irradiation of the disk caused by light deflection by the central black hole. At present, no such complete model exists that is suitable for inclusion with standard data reduction software, e.g., the X-ray spectral fitting package XSPEC (Arnaud 1996). As high-quality observational data on black-hole accretion disks become increasingly available (e.g., McClintock & Remillard 2004), the need for such a model has become urgent. In this paper we present the tools for a general relativistic model of an accretion disk around a Kerr black hole, and describe a numerical code for computing the observed blackbody spectrum of the disk. The code is efficient, and we have developed the appropriate software for interfacing it with XSPEC for analyzing spectral data.

Two basic approaches have been described in the literature for calculating the observed spectrum of an accretion disk around a Kerr black hole. The first method makes use of “transfer functions” (Cunningham 1975, 1976; Laor 1991; Speith et al. 1995; Agol & Krolik 2000; Dovčiak et al. 2004). In this approach, all the information about the Doppler boost due to the disk rotation as well as the relativistic light deflection in the vicinity of the black hole is contained in a transfer function, which operates as an integration kernel for calculating the overall disk spectrum. The transfer function has been calculated and discussed in great detail by Speith et al. (1995), who have provided a fast and easy-to-use computer program to do the calculations. The second method uses the technique of “ray-tracing” (Rauch & Blandford 1994; Fanton et al. 1997; Čadež et al. 1998; Müller & Camenzind 2004; Schnittman

& Bertschinger 2004). In this method one divides the image of the disk on the observer’s sky into a number of small elements. For each image element, the orbit of a photon is traced backward from the observer by following the geodesics in a Kerr spacetime, until the orbit crosses the plane of the disk. The flux density of the radiation emitted by the disk at that point, as well as the redshift factor of the photon and the angle between the wavevector of the photon and the normal to the disk surface, are calculated. The observed flux density contributed by each image element is thus obtained, and summing over all the elements gives the total observed flux density of the disk (see eq. [E7] below).

In this paper we use the ray-tracing approach, which we find more straightforward for numerical computations. We follow the procedures described by Fanton et al. (1997) and Čadež et al. (1998), who used elliptic integrals to simplify the calculation of the orbit of a photon in the background of a Kerr black hole (see also Rauch & Blandford 1994). Fanton et al.’s code was written for computing line emission from disks, whereas our code is designed for the continuum blackbody emission. We have made several improvements to Fanton et al.’s calculations; in particular, we include the effect of returning radiation, and we allow a nonzero torque to be set at the inner edge of the disk.

Using our code, we have calculated spectra corresponding to a three-dimensional grid of models spanning different values of the black hole spin parameter $a_* \equiv a/M$, disk inclination angle ϑ_{obs} , and dimensionless torque parameter η (defined in eq. [2]). We have also developed associated software which goes by the model name KERRBB for use with XSPEC. KERRBB reads in the above table of spectra and uses it to fit spectral data. In addition to the three parameters, a_* , ϑ_{obs} , and η spanned by the table, other parameters such as the mass of the black hole M , the distance to the source D , the mass accretion rate of the disk \dot{M} , and the spectral hardening factor f_{col} (see eqs. [E5] and [E6]), are also included. The user can also decide whether to assume isotropic emission from the disk surface or to include a standard limb-darkening law (eq. [D20]). The model works efficiently within XSPEC and some sample results are presented.

The paper is organized as follows. In §2 we summarize the assumptions behind our model, and in §3 we present the basic mathematical formalism. We discuss the effect of returning radiation in §3.1 and show examples of calculated spectra in §3.2, where we explain how the spectrum is affected by parameters such as the spin of the black hole, the inclination of the disk, and the torque on the inner edge of the disk. In §4 we apply KERRBB to spectral data on three black hole X-ray binaries, 4U1543-47, XTE J1550-564, and GRO J1655-40, and compare the results to those obtained with other models. We conclude with a summary in §5.

The ray-tracing technique involves complicated mathematics to describe the orbits of

photons in Kerr spacetime. Although many of these formulae can be found in the literature (e.g., Chandrasekhar 1983; Rauch & Blandford 1994; Fanton et al. 1997; Čadež et al. 1998), we feel it is important to present the relevant mathematics in full detail to make the paper more useful to future workers in this field. To avoid distracting the reader, we give the technical details in Appendixes A–E.

In Appendix F we compare KERRBB with GRAD—a subroutine in XSPEC for calculating the blackbody spectrum of a Keplerian disk around a nonrotating ($a_* = 0$) black hole. We show that KERRBB and GRAD give consistent results, once some errors in GRAD are corrected.

2. Basic Assumptions

Throughout the paper we use units in which $G = c = h = 1$, where G is the Newtonian constant, c is the speed of light, and h is the Planck constant. We use cylindrical coordinates (t, r, z, φ) as described by Page & Thorne (1974). In these coordinates, the rotation axis of the black hole is along the z -axis, and the equatorial plane corresponds to $z = 0$.

We consider a geometrically thin and optically thick Keplerian accretion disk around a Kerr black hole, with the spin axis of the black hole perpendicular to the disk plane. The black hole has a mass M and a specific angular momentum a , where $-M \leq a \leq M$. The disk has an inner boundary of radius r_{in} , and an outer boundary of radius $r_{\text{out}} \gg r_{\text{in}}$ (KERRBB assumes $r_{\text{out}} = 10^6 M$).

In the standard theory of accretion disks, it is usually assumed that the torque at the inner boundary of the disk is zero. However, this assumption has only been justified for nonmagnetized or weakly magnetized flows (Muchotrzeb & Paczyński 1982; Abramowicz & Kato 1989) and for very thin disks (Afshordi & Paczyński 2003). Recent theoretical works on accretion disks have suggested that a nonzero torque at the inner boundary can arise from a magnetic field which either connects a disk to a central black hole, or couples a disk to the material in the plunging region (Krolik 1999; Gammie 1999; Agol & Krolik 2000; Li 2000, 2002a,b, 2004; Wang et al. 2002, 2003; Uzdensky 2004a,b). Although this issue is still under debate (Paczyński 2000; Armitage et al. 2001; Hawley & Krolik 2002; Afshordi & Paczyński 2003; Li 2003a,b), to make our model as general as possible we assume that the torque at the inner boundary of the disk can have any nonnegative value.

In the presence of a torque $g_{\text{in}} \geq 0$ at the inner edge, the total power of the disk, i.e. the net amount of energy flowing out of the disk per unit time as measured by an observer

at infinity, is (Li 2002a)¹

$$\mathcal{L}_{\text{total}} = g_{\text{in}}\Omega_{\text{in}} + \epsilon_{\text{in}}\dot{M} , \quad (1)$$

where Ω_{in} is the angular velocity of the disk inner boundary, \dot{M} is the mass accretion rate of the disk, and $\epsilon_{\text{in}} = 1 - E_{\text{in}}^{\dagger}$ is the specific gravitational binding energy at the inner boundary, where E_{in}^{\dagger} is the specific energy of disk particles at the inner boundary.

Equation (1) shows that the total power of the disk comes from two sources: the gravitational binding energy between the disk and the black hole, and a contribution from the torque at the inner boundary of the disk (whenever the torque is nonzero). If the torque is produced by the black hole, then the power source for the second component is the spin energy of the black hole.

Let us define a dimensionless parameter

$$\eta \equiv \frac{g_{\text{in}}\Omega_{\text{in}}}{\epsilon_{\text{in}}\dot{M}} , \quad (2)$$

which measures the ratio of the power from the torque to the power from the gravitational binding energy of the accreting gas. Then we have

$$\mathcal{L}_{\text{total}} = (1 + \eta)\epsilon_{\text{in}}\dot{M} . \quad (3)$$

In this paper we treat η as a free parameter that can have any nonnegative value. It is useful to define an effective mass accretion rate

$$\dot{M}_{\text{eff}} \equiv (1 + \eta)\dot{M} , \quad (4)$$

such that the total power of the disk is simply

$$\mathcal{L}_{\text{total}} = \epsilon_{\text{in}}\dot{M}_{\text{eff}} . \quad (5)$$

With our conventions, $\eta = 0$ corresponds to the case when the torque at the inner boundary of the disk is zero (we call this *the standard case*), and $\eta = \infty$ corresponds to $\dot{M} = 0$ (we call this *the nonaccreting case*). In these two extreme cases, all the power of the disk comes from either accretion ($\eta = 0$) or from the torque at the inner boundary ($\eta = \infty$).

¹When the effect of returning radiation is considered, the total power of the disk corresponds to the energy-at-infinity carried away from the disk per unit coordinate time by the photons that permanently leave the disk—they either escape to infinity or fall into the black hole. See §3.1 for details.

The nonaccreting case is similar to the case of a “dead disk” around a magnetized spinning neutron star (Syunyaev & Shakura 1977), in the sense that both correspond to a zero mass accretion rate. However, the nonaccreting case considered in this paper is not necessarily in a “dead” state. If the black hole rotates fast and the inner boundary of a nonaccreting disk is located at the marginally stable orbit close to the horizon of the black hole, then a disk powered by the spin energy of the black hole can, in fact, be very bright (Li 2004).

The model and the computer code described in this paper apply to a geometrically thin Keplerian disk with its inner edge located at any $r_{\text{in}} \geq r_{\text{ms}}$, where r_{ms} is the radius of the marginally stable orbit. For simplicity, in all plots presented in the paper, and in the model which we have developed for use with XSPEC, we assume that $r_{\text{in}} = r_{\text{ms}}$.

We assume that the disk radiates like a blackbody. However, due to the complicated scattering processes in the disk atmosphere (predominantly electron scattering and Comptonization), the color temperature T_{col} of the emitted radiation is generally higher than the effective temperature T_{eff} of the disk (Ross et al. 1992; Shimura & Takahara 1993, 1995; Davis et al. 2004). To take this effect into account, we follow Shimura & Takahara (1995) and Ebisawa et al. (2003) and assume that the ratio $f_{\text{col}} = T_{\text{col}}/T_{\text{eff}}$ is a constant (see eqs. [E4]-[E6]). We take $f_{\text{col}} = 1.7$, the mean value recommended by Shimura & Takahara (1995), when we model observations in §4. Undoubtedly, it is an over simplification to model the spectral modification due to Comptonization and electron scattering with a single scaling parameter, but this is a standard approach in the literature and is the best that we can do at this time.

3. Mathematical Formalism for the Calculation of the Observed Spectrum of Disk Radiation

3.1. Effects of the returning radiation

Because of the gravity of the central black hole, not all of the radiation emitted by the disk escapes to infinity: a part of it, which we call “returning radiation,” returns to the disk or is permanently captured by the black hole. The returning radiation that strikes the disk will interact with the disk particles and eventually be scattered or absorbed. For simplicity, we make the following assumption: All the radiation returning to the disk in the region beyond the inner boundary is absorbed by the disk, then reprocessed and reradiated. All the radiation returning in the region inside the inner boundary (i.e., the plunging region) is advected or scattered inward by the infalling gas (which has a large inward velocity), and

is captured by the black hole (Agol & Krolik 2000). In this subsection we study the effects of the returning radiation on the emission of the disk and the evolution of the central black hole.

The mathematics for studying the effect of the returning radiation is presented in Appendix D. In brief, considering the effect of returning radiation, at each point in the disk the net flux density F is composed of two nonnegative components: an outgoing component F_{out} which represents the flux density of the energy emitted by the disk *in situ*; and an ingoing component F_{in} , which is the flux density in the returning radiation, i.e. radiation emitted elsewhere and focused back onto the disk by the gravity of the black hole. In the steady state, the net flux density F is determined by the balance of the energy and angular momentum in the disk: $F = F_0 + F_S$, where F_0 is the standard solution for the flux density when the effect of returning radiation is ignored (eq. [D11]), and F_S represents the work done by the returning radiation on the disk (eq. [D12]). The total outgoing flux density is then $F_{\text{out}} = F + F_{\text{in}} = F_0 + F_{\text{in}} + F_S$ (eq. [D17]). The inclusion of F_S in our energy balance equation is the main difference between our calculations and those of Agol & Krolik (2000). Note, however, that this has very little effect on the flux or spectrum of a standard disk.

The self-irradiation of the disk arising from returning radiation is essentially a nonlocal process. Both F_{in} and F_S of the incoming radiation—and also F_{out} at the point on the disk where the incoming photons cross the disk—are functionals of F_{out} at the point on the disk where the incoming photons were emitted. Therefore, F_{out} (and thus F_{in} and F_S) must be obtained by solving the following functional equation

$$F_{\text{out}} = F_0 + F_{\text{in}}[F_{\text{out}}] + F_S[F_{\text{out}}].$$

Self-consistent solutions for F_{out} , F_{in} , and F_S can be obtained by an iterative method using ray-tracing (see Appendix D).

In Figure 1 we show the solutions of F_{in} and F_S for the returning radiation as functions of disk radius, for the case of a Kerr black hole of $a = 0.999M$ with $\eta = 0$ (upper panel) and $\eta = \infty$ (lower panel). The radiation emitted by the disk is assumed to be isotropic in the disk frame, rather than limb-darkened (see eq. [D20] in Appendix D). As mentioned earlier, in all figures in this paper we assume that the inner boundary of the disk is at the marginally stable orbit, $r_{\text{in}} = r_{\text{ms}}$. For comparison, the outgoing flux density when the returning radiation is ignored (F_0 , eq. [D11]) is also shown. The flux densities F_{in} and F_S always have the following asymptotic behaviors: $F_{\text{in}} \propto r^{-3}$, $F_S \propto r^{-7/2}$ for $r \gg r_{\text{in}}$. Thus, asymptotically, F_{in} behaves as if it is produced by a “lamp” on the axis of the black hole, while F_S behaves like it is produced by a torque at the inner boundary of the disk. We remind the reader of the asymptotic behavior of F_0 : $F_0 \propto r^{-3}$ when $\eta = 0$, $F_0 \propto r^{-7/2}$ when $\eta = \infty$. This asymptotic behavior is the same as that in the Newtonian case (see, e.g.,

Syunyaev & Shakura 1977), which is not surprising since at large radii the effect of relativity is unimportant.

From Figure 1 we see that, for the case $\eta = 0$ (upper panel), the flux density of the returning radiation is always dominated by the original outgoing flux density F_0 , except near the inner boundary of the disk where F_0 and F_S approaches zero but F_{in} remains finite. When η is large (lower panel), at small radii the flux density is dominated by the original outgoing flux density F_0 , while at large radii the flux density is dominated by that of the returning radiation (F_{in}). Since at large radii F_{in} is always $\propto r^{-3}$, which is the same as the asymptotic behavior of $F_0(\eta = 0)$, the lower panel of Figure 1 indicates that at large disk radii the signature of a large torque at the inner boundary is smeared out by the returning radiation. This makes it hard to detect the torque at the disk inner boundary by observing the spectrum of the disk (see §3.2 for more discussion).

From Figure 1 we also see that F_S is always less important than F_{in} .

A photon emitted by the disk has three possible fates: it may be captured by the black hole, return to the disk, or escape to infinity. Thus, when the returning radiation is considered, we have three different definitions for the “power” of the disk: 1) The *total emission* of the disk, which is the total energy-at-infinity emitted by the disk per unit coordinate time (i.e., the total energy-at-infinity carried away from the disk per unit coordinate time by all photons emitted by the disk, whether the photons escape to infinity, fall into the black hole, or return to the disk)

$$P_{\text{emit}} = 4\pi \int_{r_{\text{in}}}^{\infty} E^\dagger F_{\text{out}} r dr, \quad (6)$$

where E^\dagger is the specific energy of a disk particle on a circular orbit of radius r (Page & Thorne 1974; Thorne 1974). 2) The *total power* of the disk, defined by equations (D22) and (1), which is the total energy-at-infinity carried away from the disk per unit coordinate time by the “net” radiation, i.e., the photons that permanently leave the disk—they either escape to infinity or fall into the black hole. 3) The *total luminosity* of the disk, which is the total energy-at-infinity carried away from the disk per unit coordinate time by the photons that escape to infinity.

By definition, the total emission of the disk, P_{emit} , can be decomposed into three components: $P_{\text{emit,BH}}$, for the radiation that falls into the black hole; $P_{\text{emit,ret}}$, for the radiation that returns to the disk; and $P_{\text{emit,esc}}$, for the radiation that escapes to infinity. Therefore, we can define three fractions

$$\iota_{\text{BH}} \equiv \frac{P_{\text{emit,BH}}}{P_{\text{emit}}}, \quad \iota_{\text{ret}} \equiv \frac{P_{\text{emit,ret}}}{P_{\text{emit}}}, \quad \iota_{\text{esc}} \equiv \frac{P_{\text{emit,esc}}}{P_{\text{emit}}}. \quad (7)$$

Clearly, the three ratios satisfy $\iota_{\text{BH}} + \iota_{\text{ret}} + \iota_{\text{esc}} = 1$.

By the conservation of energy, we must have

$$P_{\text{emit,esc}} + P_{\text{emit,BH}} = \mathcal{L}_{\text{total}} , \quad (8)$$

where $\mathcal{L}_{\text{total}}$ is the total power of the disk. So we can define two other ratios

$$f_{\text{BH}} \equiv \frac{P_{\text{emit,BH}}}{\mathcal{L}_{\text{total}}} , \quad f_{\text{esc}} \equiv \frac{P_{\text{emit,esc}}}{\mathcal{L}_{\text{total}}} , \quad (9)$$

which respectively represent the fraction of the energy going into the black hole and the fraction of the energy escaping to infinity in the “net” energy radiated by the disk. The two ratios must satisfy $f_{\text{BH}} + f_{\text{esc}} = 1$.

The fractions with respect to the “total” radiation, ι_{ret} , ι_{BH} , and ι_{esc} , are shown as functions of the spin of the black hole in Figure 2. Again, we assume that the radiation emitted by the disk is isotropic in the disk frame. Two extreme cases are shown: a standard Keplerian disk, where $g_{\text{in}} = 0$ (equivalent to $\eta = 0$, thin lines); and a nonaccreting disk, where $\dot{M} = 0$ but $g_{\text{in}} \neq 0$ (equivalent to $\eta = \infty$, thick lines). For the $\eta = 0$ case, we show the spin of the black hole from $a = 0$ to $a = 0.9999M$. By considering the thermodynamics of black holes, Agol & Krolik (2000) argued that a nonaccreting disk ($\eta = \infty$) can exist only for $a > 0.3594M$. A physical explanation for this is that a black hole rotates faster than the inner boundary of the disk (at the marginally stable orbit) only if $a > 0.3594M$. Therefore, if $a \leq 0.3594M$ a black hole cannot exert a positive torque on the disk (Li 2000, 2002a). Hence, for the case of a nonaccreting disk, we show the spin of the black hole from $a = 0.3594M$ to $a = 0.9999M$.

The corresponding fractions with respect to the “net” radiation, f_{BH} and f_{esc} , are shown in Figure 3 (upper panel). To check the conservation of energy, i.e. equation (8), the difference between the computed $f_{\text{BH}} + f_{\text{esc}}$ and 1 is also shown (lower panel). Within the errors of the computation the conservation of energy is confirmed.

From Figures 2 and 3 we see that the effect of the returning radiation crucially depends on the spin of the black hole and the torque at the inner boundary of the disk. For a standard accretion disk ($\eta = 0$) around a Schwarzschild black hole ($a = 0$), 1.7% of the total radiation emitted by the disk returns to the disk, 0.66% is captured by the black hole, and the remaining 97.6% escapes to infinity. For a standard accretion disk ($\eta = 0$) around a Kerr black hole of $a = 0.9999M$, 27% of the total radiation emitted by the disk returns to the disk, 4% is captured by the black hole, and 69% escapes to infinity. For a nonaccreting disk ($\eta = \infty$) around a Kerr black hole of $a = 0.9999M$, 59% of the total radiation emitted by the disk returns to the disk, 7% is captured by the black hole, and 34% escapes to infinity.

Therefore, the effect of the returning radiation is most important for a fast spinning black hole and a directly rotating disk (rotating in the same direction as the black hole) with a large torque at its inner boundary. The obvious reason for this is that as a goes up the inner boundary of the disk shrinks, and when $g_{\text{in}} > 0$ more energy is dissipated in and radiated from the inner region of the disk, which is close to the central black hole.

In terms of the “net” radiation of the disk, for a standard accretion disk around a Schwarzschild black hole, about 0.7% of the “net” radiation is captured by the black hole, and the remaining 99.3% escapes to infinity. For a standard accretion disk around a Kerr black hole of $a = 0.9999M$, about 6% of the “net” radiation is captured and 94% escapes to infinity. For a nonaccreting disk around a Kerr black hole of $a = 0.9999M$, about 17% of the “net” radiation is captured and 83% escapes to infinity.

Similar results have been obtained by Agol & Krolik (2000) using the “transfer function” approach. However, in their calculations, Agol and Krolik ignored the stress of the returning radiation (i.e., the term F_S) and obtained a fraction for the radiation captured by the black hole in the “net” radiation that is somewhat smaller than the fraction that we have obtained. For example, for a nonaccreting disk around a Kerr black hole of $a = 0.9999M$, they find $f_{\text{BH}} = 15\%$, while we obtain $f_{\text{BH}} = 17\%$.

Figures 1–3 show that when the black hole is rotating rapidly and there is a large torque at the inner boundary of the disk the effect of returning radiation is extremely important.

In order to study the effect of the radiation that is captured by the black hole on the spinup/spindown of the black hole, following Thorne (1974) we define a capture function C for each photon emitted by the disk at radius r : $C = 1$ if the photon is eventually captured by the black hole, and $C = 0$ if the photon escapes to infinity or returns to the disk. The calculation of the capture function is described in Appendix A.3.

Here we focus on the case when the stress at the inner boundary of the disk is zero, i.e., $g_{\text{in}} = 0$. Then, the torque that spins up/down the black hole comes from two sources: gas accreted from the disk, and radiation captured by the black hole. Then, the resultant spinup/spindown of the black hole is governed by (Thorne 1974)

$$\frac{da_*}{d \ln M} = \frac{L_{\text{in}}^\dagger + \zeta_L}{M \left(E_{\text{in}}^\dagger + \zeta_E \right)} - 2a_* , \quad a_* \equiv \frac{a}{M} , \quad (10)$$

where L_{in}^\dagger is the specific angular momentum of disk particles at the inner boundary, and

$$\zeta_E \equiv \frac{3}{2\pi r_g^2} \int_{r_{\text{in}}}^{\infty} \left[\int_{\Omega_+} C \Upsilon(-n_t) \cos \theta d\Omega \right] \tilde{f}_{\text{out}} r dr , \quad (11)$$

$$\zeta_L \equiv \frac{3}{2\pi r_g^2} \int_{r_{\text{in}}}^{\infty} \left(\int_{\Omega_+} C\Upsilon n_\varphi \cos\theta d\Omega \right) \tilde{f}_{\text{out}} r dr, \quad (12)$$

where $r_g = M$ is the gravitational radius of the black hole, n_t and n_φ are given by equation (D5). See Appendix D for the meanings of θ , Ω , Ω_+ , and Ω_- . For convenience, in equations (11) and (12) we have used a dimensionless outgoing flux function \tilde{f}_{out} defined by

$$F_{\text{out}} = \frac{3\dot{M}_{\text{eff}}}{8\pi r_g^2} \tilde{f}_{\text{out}}. \quad (13)$$

The function $da_*/d\ln M$, which is defined by equation (10) and is a function of a_* only when $r_{\text{in}} = r_{\text{ms}}$, is plotted in Figure 4 (upper panel). The value of a at which $da_*/d\ln M = 0$ gives the equilibrium spin of the black hole [which is called the ‘‘canonical state’’ by Thorne (1974)]: $a = a_{\text{eq}}$. When the black hole is in a state of $a < a_{\text{eq}}$, the effect of accretion from the disk dominates, which will spin up the black hole, until the equilibrium state $a = a_{\text{eq}}$ is reached. On the other hand, when the black hole is in a state of $a > a_{\text{eq}}$, the effect of the capture of photons dominates, which will spin down the black hole to the equilibrium state $a = a_{\text{eq}}$. When the disk emission is isotropic, we obtain $a_{\text{eq}} = 0.9983M$, and when the disk emission is limb-darkened, we obtain $a_{\text{eq}} = 0.9986M$.² These results show that the limb-darkening effect does not significantly affect the gross disk radiation.

The efficiency of an accretion disk in converting rest mass into outgoing radiation is defined by the ratio of the total luminosity of the disk to the mass-energy accretion rate as measured at infinity, which is given by $1 - E_{\text{in}}^\dagger - \zeta_E$ (Thorne 1974). In the lower panel of Figure 4 we show the efficiency of a standard accretion disk as a function of the spin of the black hole when the effect of the returning radiation is considered. In the canonical state, the total efficiency is 0.309 when the disk emission is isotropic and 0.315 when the emission is limb-darkened. When the effect of the returning radiation is ignored, the radiation efficiency of a standard disk is 0.326 when $a = 0.9983M$, and 0.331 when $a = 0.9986M$.

For comparison, the results of Thorne (1974) are also shown in the lower panel of Figure 4 (the two plus signs). Without considering the effect of the radiation returning to the disk, Thorne obtained: $a_{\text{eq}} = 0.9978M$ when the disk radiation is isotropic, and $a_{\text{eq}} = 0.9982M$ when the disk radiation is limb-darkened. The corresponding radiation efficiencies of the disk are respectively 0.302 and 0.308.

²These numerical results are correct only if accretion from a thin disk and capture of photons is the unique process to spin up/down the black hole, and if the torque at the inner boundary of the disk is zero.

3.2. Blackbody radiation spectrum from a Keplerian accretion disk

The energy flux density of the blackbody radiation emitted by an accretion disk around a black hole as observed by a remote observer— $F_{E_{\text{obs}}}$, where E_{obs} is the photon energy—is given by equation (E7). However, for the purpose of comparison with X-ray observations, it is more convenient to use the photon number flux density rather than the energy flux density. So we define $N_{\text{obs}} \equiv F_{E_{\text{obs}}}/E_{\text{obs}}$.

For convenience, let us define

$$d\tilde{\Omega}_{\text{obs}} \equiv \left(\frac{D}{r_g}\right)^2 d\Omega_{\text{obs}}, \quad (14)$$

where D is the distance from the observer to the black hole and $d\Omega_{\text{obs}}$ is the element of the solid angle subtended by the image of the disk on the observer’s sky. With the above definition, $d\tilde{\Omega}_{\text{obs}}$ defined above is independent of the distance D . Then, by equations (E7) and (E4), the formula for calculating N_{obs} is

$$N_{E_{\text{obs}}} = N_0 \left(\frac{E_{\text{obs}}}{\text{keV}}\right)^2 \int \frac{d\tilde{\Omega}_{\text{obs}}}{\exp\left[\mu \left(\frac{E_{\text{obs}}}{\text{keV}}\right) g^{-1} \tilde{f}_{\text{out}}^{-1/4}\right] - 1}, \quad (15)$$

where g is the photon redshift (defined by eq. [E3]), \tilde{f}_{out} is defined by equation (13), and

$$N_0 = 0.07205 f_{\text{col}}^{-4} \left(\frac{M}{M_{\odot}}\right)^2 \left(\frac{D}{\text{kpc}}\right)^{-2} \text{ photons keV}^{-1} \text{ cm}^{-2} \text{ sec}^{-1}, \quad (16)$$

$$\mu = 0.1202 f_{\text{col}}^{-1} \left(\frac{\dot{M}_{\text{eff}}}{10^{18} \text{g sec}^{-1}}\right)^{-1/4} \left(\frac{M}{M_{\odot}}\right)^{1/2}, \quad (17)$$

where f_{col} is the spectrum hardening factor defined by equation (E5).

Some examples of the observed spectra calculated with our ray-tracing code are shown in Figures 5–9. In Figures 5–8 we assume the disk radiation is isotropic in the frame corotating with the disk, i.e., there is no limb-darkening, whereas in Figure 9 we include limb-darkening according to equation (D20).

In the upper panel of Figure 5, we show the dependence of the observed spectrum on the spin of the black hole. The disk has $\eta = 0$ (zero-torque) and an inclination angle $\vartheta_{\text{obs}} = 30^\circ$ (for other parameters see the caption of the figure). Different lines correspond to different spins of the black hole: $a/M = 0, 0.5, 0.9$, and 0.999 (left to right). We see that the spectrum becomes harder as the spin of the black hole goes up. Physically, this is caused by the fact that when M is fixed and a/M increases, the radius of the inner edge of the

disk (by assumption located at the marginally stable orbit) decreases, so that the disk has a higher radiation efficiency (see Fig. 4, lower panel) and a higher temperature. We also see another effect: as a/M increases, the flux density at low energies increases even though this radiation comes from large radii where the spin of the black hole should have negligible effect. This increase in flux density is caused by the returning radiation. As a/M goes up, more radiation emitted by the disk in the inner region is focused back to the disk by the gravity of the black hole (Figs. 2 and 3). This increases the radiation of the disk even at large radii (corresponding to the low energy end of the spectrum).

In the lower panel of Figure 5, we test the effect on the observed spectrum of the inclination angle of the disk. The case considered is for $\eta = 0$ and $a/M = 0.9$. Different lines correspond to different inclination angles of the disk: $\vartheta_{\text{obs}} = 0^\circ, 40^\circ, 70^\circ$ and 85° . At the low energy end, the flux density goes down as ϑ_{obs} increases. This is caused by the projection effect. The low energy radiation is primarily emitted by the disk at large radii, where the effect of relativity is not important. The projection causes the flux density of the disk radiation to be proportional to $\cos \vartheta_{\text{obs}}$. At the high energy end, the flux density goes up as ϑ_{obs} increases. This is caused by the effects of Doppler beaming and gravitational focusing. The high energy radiation is primarily emitted by the disk in the region near the black hole, where the orbital velocity of the disk is mildly relativistic so that special relativistic beaming boosts the disk radiation to higher energy. In addition, near the black hole, the gravity of the black hole is strong and focuses the disk radiation back to the disk plane, thereby modifying the projection effect. The joint action of the two effects leads to an enhancement at the high energy end of the observed spectrum.

Figure 6 shows the effect of the returning radiation on the observed spectrum of the disk. The three panels correspond to $\eta = 0$ (upper panel, the standard disk case), $\eta = 1$ (middle panel), and $\eta = \infty$ (lower panel, the nonaccreting case). The black hole has a spin $a/M = 0.999$, and the disk has an inclination angle $\vartheta_{\text{obs}} = 30^\circ$ (other parameters are given in the caption of the figure). The spectra when returning radiation is included are shown with solid lines, and those without the returning radiation are shown with dashed lines. We see that the returning radiation enhances the disk radiation (especially at the high energy end), and the effect is more prominent for a disk with a larger torque at its inner boundary. For the standard disk with $\eta = 0$ (upper panel), where the power of the disk comes purely from disk accretion, the effect of the returning radiation is almost indistinguishable from the effect of a change in the mass accretion rate: The dotted line (almost coincident with the solid line) represents a disk spectrum minus the returning radiation with the same parameters except that the mass accretion rate is larger by a factor of 1.23. For the case $\eta = 1$ (middle panel), for which the power of the disk comes equally from disk accretion and a torque at the inner boundary of the disk, the effect of the returning radiation can again be well approximated by

adjusting the effective mass accretion rate. The dotted line represents the spectrum without the returning radiation of a disk with the same parameters except that the effective mass accretion rate is larger by a factor of 1.7. In this case also, the dotted line agrees very well with the solid line. However, when η is very large, e.g. for the nonaccreting case with $\eta = \infty$ (lower panel), where the power of the disk comes purely from the torque at the inner boundary, the effect of the returning radiation is so prominent that it cannot be fitted by simply modifying the effective mass accretion rate.

Figure 7 shows the effect of a nonzero torque at the inner boundary of the disk for the case of a Schwarzschild black hole ($a = 0$). Each panel corresponds to a different value of η : 0.1, 0.3, 1 and 16.49. The last value corresponds to the case that the total efficiency of the disk is equal to unity—the upper limit for the efficiency of a Keplerian disk around a nonrotating black hole. In each panel, the solid line is the spectrum when the disk has a nonzero torque at the inner boundary, and the dashed line is the spectrum when the disk has a zero torque with other parameters remaining the same. In particular, for both the solid and the dashed lines the effective mass accretion rate is $\dot{M}_{\text{eff}} = 10^{19} \text{g sec}^{-1}$, which means that the two disks have the same total power (but different mass accretion rates \dot{M} , see eqs. [4] and [5]). From the figure we see that the effect of the torque at the inner boundary is to make the spectrum harder. When the torque at the inner boundary is positive, more energy is dissipated and more radiation is emitted in the inner region of the disk where the temperature is higher. Also, the disk rotates faster there, so the Lorentz boost is more prominent. Both effects cause a hardening of the spectrum.

In the case of the returning radiation, we showed earlier that its effect can be modeled very well by adjusting the mass accretion rate in a model without returning radiation. Can the effect of a nonzero torque be similarly absorbed by adjusting the parameters of a zero-torque model? The first panel of Figure 7 shows that for $\eta = 0.1$, which corresponds to a weak torque, a zero-torque model with the same power (\dot{M}_{eff}) as the finite-torque model gives an almost indistinguishable spectrum. So, in this case, the answer to our question is a definite yes. For the cases of $\eta = 0.3, 1$, and 16.49, we see that just keeping \dot{M}_{eff} the same is not enough, since the dashed lines are noticeably different from the solid lines. However, by adjusting both \dot{M}_{eff} and f_{col} of a zero-torque model, we can get a very good fit to the finite-torque models with $\eta = 0.3$ and 1, as shown by the dotted lines; the corresponding values of these parameters are given in the caption to the Figure. Only in the extreme case $\eta = 16.49$ are we unable to fit the spectrum by adjusting \dot{M}_{eff} and f_{col} . Note that adjusting f_{col} is equivalent to adjusting the normalization, which could be done equally well by adjusting M , D , or $\cos \vartheta_{\text{obs}}$. Since none of these parameters is known precisely in a real system, one always has some freedom in the normalization. These results indicate that for a Schwarzschild black hole the spectrum of a disk with a modest torque at the inner boundary can be fitted with

a zero torque at the inner boundary by adjusting \dot{M} and the normalization.

Similar results for the case of a Kerr black hole with $a/M = 0.999$ are shown in Figure 8. Now we find that the spectrum can always be fitted by a disk with a zero torque at the inner boundary by adjusting \dot{M}_{eff} and f_{col} ; in fact, we can do this even when $\eta = \infty$. Interestingly, the effect of a nonzero torque is more important for a non-rotating black hole than for a rapidly rotating hole, e.g., note that the spectrum is significantly hardened in Figure 7 whereas there is almost no effect in Figure 8. This is caused by the effect of the returning radiation. For a nonrotating black hole, the effect of the returning radiation is not important due to the fact that the inner edge of the disk has a large radius, so the torque at the inner boundary produces a radiation flux density ($\sim r^{-7/2}$ at large radii) that is distinctly different from the radiation flux density arising from accretion ($\sim r^{-3}$ at large radii). For a fast rotating black hole, the effect of the returning radiation is important, it makes the radiation flux density of the disk more or less similar to that arising from accretion (both going as $\sim r^{-3}$ at large radii) (see Figs. 1–2 and the relevant discussions in §3.1).

Figure 8 shows another effect of the torque at the inner boundary for a rapidly spinning hole: when the torque changes from zero to nonzero and other parameters (including \dot{M}_{eff}) are left unchanged, the flux at infinity decreases (compare the solid and dashed lines). This is caused by the fact that when the torque at the inner boundary is nonzero more energy is dissipated in the inner region of the disk; for a rapidly rotating black hole the inner boundary of the disk is closer to the horizon of the black hole and so more radiation is focused to the equatorial plane.

Overall, the results shown in Figures 6–8 suggest that when modeling observational data the effects of returning radiation and nonzero torque can be ignored since they can be absorbed by modifying the mass accretion rate and the spectral hardening factor of a zero-torque model without returning radiation.

Finally, in Figure 9 we show the effect of limb-darkening (eq. [D20], Appendix D) on the observed spectra of the disk. As can be expected from equation (D20), compared to the case when the disk emission is isotropic, when the disk emission is limb-darkened we see more radiation when the disk has a low inclination angle, and we see less radiation when the disk has a high inclination angle. The effect of limb-darkening is most important when the disk is nearly edge-on: in this case the effect cannot be absorbed by simply adjusting the mass accretion rate and the spectral hardening factor.

4. Modeling the Spectra of Black Hole X-ray Binaries

To test the performance of our model KERRBB and to compare it with other models of disk spectra, we have analyzed spectral data on three black hole X-ray binaries: 4U1543–47 (hereafter U1543), XTE J1550-564 (hereafter J1550), and GRO J1655–40 (hereafter J1655). The data were obtained using the Proportional Counter Array aboard the *Rossi X-ray Timing Explorer* (*RXTE*). The data themselves and the methods of data analysis are thoroughly described in Zimmerman et al. 2004 (hereafter Z04). These three black hole binaries have all had recent outbursts that have been analyzed in detail using *RXTE* observations. Park et al. (2004) studied the 2002 outburst of U1543; Sobczak et al. (2000) analyzed the outburst of J1550 in 1998-1999; and Sobczak et al. (1999) analyzed J1655’s 1996-1997 outburst. In fitting the spectra of these sources, we followed as closely as possible the procedures described in these papers.

In addition to KERRBB and the other disk models discussed below, we used four other supplementary XSPEC models in our fits. Primary among these was the power-law model, which has two parameters: the photon index, Γ , and a normalization constant, which we will call K_{PL} . The remaining three spectral components, which model the effects of interstellar absorption, a smeared Fe absorption edge, and a Gaussian Fe line, are relatively unimportant. Because our focus was on the disk models, we froze a number of the extraneous parameters in these other spectral components to minimize their influence on our fits by fixing the parameters at average values obtained from the previously cited papers (see Z04). The spectra were fitted using XSPEC over the energy range $\approx 3 - 20$ keV. All of the data sets correspond to the high/soft state, for which the accretion flow is believed to be dominated by a geometrically thin, optically thick disk component of emission that contributes $\gtrsim 90\%$ of the flux (McClintock & Remillard 2004). For further details on the data and the analysis techniques, see Z04.

In addition to (i) KERRBB, the other XSPEC models we considered were: (ii) GRAD: a general relativistic code for non-spinning black holes (Hanawa 1989); (iii) DISKPN: a disk model employing a pseudo-Newtonian potential (Gierliński et al. 1999); (iv) EZDISKBB: a Newtonian model with a zero-torque inner boundary condition (Z04); and (v) DISKBB: a Newtonian model (Mitsuda et al. 1984) which includes a finite torque at the inner edge of the disk (Gierliński et al. 1999; Z04). Note that KERRBB is the most complete model of these five since it includes the effects of general relativity and can handle a black hole with any spin and any nonnegative torque at the inner edge of the disk. In this section we assume that the torque is zero ($\eta = 0$). Likewise the torque at the inner disk edge is zero for all of the other models except DISKBB (see below). For the specific case of a non-spinning black hole ($a = 0$), KERRBB should agree with GRAD, but there are in fact

some deviations because of an error in GRAD discussed in Appendix F. In order to facilitate comparison between KERRBB and GRAD, we did not include the returning radiation in KERRBB in the calculations reported here. As we have shown in §3.2, the effect is in any event small for $\eta = 0$, and can be absorbed in the fitted value of \dot{M} . Of the other three models, DISKPN should be closest to KERRBB since it attempts to include some relativistic effects through the pseudo-Newtonian potential of Paczyński & Wiita (1980). The main difference between the final two Newtonian models is that EZDISKBB includes a zero-torque boundary condition at the inner edge of the disk whereas DISKBB has a finite torque. As argued in Z04, the zero-torque condition is expected to be valid in a number of situations. Furthermore, even in those cases in which a finite torque might be expected, it is unlikely that the specific magnitude of the torque would be equal to the value assumed in DISKBB.

4.1. Comparison of normalizations

For our first comparison, we analyzed data from ten epochs each on U1543 and J1550 (see Z04 for details of the particular observations). We fixed the mass of the black hole and the inclination of the disk at their respective estimated values of $9.4M_{\odot}$ and 20.7° for U1543 (Orosz et al. 1998; Orosz 2004) and $10.6M_{\odot}$ and 73.5° for J1550 (Orosz et al. 2002). We also assumed that the two black holes are not spinning ($a = 0$) and fixed the inner edge of the disk at the marginally stable orbit ($r_{\text{in}} = r_{\text{ms}} = 6M$). The constancy of this inner disk radius over a wide range of X-ray luminosity has been established in synoptic studies of several black hole binaries (Tanaka & Lewin 1995; Sobczak et al. 2000). Although there are reasonable estimates of the distances to the sources, we left the distance D as an adjustable parameter; in effect, this parameter played the role of a normalization in these calculations. We also left the mass accretion rate \dot{M} as a free parameter, and used a spectral hardening factor $f_{\text{col}} = 1.7$ (Shimura & Takahara 1995).

Figure 10 shows the results of fitting the data on U1543 with the five models. We see a remarkably consistent pattern. KERRBB and GRAD agree almost perfectly in their estimates of both D and \dot{M} ; DISKPN has modest deviations from these two models; EZDISKBB deviates somewhat more; and DISKBB deviates in both parameters by an enormous factor. Table 1 gives the average ratio by which the estimated parameters obtained with each of the models deviates from the value obtained with KERRBB. Here and in what follows, we assume that the result from KERRBB is correct and view any deviation from it as a measure of the error in a particular model.

To understand the patterns seen in Figure 10, we note that each model adjusts two

parameters to the data. These parameters are obtained essentially by fitting the integrated flux from the source and the position of the peak in the spectrum; the latter in effect measures the peak temperature (as observed at infinity) of the emission from the disk. For a non-rotating black hole, the radiative efficiency of KERRBB and GRAD is $\epsilon = 1 - (8/9)^{1/2} = 0.057$; that is, for a given \dot{M} , the luminosity is equal to $0.057\dot{M}c^2$. In contrast, DISKPN has $\epsilon = 0.0625$ and EZDISKBB has $\epsilon = 0.0833$. Thus, these models produce the same luminosity with a smaller \dot{M} . Moreover, for a given luminosity, the fully relativistic models KERRBB and GRAD include Doppler and gravitational redshift factors, whereas the other models do not. These cause additional deviations. The net effect is that the estimate of \dot{M} obtained with DISKPN is lower than the correct relativistic result by a factor of ~ 0.6 , while \dot{M} with EZDISKBB is only a quarter of the correct value. The variations in the derived values of D with the various models are straightforward to understand — each model adjusts D so as to fit the observed flux \propto luminosity/ D^2 .

Compared to the other models, DISKBB makes an extraordinarily large error: the estimate of \dot{M} is reduced by more than a factor of 50 relative to KERRBB. The reason for this is well understood (e.g., Kubota et al. 1998; Gierliński et al. 2001; Z04), though not widely appreciated. DISKBB assumes a finite torque at the inner edge and so its radiative efficiency is three times that of EZDISKBB: $\epsilon = 0.25$. Furthermore, this model has its temperature maximum at the inner edge of the disk, whereas all the other models have their maxima at larger radii. Therefore, it predicts a substantially larger value of T_{\max} for a given luminosity. Since the spectral fit tries to reproduce the position of the peak in the observed spectrum, both effects act in the same direction and lead to a large decrease in the estimated value of \dot{M} . Despite this well-known deficiency in DISKBB, the model is still widely used to model spectra of black hole X-ray binaries.

Some authors have used DISKBB but included correction factors to make the results more consistent with other models. For example, Zhang et al. (1997) and Gierliński & Done (2004) apply correction factors to the temperature and the flux derived from DISKBB. Other authors have attempted to include these corrections in the spectral hardening factor f_{col} (see Davis et al. 2004 for a review of this topic). While these approaches have some merit, we feel it is better to use the correct model, viz., EZDISKBB if one wishes to assume a Newtonian model, DISKPN if one is interested in a pseudo-Newtonian potential, and KERRBB if one would like to include all relativistic effects including returning radiation, and would like to consider different black hole spins and inner torques. (GRAD is valid only for a non-rotating hole.) Indeed, if we apply the approach of Zhang et al. (1997) and Gierliński & Done (2004) to DISKBB or EZDISKBB for U1543, where we expect $\dot{M}/D^2 \propto 1/g_{\text{GR}}$ where g_{GR} is the relativistic correction factor introduced by Zhang et al. (1997), we get $\dot{M}/D^2 \approx 0.22$ for the DISKBB results, and $\dot{M}/D^2 \approx 0.68$ for the EZDISKBB results in Table 1. These corrections

improve somewhat the results of the models without relativistic corrections ($\dot{M}/D^2 \approx 0.18$ for DISKBB and ≈ 0.56 for EZDISKBB), but are still far from the correct relativistic results of KERRBB, which by definition imply $\dot{M}/D^2 = 1$.

In the case of J1550, which is nearly edge-on, we find that the relativistic corrections introduced by Zhang et al. (1997) do not improve the results of DISKBB and EZDISKBB at all. Indeed, from Table 1 of Zhang et al. (1997), by interpolation we have $g_{\text{GR}} \approx 1.14$ for $\theta = 73.5^\circ$ and $a_* = 0$, which brings the results of DISKBB and EZDISKBB farther from the results of KERRBB (see Table 2).

We turn now to a comparison of the results for J1550 obtained using the five models; these results are summarized in Figure 11 and Table 2. Similar patterns are seen as in the case of U1543, but there are also differences. The latter are all caused by the fact that U1543 is a nearly face-on system ($\vartheta_{\text{obs}} = 20.7^\circ$) whereas J1550 is a nearly edge-on system ($\vartheta_{\text{obs}} = 73.5^\circ$). For the three nonrelativistic models, viz., DISKPN, EZDISKBB, and DISKBB, the effect of inclination is straightforward: the flux simply decreases by a factor of $\cos \vartheta_{\text{obs}}$, and there is no change in the spectral shape. However, the two relativistic models KERRBB and GRAD have additional effects. First, they have stronger Doppler beaming for an edge-on system like J1550 and consequently appear brighter and hotter for a given \dot{M} . Second, because of light deflection, the effective projected area of the disk as viewed by the observer is larger than one might expect with a simple $\cos \vartheta_{\text{obs}}$ scaling, especially for the hot inner regions of the disk. For both reasons, these two models are able to fit a given observed flux with a smaller value of \dot{M} than one might expect by naively scaling from a face-on system like U1543. As a result the ratios in Table 2 corresponding to DISKPN, EZDISKBB, and DISKBB are higher by a factor of $\sim 2 - 3$ relative to those in Table 1. In addition, we see that the values obtained with GRAD are higher than those from KERRBB. This is the result of the error in GRAD pointed out in Appendix F. The error has almost no effect for a face-on system like U1543, but becomes more serious for edge-on systems.

Finally, we note that the χ^2 values of the fits vary somewhat erratically from one epoch to the next. Epochs 2 and 3 of U1543 are relatively bad for all models, while epochs 6 and 9 of J1550 are bad for three of the models (DISKPN, EZDISKBB, and DISKBB) but perfectly reasonable for the other two models (KERRBB and GRAD). In the case of our third source, J1655, we obtained large χ^2 values for all except the first two epochs. For this reason, we did not include this source for the calculations discussed in this subsection.

4.2. Estimating the black hole spin

In the previous subsection, we treated the distance D to each source as a free parameter (equivalent to the normalization) and fitted D and \dot{M} from the data. However, we do have independent estimates of the distances: 7.5 ± 1.0 kpc for U1543 (Orosz et al. 1998, 2002); $5.9_{-3.1}^{+1.7}$ kpc for J1550 (Orosz et al. 2002); and 3.2 ± 0.2 kpc for J1655 (Hjellming & Rupen 1995). By using this additional information we should in principle be able to constrain the spin of the black hole (Zhang et al. 1997). (Note that we fixed $a = 0$ in §4.1.) In the case of KERRBB, the calculation is straightforward—we simply fix the value of D and let $a_* \equiv a/M$ and \dot{M} be the free parameters. For the other models, however, a_* is not an adjustable parameter. In the case of the three non-relativistic models, DISKPN, EZDISKBB, and DISKBB, we allow the radius of the inner edge r_{in} and \dot{M} to be the free parameters. Having fitted r_{in} from the data, we then use the ratio r_{in}/M to estimate a_* , assuming that the inner edge is at the marginally stable orbit corresponding to the particular spin parameter. This procedure is somewhat arbitrary, but is fairly standard practice in the literature. We have not attempted a similar exercise with GRAD.

Figure 12 shows the estimated spin parameter a_* for each of the 10 observations of U1543 and J1550, and the first two observations of J1655 (with $M = 7.0M_{\odot}$ and $\vartheta_{\text{obs}} = 69.5^{\circ}$; Orosz & Bailyn 1997). We have ignored the remaining 8 observations of J1655 because (for some unexplained reason) the χ^2 values are very large. In the case of U1543, KERRBB gives a consistent estimate of $a_* \sim 0.6$ for all the epochs. The near-constancy of the estimate is notable, especially since the luminosity and the mass accretion rate do vary from one epoch to the next (see Fig. 10). The models DISKPN and EZDISKBB give different values of a_* , suggesting that it is dangerous to use these models to estimate the black hole spin. The model DISKBB is especially poor—in the case of both U1543 and J1550, it gives estimates of the disk inner edge that are too large ($> 9M$) to be consistent with any choice of the spin parameter. The results are more variable in the case of J1550. We find with KERRBB values of a_* ranging all the way from -0.8 to -0.1 . In part this is because the spectra are less sensitive to the value of a_* when the parameter is negative, but in part it might also reflect the quality of the data (e.g., the very uncertain distance to the source; see below). In the case of J1655, the two epochs that we have analyzed give $a_* \sim 0.6 - 0.7$, slightly larger than for U1543.

The ability to estimate a_* depends on having independent estimates of the disk inclination ϑ_{obs} , the black hole mass M , the distance to the source D , and the spectral hardening factor f_{col} . However, even for the best sources, there are substantial uncertainties in these parameters. Table 3 shows for one epoch of U1543 how the fitted value of a_* varies as each of the four input parameters is allowed to range over its 1σ range of uncertainty. Leaving

aside f_{col} , we see that the uncertainties in the other three parameters are not particularly severe for this favorable case of U1543. Even allowing for the uncertainties it appears that one could infer that $a_* > 0.5$. The spectral hardening factor, however, introduces a large uncertainty. The value of this parameter is not well constrained. Shimura & Takahara (1995) suggested a value of 1.7, but said that the value could be anywhere in the range from 1.5 to 1.9 (the range covered in Table 3). A recent comprehensive analysis by Davis et al. (2004), which includes better opacities, comes down in favor of somewhat smaller values in the range $f_{\text{col}} \sim 1.5 - 1.6$, depending on the luminosity of the disk. For such values, the spin estimates go up by a modest amount, to $a_* \sim 0.7 - 0.8$ for U1543 and ~ 0.8 for J1655. Apart from the question of what is the correct value of f_{col} to use, a more serious concern is that it is a rather severe simplification to model the spectral modification due to Comptonization and opacity effects with a single scaling parameter f_{col} . It is hard to quantify the error from this approximation. In our opinion, if one wishes to estimate black hole spin via spectral fitting, one must first develop more reliable spectral models of disk atmospheres. The work of Davis et al. (2004) is a first step in this direction.

In the case of J1550, the distance is highly uncertain: $D = 2.8 - 7.6$ kpc (Orosz et al. 2002). Correspondingly, a_* is poorly constrained. We analyzed the 10 observations of this source using the two extreme 1σ values of D and obtained values of a_* ranging all the way from -1 to $+0.7$. This emphasizes once again that we cannot hope to constrain the spin of a black hole via spectral fitting unless we have accurate input parameters.

5. Summary

We have developed a ray-tracing computer code to calculate the spectrum of a thin accretion disk around a black hole, assuming that the emission from each point on the surface of the disk is locally blackbody-like with a constant spectral hardening factor f_{col} . The code includes all relativistic effects. It also includes the effect of self-irradiation whereby radiation emitted at one point on the disk is deflected by the gravity of the black hole and illuminates another part of the disk. The code can handle any value of the black hole spin, the disk inclination, the disk inner radius ($r_{\text{in}} \geq r_{\text{ms}}$), and the torque on the inner edge (the dimensionless parameter η). It also allows the user to choose between isotropic emission and a Chandrasekhar (1950) limb-darkening law (eq. [D20]).

In terms of the scope of the calculations, the present work is not markedly different from previous studies. For instance, Fabian et al. (1989) and Stella (1990) calculated line emission from a relativistic disk around a non-rotating black hole, while Laor (1991) repeated the calculation for a rapidly rotating black hole with a specific value of $a/M = 0.998$ (i.e., a

nearly maximally rotating hole). Our code calculates the continuum emission, rather than the line emission, and is more comparable to the blackbody continuum models calculated by Hanawa (1989) and Ebisawa et al. (1991) for a disk around a non-rotating black hole and by Cunningham (1975, 1976) and Gierliński et al. (2001) for a disk around a rotating black hole. Our model supersedes Cunningham’s model by including a torque at the inner boundary of the disk, and that of Gierliński et al. by including both the torque and the effect of the returning radiation. The calculations of Agol & Krolik (2000) are very close to the present work. The only difference is that they did not include the additional energy released as a result of the torque applied by the returning radiation (the term F_S in §3.1 and Appendix D). As we have shown, this term is quantitatively not important.

Using the ray-tracing code, we have calculated tables of spectra and developed a model called KERRBB for use with the X-ray spectral fitting package XSPEC. This model can handle black hole spins in the range $a_* = a/M = -1$ to $+0.9999$, inclinations in the range $\vartheta_{\text{obs}} = 0^\circ$ to 85° , and torque parameters in the range $\eta = 0$ to 1 . One can choose either isotropic emission or limb-darkened emission from the disk (eq. [D20]). In addition, as usual, one can set (or fit) the black hole mass M , the distance to the source D , the mass accretion rate \dot{M} , and the spectral hardening factor f_{col} . KERRBB thus goes well beyond other models that are presently available in XSPEC for fitting the continuum emission from thin disks. The other models are based on a Newtonian potential (DISKBB, EZDISKBB) or a pseudo-Newtonian potential (DISKPN), or if they solve the relativistic problem it is only for a specific case, e.g., a non-rotating black hole (GRAD, see Appendix F). KERRBB is more general and complete than any of these models. One limitation of KERRBB is that the present implementation in XSPEC only considers disks that extend down to the marginally stable orbit ($r_{\text{in}} = r_{\text{ms}}$). Disks that evaporate into a corona/ADAF at radii $r_{\text{in}} > r_{\text{ms}}$ are not yet modeled, but could easily be incorporated in the future if there is a need.

The effects of some of the model parameters on the observed spectrum are illustrated in Figures 5–9. The black hole spin parameter a/M and the inclination angle ϑ_{obs} are seen to have a strong effect on the spectrum. These model parameters must clearly be included when fitting spectral data. The effect of the returning radiation appears to be less important. At least for torque parameters $\eta \lesssim 1$, its effect can be almost completely absorbed by a rescaling of the mass accretion rate. Likewise, the effect of limb-darkening, which is important only when the disk is nearly edge-on, can otherwise be absorbed by adjusting the mass accretion rate and the normalization (Fig. 9).

Afshordi & Paczyński (2003) have argued that a thin accretion disk will have a negligible torque at its inner edge. Magnetohydrodynamic simulations of disks have found nonzero torques (Hawley & Krolik 2002), but the magnitude appears to be relatively small ($\eta \sim 0.2$)

even for relatively thick disks ($H/R \sim 0.1 - 0.2$). For such values of η , and indeed even for larger values up to $\eta \sim 1$, Figures 7 and 8 show that the effect of a finite torque can be modeled with a zero-torque disk by simply adjusting the mass accretion rate and the normalization (however, see the caveat in the following paragraph). Since \dot{M} is almost always fitted to the data, and the normalization is rarely known accurately a priori because of uncertainties in the black hole mass, source distance, disk inclination, etc., it appears that there is no particular advantage to including a finite torque in fitting spectral observations. Nevertheless, we have retained η as a parameter in KERRBB for the occasions when it might be needed.

The following additional caveat must be noted with respect to models with a finite torque at the disk inner edge. Most such models have continued viscous dissipation at radii inside r_{ms} (e.g., Krolik 1999; Gammie 1999). KERRBB calculates the effect of the torque and the radiation it produces only for radii $r \geq r_{\text{in}} = r_{\text{ms}}$, and does not include the emission from smaller radii. The model is thus incomplete. This is one more reason for not including a finite torque in fitting spectral data with KERRBB. When $\eta = 0$, no additional energy dissipation is expected for $r < r_{\text{in}}$. In this case, KERRBB includes all the emission and is self-consistent.

We have compared KERRBB with the various other models mentioned above: GRAD, DISKPN, EZDISKBB, DISKBB. As §§3.1, 3.2, Figures 10–12 and Tables 1 and 2 show, the differences are quite large (except in the case of GRAD), indicating that these models make significant errors in computing the spectra of disks. The errors are the result of the approximations made by the models, e.g., Newtonian or pseudo-Newtonian dynamics, neglect of Doppler and redshift effects, inappropriate torque at the inner edge, etc. When the relativistic corrections of Zhang et al. (1997) are applied to DISKBB and EZDISKBB, the results are improved somewhat for the low inclination case, but the differences from the results of KERRBB are still significant. For the high inclination case the relativistic corrections of Zhang et al. (1997) do not improve the nonrelativistic results of DISKBB and EZDISKBB at all.

In §3.2 we showed that, in principle, if we knew M , ϑ_{obs} and D , then we could determine the spin parameter a_* of the black hole by fitting spectral data. This was first attempted by Zhang et al. (1997) for the black hole X-ray binary J1655 (also, see Sobczak et al. 1999). For this approach to work, we need fairly accurate estimates of M , ϑ_{obs} and D (see Table 3), which are not always available (e.g., the distance to J1550 is very uncertain and so the estimates of a_* obtained for this source in Fig. 12 are highly suspect). Moreover, even if we did have accurate estimates of these parameters, the results would still be uncertain because of the questionable blackbody assumption. Non-blackbody effects are usually modeled by

means of the spectral hardening factor f_{col} , and a value $f_{\text{col}} = 1.7$ is conventionally used (Shimura & Takahara 1995). Using this value, and allowing ϑ_{obs} , M and D to vary over their allowed 1σ ranges, we estimate for the source U1543 that $a_* \sim 0.5 - 0.7$ (Table 3). If instead we assume $f_{\text{col}} \sim 1.5 - 1.6$, as in the recent paper of Davis et al. (2004), then we find a somewhat more rapidly rotating black hole with $a_* \sim 0.7 - 0.8$. On the other hand, if we allow the full range of uncertainty as estimated by Shimura & Takahara (1995), viz. $f_{\text{col}} \sim 1.5 - 1.9$, then a_* could be as low as ~ 0.3 . This illustrates that the biggest obstacle to estimating black hole spin via this method is the uncertainty in modeling the emitted spectrum from the disk. The crude treatment in terms of a simple hardening factor f_{col} needs to be improved significantly before we can make full use of spectral observations of black hole accretion disks. More work along the lines of Davis et al. (2004) is highly desirable.

Other limitations include the fact that the model assumes that the disk is perfectly flat with zero vertical thickness, and all the returning radiation is absorbed by the disk and reemitted as blackbody radiation. A real disk has a finite thickness which moreover varies with radius (i.e., the disk is flared); it probably also has a substantial warp. These complications will modify the effect of returning radiation and will also change the geometrical projection factors needed when computing the observed spectrum. Furthermore, at least a part of the returning radiation is scattered by the disk, which adds a high-energy component to the spectrum (Cunningham 1976). Modeling such effects would involve too many additional parameters and we have not attempted it.

LXL acknowledges Massimo Calvani and Claudio Fanton for discussions on ray-tracing and for sharing their computer code, Craig Gordon and Keith Arnaud for helps on loading KERRBB to XSPEC. LXL’s research was supported by NASA through Chandra Postdoctoral Fellowship grant number PF1-20018 awarded by the Chandra X-ray Center, which is operated by the Smithsonian Astrophysical Observatory for NASA under contract NAS8-39073. EZ, RN and JEM’s research was supported in part by NASA grants NAG5-9930 and NAG5-10780 and NSF grant AST 0307433.

A. Integration of Photon Orbits in a Kerr Spacetime I: The $E_\infty \neq 0$ Case

The general orbit of a photon (indeed for any particle) in a Kerr spacetime is described by three constants of motion (Carter 1968): the energy-at-infinity E_∞ , the angular momentum about the axis of the black hole L_z , and another constant \mathcal{Q} (when $a = 0$, $\mathcal{Q} + L_z^2$ is the

square of the total angular momentum). Let us write $L_z = \lambda E_\infty$ and $\mathcal{Q} = QE_\infty^2$.³ Then, the equations governing the orbital trajectories are separable. Since the system is stationary and axisymmetric, only the motions in the r - and ϑ -directions are required in the calculation of the radiation spectrum from the disk. The motion in the $r - \vartheta$ plane is governed by (Bardeen et al. 1972; Chandrasekhar 1983)

$$\int_{r_e}^r \frac{dr}{\sqrt{R(r)}} = \pm \int_{\vartheta_e}^{\vartheta} \frac{d\vartheta}{\sqrt{\Theta(\vartheta)}}, \quad (\text{A1})$$

where

$$R(r) = r^4 + (a^2 - \lambda^2 - Q)r^2 + 2M[Q + (\lambda - a)^2]r - a^2Q, \quad (\text{A2})$$

$$\Theta(\vartheta) = Q + a^2 \cos^2 \vartheta - \lambda^2 \cot^2 \vartheta, \quad (\text{A3})$$

and r_e and ϑ_e are the starting values of r and ϑ . The \pm signs in equation (A1) must be carefully chosen according to the sign of $dr/d\vartheta$ on the orbit of the photon.

Define $\mu = \cos \vartheta$, then equation (A1) becomes

$$\int_{r_e}^r \frac{dr}{\sqrt{R(r)}} = \pm \int_{\mu_e}^{\mu} \frac{d\mu}{\sqrt{\Theta_\mu(\mu)}}, \quad (\text{A4})$$

where $\mu_e = \cos \vartheta_e$ and

$$\Theta_\mu(\mu) = Q + (a^2 - \lambda^2 - Q)\mu^2 - a^2\mu^4 = a^2(\mu_-^2 + \mu^2)(\mu_+^2 - \mu^2), \quad (\text{A5})$$

and μ_\pm^2 are defined by

$$\mu_\pm^2 = \frac{1}{2a^2} \left\{ [(\lambda^2 + Q - a^2)^2 + 4a^2Q]^{1/2} \mp (\lambda^2 + Q - a^2) \right\}. \quad (\text{A6})$$

For a photon crossing the equatorial plane (which is the case that we are interested in), we have $Q > 0$. Then, both μ_+^2 and μ_-^2 are nonnegative. Note, $\mu_+^2 \mu_-^2 = Q/a^2$.

For a photon emitted by the disk, we have $\vartheta_e = \pi/2$ and $\mu_e = 0$, so μ^2 can never exceed μ_+^2 since otherwise $\sqrt{\Theta_\mu}$ and $\sqrt{\Theta}$ become imaginary. Then, the integral over μ can be worked out with the inverse Jacobian elliptic integral (Byrd & Friedman 1954, eq. 213.00)

$$\int_{\mu}^{\mu_+} \frac{d\mu}{\sqrt{\Theta_\mu}} = \int_{\mu}^{\mu_+} \frac{d\mu}{\sqrt{a^2(\mu_-^2 + \mu^2)(\mu_+^2 - \mu^2)}} = \frac{1}{\sqrt{a^2(\mu_+^2 + \mu_-^2)}} \text{cn}^{-1} \left(\frac{\mu}{\mu_+} \middle| m_\mu \right), \quad (\text{A7})$$

³The case of $E_\infty \approx 0$ is treated separately in Appendix B.

where $0 \leq \mu < \mu_+$ and

$$m_\mu = \frac{\mu_+^2}{\mu_+^2 + \mu_-^2}. \quad (\text{A8})$$

In this paper we use the convention for the modulus in an elliptic integral (e.g., m_μ in the above inverse Jacobian elliptic integral) which is the same as that of Abramowitz & Stegun (1972), and differs from that of Byrd & Friedman (1954) by a square.

The integral over r can also be worked out with inverse Jacobian elliptic integrals. To do so, we need to find out the four roots of $R(r) = 0$. Since $R(r \rightarrow \pm\infty) = \infty$ and $R(r = 0) = -a^2Q \leq 0$, $R(r) = 0$ has at least two real roots. The remaining two roots can be either real or complex (in the latter case the two must be complex conjugates of each other). We consider the two cases separately:

Case A. $R(r) = 0$ has four real roots Let us denote the four roots by $r_1, r_2, r_3,$ and r_4 , with $r_1 \geq r_2 \geq r_3 \geq r_4$. By equation (A2), we have $r_1 + r_2 + r_3 + r_4 = 0$ and $r_1 r_2 r_3 r_4 = -a^2Q \leq 0$; the latter implies that r_4 must be ≤ 0 . Physically allowed regions for photons are given by $R \geq 0$, i.e., $r \geq r_1$ (region I) and $r_3 \leq r \leq r_2$ (region II). (Although $R \geq 0$ also for $r \leq r_4$, this region is unphysical since $r_4 \leq 0$.)

In region I ($r \geq r_1$), the integral over r can be worked out by the following integration (Byrd & Friedman 1954, eq. 258.00)

$$\begin{aligned} \int_{r_1}^r \frac{dr}{\sqrt{R}} &= \int_{r_1}^r \frac{dr}{\sqrt{(r-r_1)(r-r_2)(r-r_3)(r-r_4)}} \\ &= \frac{2}{\sqrt{(r_1-r_3)(r_2-r_4)}} \operatorname{sn}^{-1} \left[\sqrt{\frac{(r_2-r_4)(r-r_1)}{(r_1-r_4)(r-r_2)}} \middle| m_4 \right], \end{aligned} \quad (\text{A9})$$

where

$$m_4 = \frac{(r_1-r_4)(r_2-r_3)}{(r_1-r_3)(r_2-r_4)}. \quad (\text{A10})$$

It is easy to show that

$$0 \leq \sqrt{\frac{(r_2-r_4)(r-r_1)}{(r_1-r_4)(r-r_2)}} < 1, \quad 0 \leq m_4 \leq 1,$$

when $r_1 \neq r_2$. Thus, the inverse Jacobian elliptic function sn^{-1} in equation (A9) is well defined.

When $r_1 = r_2$, the integral in equation (A9) becomes $\propto \text{sn}^{-1}(1|1) = \infty$. In this case the integral over r needs special treatment. Indeed, when $r_1 = r_2$, the integral over r can be expressed in terms of a logarithm,

$$\begin{aligned} \int \frac{dr}{\sqrt{R}} &= \int \frac{dr}{(r-r_1)\sqrt{(r-r_3)(r-r_4)}} = -\frac{1}{\sqrt{(r_1-r_3)(r_1-r_4)}} \\ &\times \ln \left[\frac{\sqrt{(r-r_3)(r-r_4)}}{r-r_1} + \frac{2r_3r_4 - r_1(r_3+r_4) + (2r_1-r_3-r_4)r}{2(r-r_1)\sqrt{(r_1-r_3)(r_1-r_4)}} \right] \\ &= -\frac{1}{\sqrt{(r_1-r_3)(r_1-r_4)}} \\ &\times \ln \left[\frac{\sqrt{(r-r_3)(r-r_4)}}{r-r_1} + \frac{r_1^2 + r_3r_4 + 2r_1r}{(r-r_1)\sqrt{(r_1-r_3)(r_1-r_4)}} \right], \end{aligned} \quad (\text{A11})$$

where in the last step we have used $2r_1 + r_3 + r_4 = 0$.

In region II ($r_3 \leq r \leq r_2$), the integral over r can be worked out by the following integration (Byrd & Friedman 1954, eq. 255.00)

$$\begin{aligned} \int_r^{r_2} \frac{dr}{\sqrt{R}} &= \int_r^{r_2} \frac{dr}{\sqrt{(r_1-r)(r_2-r)(r-r_3)(r-r_4)}} \\ &= \frac{2}{\sqrt{(r_1-r_3)(r_2-r_4)}} \text{sn}^{-1} \left[\sqrt{\frac{(r_1-r_3)(r_2-r)}{(r_2-r_3)(r_1-r)}} \middle| m_4 \right]. \end{aligned} \quad (\text{A12})$$

It can be shown that

$$0 \leq \sqrt{\frac{(r_1-r_3)(r_2-r)}{(r_2-r_3)(r_1-r)}} \leq 1,$$

so the inverse Jacobian elliptic function sn^{-1} in equation (A12) is well defined when $r_1 \neq r_2$.

Again, we need special treatment for the case $r_1 = r_2$: the integral over r is then given by

$$\begin{aligned} \int \frac{dr}{\sqrt{R}} &= \int \frac{dr}{(r_1-r)\sqrt{(r-r_3)(r-r_4)}} = \frac{1}{\sqrt{(r_1-r_3)(r_1-r_4)}} \\ &\times \ln \left[\frac{\sqrt{(r-r_3)(r-r_4)}}{r_1-r} + \frac{r_1^2 + r_3r_4 + 2r_1r}{(r_1-r)\sqrt{(r_1-r_3)(r_1-r_4)}} \right]. \end{aligned} \quad (\text{A13})$$

Case B. $R(r) = 0$ has two complex roots and two real roots Let us assume that r_1 and r_2 are complex, r_3 and r_4 are real and $r_3 > r_4$. Then, we must have $r_1 = r_2^*$, where \star stands

for complex conjugate. Since $r_1 r_2 r_3 r_4 = |r_1|^2 r_3 r_4 = -a^2 Q \leq 0$, r_4 must be ≤ 0 and r_3 must be ≥ 0 . [Thus, it is impossible that $r_3 = r_4$, since otherwise it gives $r_3 = r_4 = 0$, which by eq. (A2) implies that $Q = \lambda - a = 0$ and $r_1 = r_2 = 0$ too.] Since $R \geq 0$ implies $r \geq r_3$ or $r \leq r_4$, the physically allowed region for photons is given by $r \geq r_3$.

Define $u = \Re(r_1) = \Re(r_2)$ and $v = \Im(r_1) = -\Im(r_2)$, where \Re and \Im denote the real and imaginary parts of a complex number. Then, the integral over r can be worked out with the following integration (Byrd & Friedman 1954, eq. 260.00)

$$\begin{aligned} \int_{r_3}^r \frac{dr}{\sqrt{R}} &= \int_{r_3}^r \frac{dr}{\sqrt{(r-r_1)(r-r_2)(r-r_3)(r-r_4)}} \\ &= \frac{1}{\sqrt{AB}} \operatorname{cn}^{-1} \left[\frac{(A-B)r + r_3 B - r_4 A}{(A+B)r - r_3 B - r_4 A} \middle| m_2 \right], \end{aligned} \quad (\text{A14})$$

where

$$A^2 = (r_3 - u)^2 + v^2, \quad B^2 = (r_4 - u)^2 + v^2, \quad (\text{A15})$$

and

$$m_2 = \frac{(A+B)^2 - (r_3 - r_4)^2}{4AB}. \quad (\text{A16})$$

It is easy to verify that

$$\left[\frac{(A-B)r + r_3 B - r_4 A}{(A+B)r - r_3 B - r_4 A} \right]^2 = 1 - \frac{4AB(r-r_3)(r-r_4)}{[(A+B)r - r_3 B - r_4 A]^2} \leq 1,$$

for $r \geq r_3$. Using the identity $(2AB)^2 - [A^2 + B^2 - (r_3 - r_4)^2]^2 = 4(r_3 - r_4)^2 v^2 > 0$, we have

$$-2AB < A^2 + B^2 - (r_3 - r_4)^2 < 2AB.$$

Then we can show that

$$0 < m_2 < 1.$$

Hence, the inverse Jacobian elliptic function cn^{-1} in equation (A14) is well defined.

Therefore, if we can find the four roots of $R = 0$, we can work out the integral over r . The standard procedure for finding the roots of a quartic equation can be found in, e.g., Birkhoff & Mac Lane (1965); Zwillinger (2002).

Each photon emitted by the disk has three possible fates: escaping to infinity, returning to the disk, or being captured by the black hole. In the following we discuss the solutions for the photon orbits for each of those the possibilities separately.

A.1. Solutions for photons escaping to infinity

We consider an observer at infinity (in practice corresponding to the limit that the distance from the black hole to the observer is \gg the radius of the disk) with a polar angle ϑ_{obs} , and calculate the orbit of a photon that reaches him/her. As the photon leaves the disk, we have $\vartheta = \vartheta_e = \pi/2$ and $\mu = \mu_e = \cos \vartheta_e = 0$. As the photon reaches the observer, we have $\vartheta = \vartheta_{\text{obs}}$ and $\mu = \mu_{\text{obs}} \equiv \cos \vartheta_{\text{obs}}$.

The position of a photon on the sky as seen by the observer is specified by a pair of impact parameters (α, β) (see Figure 13 and the second part of Appendix C for details). The coordinate α measures the displacement of the photon image perpendicular to the projection of the rotation axis of the black hole, and β measures the displacement parallel to the projection of the axis. The line of sight to the black hole center marks the origin of the coordinates, where $\alpha = \beta = 0$. It can be checked that as the photon reaches the observer, on the photon orbit we have $d\vartheta/dr > 0$ (i.e., $d\mu/dr < 0$) if $\beta > 0$, and $d\vartheta/dr < 0$ (i.e., $d\mu/dr > 0$) if $\beta < 0$. Therefore, when $\beta > 0$, the photon must encounter a turning point at $\mu = \mu_+$: μ starts from 0, goes up to μ_+ , then goes down to μ_{obs} (which is $\leq \mu_+$ according to the earlier argument). When $\beta < 0$, the photon must not encounter a turning point at $\mu = \mu_+$: μ starts from 0 and monotonically increases to μ_{obs} .

Based on the above arguments, we can calculate the total integration over μ along the path of the photon from the disk to the observer. The results are

$$\tau_\mu \equiv \int_{\mathcal{S}_{\text{ph}}} \frac{d\mu}{\sqrt{\Theta_\mu}} = \begin{cases} \left(\int_0^{\mu_+} + \int_{\mu_{\text{obs}}}^{\mu_+} \right) \frac{d\mu}{\sqrt{\Theta_\mu}}, & (\beta > 0) \\ \int_0^{\mu_{\text{obs}}} \frac{d\mu}{\sqrt{\Theta_\mu}} = \left(\int_0^{\mu_+} - \int_{\mu_{\text{obs}}}^{\mu_+} \right) \frac{d\mu}{\sqrt{\Theta_\mu}}, & (\beta < 0) \end{cases}, \quad (\text{A17})$$

where $\int_{\mathcal{S}_{\text{ph}}}$ stands for the integration along the path of the photon. Note, by definition, τ_μ is positive. Substituting equation (A7) into equation (A17), we get

$$\tau_\mu = \frac{1}{\sqrt{a^2(\mu_+^2 + \mu_-^2)}} \left[K(m_\mu) + \text{sign}(\beta) \text{cn}^{-1} \left(\frac{\mu_{\text{obs}}}{\mu_+} \middle| m_\mu \right) \right], \quad (\text{A18})$$

where $\text{sign}(\beta) = 1$ if $\beta > 0$, 0 if $\beta = 0$, and -1 if $\beta < 0$; $K(m)$ is the complete elliptic integral of the first kind.

Now let us consider the integration over r . Since the observer is at infinity, the photon reaching him/her must have been moving in the allowed region defined by $r \geq r_1$ when $R = 0$ has four real roots (case A), or the allowed region defined by $r \geq r_3$ when $R = 0$ has two complex roots and two real roots (case B). There are then two possibilities for the photon during its trip: it has encountered a turning point at $r = r_+$ ($r_+ = r_1$ in case A, $r_+ = r_3$ in

case B), or it has not encountered any turning point in r . Define

$$\tau_\infty \equiv \int_{r_+}^{\infty} \frac{dr}{\sqrt{R}}, \quad \tau_e \equiv \int_{r_+}^{r_e} \frac{dr}{\sqrt{R}}, \quad (\text{A19})$$

where r_e is the radius in the disk where the photon is emitted. Obviously, according to equation (A4), a necessary and sufficient condition for the occurrence of a turning point in r on the path of the photon is that $\tau_\infty < \tau_\mu$. Then, the total integration over r along the path of the photon from the disk to the observer is

$$\tau_r \equiv \int_{S_{\text{ph}}} \frac{dr}{\sqrt{R}} = \begin{cases} \tau_\infty + \tau_e, & (\tau_\infty < \tau_\mu) \\ \int_{r_e}^{\infty} \frac{dr}{\sqrt{R}} = \tau_\infty - \tau_e, & (\tau_\infty \geq \tau_\mu) \end{cases}. \quad (\text{A20})$$

By definition, τ_∞ , τ_e , and τ_r are all positive. According to equation (A4), we must have $\tau_r = \tau_\mu$ for the orbit of a photon.

Case A: $R = 0$ has four real roots When $r_1 \neq r_2$, substitute equation (A9) into equation (A19) and set $r_+ = r_1$. We obtain

$$\tau_\infty = \frac{2}{\sqrt{(r_1 - r_3)(r_2 - r_4)}} \operatorname{sn}^{-1} \left(\sqrt{\frac{r_2 - r_4}{r_1 - r_4}} \middle| m_4 \right), \quad (\text{A21})$$

$$\tau_e = \frac{2}{\sqrt{(r_1 - r_3)(r_2 - r_4)}} \operatorname{sn}^{-1} \left[\sqrt{\frac{(r_2 - r_4)(r_e - r_1)}{(r_1 - r_4)(r_e - r_2)}} \middle| m_4 \right]. \quad (\text{A22})$$

Substituting equations (A21) and (A22) into equation (A20) and letting $\tau_r = \tau_\mu$, we can solve for r_e —the radius in the disk where the photon is emitted. The solution is

$$r_e = \frac{r_1(r_2 - r_4) - r_2(r_1 - r_4) \operatorname{sn}^2(\xi_4 | m_4)}{(r_2 - r_4) - (r_1 - r_4) \operatorname{sn}^2(\xi_4 | m_4)}, \quad (\text{A23})$$

where

$$\xi_4 \equiv \frac{1}{2}(\tau_\mu - \tau_\infty) \sqrt{(r_1 - r_3)(r_2 - r_4)}. \quad (\text{A24})$$

Since $\operatorname{sn}^2(-\xi_4 | m_4) = \operatorname{sn}^2(\xi_4 | m_4)$, the solution given by equation (A23) applies whether $\tau_\mu - \tau_\infty$ is positive or negative, i.e. no matter whether there is a turning point in r or not along the path of the photon. Equation (A23) is essentially equivalent to equation (37) of Čadež et al. (1998).

When $r_1 = r_2$, the integration from $r = r_1$ to any $r > r_1$ is infinite (see eq. [A11]), so $\tau_\infty = \infty$ and there cannot be a turning point in r . Then, by equation (A11), we have

$$\tau_r = \int_{r_e}^{\infty} \frac{dr}{\sqrt{R}} = \frac{1}{\sqrt{(r_1 - r_3)(r_1 - r_4)}} \left\{ -\ln \left[1 + \frac{2r_1}{\sqrt{(r_1 - r_3)(r_1 - r_4)}} \right] \right\}$$

$$+ \ln \left[\frac{\sqrt{(r_e - r_3)(r_e - r_4)}}{r_e - r_1} + \frac{r_1^2 + r_3 r_4 + 2r_1 r_e}{(r_e - r_1)\sqrt{(r_1 - r_3)(r_1 - r_4)}} \right] \}. \quad (\text{A25})$$

Setting $\tau_r = \tau_\mu$, we then obtain the solution for r_e

$$r_e = \frac{r_3 r_4 - \left[\gamma r_1 + (r_1^2 + r_3 r_4) / \sqrt{(r_1 - r_3)(r_1 - r_4)} \right]^2}{r_1 \left\{ 1 - \left[\gamma - 2r_1 / \sqrt{(r_1 - r_3)(r_1 - r_4)} \right]^2 \right\}}, \quad (\text{A26})$$

where the identity $2r_1 + r_3 + r_4 = 0$ has been used, and

$$\gamma \equiv \left[1 + \frac{2r_1}{\sqrt{(r_1 - r_3)(r_1 - r_4)}} \right] \exp \left[\tau_\mu \sqrt{(r_1 - r_3)(r_1 - r_4)} \right]. \quad (\text{A27})$$

The numerical value for r_e obtained from equation (A26) should be substituted back in equation (A25) (with $\tau_r = \tau_\mu$) to check if r_e is a true root, since the square operation in the process of solving equation (A25) might produce a false root.

Case B: $R = 0$ has two complex roots and two real roots. Substituting equation (A14) into equation (A19) and setting $r_+ = r_3$, we obtain

$$\tau_\infty = \frac{1}{\sqrt{AB}} \text{cn}^{-1} \left(\frac{A - B}{A + B} \middle| m_2 \right), \quad (\text{A28})$$

$$\tau_e = \frac{1}{\sqrt{AB}} \text{cn}^{-1} \left[\frac{(A - B)r_e + r_3 B - r_4 A}{(A + B)r_e - r_3 B - r_4 A} \middle| m_2 \right]. \quad (\text{A29})$$

Substituting equation (A28) and (A29) into equation (A20) and letting $\tau_r = \tau_\mu$, we can solve for r_e . The solution is

$$r_e = \frac{r_4 A - r_3 B - (r_4 A + r_3 B) \text{cn}(\xi_2 | m_2)}{(A - B) - (A + B) \text{cn}(\xi_2 | m_2)}, \quad (\text{A30})$$

where

$$\xi_2 \equiv (\tau_\mu - \tau_\infty) \sqrt{AB}. \quad (\text{A31})$$

Since $\text{cn}(-\xi_2 | m_2) = \text{cn}(\xi_2 | m_2)$, the solution given by equation (A30) applies no matter whether $\tau_\mu - \tau_\infty$ is positive or negative, i.e. no matter whether there is a turning in r or not along the path of the photon. Equation (A30) is essentially equivalent to equation (39) of Čadež et al. (1998), although equation (A30) is much simpler.

In the above derivation we have implicitly assumed that $r_+ > r_H$, where r_H is the radius of the horizon of the black hole. If $r_+ \leq r_H$, then obviously the orbit of the photon cannot have a turning point at $r = r_+$, since if a photon falls into a black hole it cannot get out. Therefore, when $r_+ \leq r_H$, the solutions given by equations (A23) and (A30) hold only if $\tau_\mu < \tau_\infty$, i.e. when there is no turning in r along the path of the photon. Finally, the solution that we have found above for r_e represents a physical solution—i.e., it represents a photon emitted by the disk—only if it satisfies $r_{\text{in}} \leq r_e \leq r_{\text{out}}$, where r_{in} is the radius of the inner boundary of the disk, and r_{out} is the radius of the outer boundary of the disk.

A.2. Solutions for photons returning to the disk

A photon returning to the disk must satisfy $\mu = 0$ (i.e., $\vartheta = \pi/2$) as it approaches the disk at radius r_a . Since as it leaves the disk at radius r_e it must also have $\mu = 0$, the photon must have encountered a turning in ϑ during its trip. Therefore, along the path of the photon, μ must first increase from $\mu = 0$ to $\mu = \mu_+$, then decrease from $\mu = \mu_+$ to $\mu = 0$.⁴ Then, along the path of the photon the total integration over μ is

$$\tau_\mu = 2 \int_0^{\mu_+} \frac{d\mu}{\sqrt{\Theta_\mu}} = \frac{2}{\sqrt{a^2(\mu_+^2 + \mu_-^2)}} K(m_\mu). \quad (\text{A32})$$

The integration over r depends on the allowed region which the photon moves in. In case A ($R = 0$ has four real roots), there are two allowed regions: region I and region II. If the photon moves in region I, which is bounded at $r = r_1$, it may encounter a turning point at $r = r_1$. If the photon moves in region II, which is bounded at $r = r_2$ and $r = r_3$, it may encounter many turning points at $r = r_2$ and $r = r_3$. In case B ($R = 0$ has two complex roots and two real roots), there is only one allowed region that is given by $r \geq r_3$, so the photon may encounter a turning point at $r = r_3$. In each of these cases the path of the photon also depends on the fact whether r_H appears in the region that the photon moves in, and on the direction of the photon as it approaches $r = r_a$ in the disk, determined by the value of $k_r = k_a(\partial/\partial r)^a$ at $r = r_a$, where k^a is the four-wavevector of the photon. Let us discuss each of these cases separately.

Case A1: $R = 0$ has four real roots, region I ($r \geq r_1$) If $r_1 \neq r_2$, the fundamental

⁴Of course this assumes that the returning photon crosses the equatorial plane only once. This is reasonable since we assume that as the photon reaches the equatorial plane it will be captured by either the disk or the gas in the plunging region.

integral over r is given by equation (A9). Let us define

$$\tau_a \equiv \int_{r_1}^{r_a} \frac{dr}{\sqrt{R}} = \frac{2}{\sqrt{(r_1 - r_3)(r_2 - r_4)}} \operatorname{sn}^{-1} \left[\sqrt{\frac{(r_2 - r_4)(r_a - r_1)}{(r_1 - r_4)(r_a - r_2)}} \middle| m_4 \right]. \quad (\text{A33})$$

Other relevant integrations are τ_∞ and τ_e , defined by equations (A21) and (A22) respectively.

When $k_r < 0$ at $r = r_a$, i.e., the photon approaches r_a from the side of $r > r_a$, the solution for r_e is determined by the equation $\tau_\mu = \tau_r$, where the integral over r along the path of the photon is (there is no turning point in r)

$$\tau_r = \int_{r_a}^{r_e} \frac{dr}{\sqrt{R}} = \left(\int_{r_1}^{r_e} - \int_{r_1}^{r_a} \right) \frac{dr}{\sqrt{R}} = \tau_e - \tau_a. \quad (\text{A34})$$

Obviously, if $\tau_\mu \geq \tau_\infty - \tau_a$, then $r_e = \infty$, which is of course not a solution for a photon returning to the disk. So, the solution for r_e exists only if $\tau_\mu < \tau_\infty - \tau_a$, which is given by the solution to $\tau_\mu = \tau_e - \tau_a$. The solution is

$$r_e = \frac{r_1(r_2 - r_4) - r_2(r_1 - r_4) \operatorname{sn}^2(\xi_{4a}|m_4)}{(r_2 - r_4) - (r_1 - r_4) \operatorname{sn}^2(\xi_{4a}|m_4)}, \quad (\text{A35})$$

where

$$\xi_{4a} \equiv \frac{1}{2}(\tau_\mu + \tau_a) \sqrt{(r_1 - r_3)(r_2 - r_4)}. \quad (\text{A36})$$

When $k_r > 0$ at $r = r_a$, i.e. the photon approaches r_a from the side of $r < r_a$, the integral over r along the path of the photon is

$$\tau_r = \begin{cases} \int_{r_e}^{r_a} \frac{dr}{\sqrt{R}} = \left(\int_{r_1}^{r_a} - \int_{r_1}^{r_e} \right) \frac{dr}{\sqrt{R}} = \tau_a - \tau_e, & (\tau_\mu \leq \tau_a) \\ \left(\int_{r_1}^{r_a} + \int_{r_1}^{r_e} \right) \frac{dr}{\sqrt{R}} = \tau_a + \tau_e, & (\tau_a < \tau_\mu < \tau_a + \tau_\infty) \end{cases}. \quad (\text{A37})$$

When $\tau_\mu \leq \tau_a$, there is no turning point in r ; when $\tau_a < \tau_\mu < \tau_\infty$, there is a turning point at $r = r_1$; and when $\tau_\mu \geq \tau_a + \tau_\infty$, a solution for r_e does not exist. Setting $\tau_r = \tau_\mu$, we can solve for r_e . The solution is given by equation (A35) with ξ_{4a} replaced by

$$\xi_{4a} \equiv \frac{1}{2}(\tau_\mu - \tau_a) \sqrt{(r_1 - r_3)(r_2 - r_4)}. \quad (\text{A38})$$

Since $\operatorname{sn}^2(-\xi_{4a}|m_4) = \operatorname{sn}^2(\xi_{4a}|m_4)$, the above solution applies if $\tau_\mu < \tau_a + \tau_\infty$, no matter whether there is a turning point in r or not.

Of course, when $r_H \geq r_1$, there cannot be a turning point in r along the path of the photon. Then, when $k_r > 0$, the solution is given by equations (A35) and (A38) if and only if $\tau_\mu < \tau_a$.⁵

Now let us consider the case $r_1 = r_2$. In region I the fundamental integral over r is given by equation (A11). Since the integration from $r = r_1$ to any $r > r_1$ is infinite, there cannot be a turning point along the path of the photon. Let us define

$$\hat{\tau}_\infty \equiv \frac{1}{\sqrt{(r_1 - r_3)(r_1 - r_4)}} \ln \left[1 + \frac{2r_1}{\sqrt{(r_1 - r_3)(r_1 - r_4)}} \right], \quad (\text{A39})$$

$$\hat{\tau}_a \equiv \frac{1}{\sqrt{(r_1 - r_3)(r_1 - r_4)}} \ln \left[\frac{\sqrt{(r_a - r_3)(r_a - r_4)}}{r_a - r_1} + \frac{r_1^2 + r_3 r_4 + 2r_1 r_a}{(r_a - r_1)\sqrt{(r_1 - r_3)(r_1 - r_4)}} \right], \quad (\text{A40})$$

$$\hat{\tau}_e \equiv \frac{1}{\sqrt{(r_1 - r_3)(r_1 - r_4)}} \ln \left[\frac{\sqrt{(r_e - r_3)(r_e - r_4)}}{r_e - r_1} + \frac{r_1^2 + r_3 r_4 + 2r_1 r_e}{(r_e - r_1)\sqrt{(r_1 - r_3)(r_1 - r_4)}} \right]. \quad (\text{A41})$$

We have

$$\int_{r_a}^{\infty} \frac{dr}{\sqrt{R}} = \hat{\tau}_a - \hat{\tau}_\infty. \quad (\text{A42})$$

Then, when $k_r < 0$ at $r = r_a$, the integration over r along the path of the photon is

$$\tau_r = \int_{r_a}^{r_e} \frac{dr}{\sqrt{R}} = \hat{\tau}_a - \hat{\tau}_e. \quad (\text{A43})$$

The solution for r_e is determined by $\tau_r = \tau_\mu$. Obviously, if $\tau_\mu \geq \hat{\tau}_a - \hat{\tau}_\infty$, the solution for r_e does not exist. So, if $\tau_\mu < \hat{\tau}_a - \hat{\tau}_\infty$, we have the solution for r_e

$$r_e = \frac{r_3 r_4 - \left[\gamma_a r_1 + (r_1^2 + r_3 r_4) / \sqrt{(r_1 - r_3)(r_1 - r_4)} \right]^2}{r_1 \left\{ 1 - \left[\gamma_a - 2r_1 / \sqrt{(r_1 - r_3)(r_1 - r_4)} \right]^2 \right\}}, \quad (\text{A44})$$

⁵A more strict condition should be $\tau_\mu < \tau_H$, where $\tau_H = \int_{r_1}^{r_H} \frac{dr}{\sqrt{R}}$ is given by the right hand side of eq. (A33) with r_a replaced by r_H . This condition ensures that $r_e > r_H$. However, since in the final stage of our computation we select only the solutions satisfying $r_{\text{in}} \leq r \leq r_{\text{out}}$, $\tau_\mu < \tau_a$ and $\tau_\mu < \tau_H$ lead to the same final results. (Note, $r_{\text{in}} \geq r_H$ always.)

where

$$\gamma_a \equiv \exp \left[(\hat{\tau}_a - \tau_\mu) \sqrt{(r_1 - r_3)(r_1 - r_4)} \right]. \quad (\text{A45})$$

When $k_r > 0$ at $r = r_a$, the integration over r along the path of the photon is

$$\tau_r = \int_{r_e}^{r_a} \frac{dr}{\sqrt{R}} = \hat{\tau}_e - \hat{\tau}_a. \quad (\text{A46})$$

The solution for r_e is determined by $\tau_r = \tau_\mu$. Since $\int_{r_1}^{r_a} \frac{dr}{\sqrt{R}} = \infty$, the solution for r_e always exists. It is given by equation (A44) with γ_a replaced by

$$\gamma_a \equiv \exp \left[(\hat{\tau}_a + \tau_\mu) \sqrt{(r_1 - r_3)(r_1 - r_4)} \right]. \quad (\text{A47})$$

As in Appendix A.1, the value of r_e obtained above for the case of $r_1 = r_2$ should be substituted back in the original equation $\tau_r = \tau_\mu$ to check if r_e is a true solution.

Case A2: $R = 0$ has four real roots, region II ($r_3 \leq r \leq r_2$) If $r_1 \neq r_2$, the fundamental integral over r is given by equation (A12). Let us define the following integrals

$$\tau_{e2} \equiv \int_{r_e}^{r_2} \frac{dr}{\sqrt{R}} = \frac{2}{\sqrt{(r_1 - r_3)(r_2 - r_4)}} \operatorname{sn}^{-1} \left[\sqrt{\frac{(r_1 - r_3)(r_2 - r_e)}{(r_2 - r_3)(r_1 - r_e)}} \middle| m_4 \right], \quad (\text{A48})$$

$$\tau_{a2} \equiv \int_{r_a}^{r_2} \frac{dr}{\sqrt{R}} = \frac{2}{\sqrt{(r_1 - r_3)(r_2 - r_4)}} \operatorname{sn}^{-1} \left[\sqrt{\frac{(r_1 - r_3)(r_2 - r_a)}{(r_2 - r_3)(r_1 - r_a)}} \middle| m_4 \right], \quad (\text{A49})$$

$$\tau_{32} \equiv \int_{r_3}^{r_2} \frac{dr}{\sqrt{R}} = \frac{2}{\sqrt{(r_1 - r_3)(r_2 - r_4)}} K(m_4), \quad (\text{A50})$$

and

$$\tau_{3a} \equiv \int_{r_3}^{r_a} \frac{dr}{\sqrt{R}} = \left(\int_{r_3}^{r_2} - \int_{r_a}^{r_2} \right) \frac{dr}{\sqrt{R}} = \tau_{32} - \tau_{a2}. \quad (\text{A51})$$

When $r_H \geq r_3$, there cannot be a turning point at $r = r_3$. However, there may be a turning point at $r = r_2$, since r_a must be between r_H and r_2 . Then, when $k_r < 0$ at $r = r_a$, the integral over r is

$$\tau_r = \begin{cases} \int_{r_a}^{r_e} \frac{dr}{\sqrt{R}} = \left(\int_{r_a}^{r_2} - \int_{r_e}^{r_2} \right) \frac{dr}{\sqrt{R}} = \tau_{a2} - \tau_{e2}, & (\tau_\mu \leq \tau_{a2}) \\ \left(\int_{r_a}^{r_2} + \int_{r_e}^{r_2} \right) \frac{dr}{\sqrt{R}} = \tau_{a2} + \tau_{e2}, & (\tau_{a2} < \tau_\mu < \tau_{a2} + \tau_{32}) \end{cases}. \quad (\text{A52})$$

When $\tau_\mu \leq \tau_{a2}$, there is no turning point in r ; when $\tau_{a2} < \tau_\mu < \tau_{a2} + \tau_{32}$, there is a turning point at $r = r_2$; and when $\tau_\mu \geq \tau_{a2} + \tau_{32}$, a solution for r_e (satisfying $r_e > r_H$) does not exist since it would have a turning point at $r = r_3$ which is impossible. Setting $\tau_r = \tau_\mu$, we can then solve for r_e . The solution is

$$r_e = \frac{r_2(r_1 - r_3) - r_1(r_2 - r_3) \operatorname{sn}^2(\xi_{4b}|m_4)}{(r_1 - r_3) - (r_2 - r_3) \operatorname{sn}^2(\xi_{4b}|m_4)}, \quad (\text{A53})$$

where

$$\xi_{4b} = \frac{1}{2}(\tau_\mu - \tau_{a2})\sqrt{(r_1 - r_3)(r_2 - r_4)}. \quad (\text{A54})$$

Since $\operatorname{sn}^2(-\xi_{4b}|m_4) = \operatorname{sn}^2(\xi_{4b}|m_4)$, the above solution applies if $\tau_\mu < \tau_{a2} + \tau_{32}$, no matter whether there is a turning point at $r = r_2$ or not.

When $r_H \geq r_3$ and $k_r > 0$ at $r = r_a$, there cannot be a turning point in r along the path of the photon. Then, the integral over r is

$$\tau_r = \int_{r_e}^{r_a} \frac{dr}{\sqrt{R}} = \left(\int_{r_e}^{r_2} - \int_{r_a}^{r_2} \right) \frac{dr}{\sqrt{R}} = \tau_{e2} - \tau_{a2}. \quad (\text{A55})$$

Setting $\tau_r = \tau_\mu$, we then get the solution for r_e . The solution exists only if $\tau_\mu \leq \tau_{3a}$, and is given by equation (A53) with ξ_{4b} replaced by

$$\xi_{4b} = \frac{1}{2}(\tau_\mu + \tau_{a2})\sqrt{(r_1 - r_3)(r_2 - r_4)}. \quad (\text{A56})$$

When $r_H < r_3$, the horizon of the black hole does not affect the motion of the photon, and the photon moves in a region bounded by r_2 and r_3 . So, the photon can have many turning points at $r = r_2$ and $r = r_3$. To properly account for this fact, we define the following two numbers

$$n \equiv \operatorname{int} \left(\frac{\tau_\mu}{2\tau_{32}} \right), \quad \tau'_\mu \equiv \tau_\mu - 2n\tau_{32}, \quad (\text{A57})$$

where $2\tau_{32}$ is a whole period of the integration over r , and $\operatorname{int}(x)$ means the integer part of a real number x . Obviously, we must have $0 \leq \tau'_\mu < 2\tau_{32}$.

Then, when $r_H < r_3$ and $k_r < 0$ at $r = r_a$, the integration over r is $\tau_r = 2n\tau_{32} + \tau'_r$, where

$$\tau'_r = \begin{cases} \left(\int_{r_a}^{r_2} - \int_{r_e}^{r_2} \right) \frac{dr}{\sqrt{R}} = \tau_{a2} - \tau_{e2}, & (\tau'_\mu \leq \tau_{a2}) \\ \left(\int_{r_a}^{r_2} + \int_{r_e}^{r_2} \right) \frac{dr}{\sqrt{R}} = \tau_{a2} + \tau_{e2}, & (\tau_{a2} < \tau'_\mu \leq \tau_{a2} + \tau_{32}) \\ \left(\int_{r_a}^{r_2} + \int_{r_3}^{r_2} + \int_{r_3}^{r_e} \right) \frac{dr}{\sqrt{R}} = \tau_{a2} + 2\tau_{32} - \tau_{e2}, & (\tau'_\mu > \tau_{a2} + \tau_{32}) \end{cases}. \quad (\text{A58})$$

When $\tau'_\mu \leq \tau_{a2}$, there are n turning points at $r = r_2$ and n turning points at $r = r_3$. When $\tau_{a2} < \tau'_\mu \leq \tau_{a2} + \tau_{32}$, there are $n + 1$ turning points at $r = r_2$ and n turning points at $r = r_3$. When $\tau'_\mu > \tau_{a2} + \tau_{32}$, there are $n + 1$ turning points at $r = r_2$ and $n + 1$ turning points at $r = r_3$. Setting $\tau_r = \tau_\mu$, we then obtain the solution for r_e . It is given by equation (A53) with ξ_{4b} replaced by

$$\xi_b = \begin{cases} \frac{1}{2}(\tau'_\mu - \tau_{a2})\sqrt{(r_1 - r_3)(r_2 - r_4)}, & (\tau'_\mu \leq \tau_{a2} + \tau_{32}) \\ \frac{1}{2}(\tau_{a2} + 2\tau_{32} - \tau'_\mu)\sqrt{(r_1 - r_3)(r_2 - r_4)}, & (\tau'_\mu > \tau_{a2} + \tau_{32}) \end{cases}. \quad (\text{A59})$$

When $r_H \geq r_3$ and $k_r > 0$ at $r = r_a$, the integration over r is $\tau_r = 2n\tau_{32} + \tau'_r$, where

$$\tau'_r = \begin{cases} \left(\int_{r_e}^{r_2} - \int_{r_a}^{r_2} \right) \frac{dr}{\sqrt{R}} = \tau_{e2} - \tau_{a2}, & (\tau'_\mu \leq \tau_{3a}) \\ \left(\int_{r_3}^{r_a} + \int_{r_3}^{r_e} \right) \frac{dr}{\sqrt{R}} = \tau_{3a} + \tau_{32} - \tau_{e2}, & (\tau_{3a} < \tau'_\mu \leq \tau_{3a} + \tau_{32}) \\ \left(\int_{r_3}^{r_a} + \int_{r_3}^{r_2} + \int_{r_e}^{r_2} \right) \frac{dr}{\sqrt{R}} = \tau_{3a} + \tau_{32} + \tau_{e2}, & (\tau'_\mu > \tau_{3a} + \tau_{32}) \end{cases}. \quad (\text{A60})$$

When $\tau'_\mu \leq \tau_{3a}$, there are n turning points at $r = r_2$ and n turning points at $r = r_3$. When $\tau_{3a} < \tau'_\mu \leq \tau_{3a} + \tau_{32}$, there are n turning points at $r = r_2$ and $n + 1$ turning points at $r = r_3$. When $\tau'_\mu > \tau_{3a} + \tau_{32}$, there are $n + 1$ turning points at $r = r_2$ and $n + 1$ turning points at $r = r_3$. Setting $\tau_r = \tau_\mu$, we then obtain the solution for r_e . It is given by equation (A53) with ξ_{4b} replaced by

$$\xi_b = \begin{cases} \frac{1}{2}(\tau'_\mu + \tau_{a2})\sqrt{(r_1 - r_3)(r_2 - r_4)}, & (\tau'_\mu \leq \tau_{3a}) \\ \frac{1}{2}(\tau_{3a} + \tau_{32} - \tau'_\mu)\sqrt{(r_1 - r_3)(r_2 - r_4)}, & (\tau'_\mu > \tau_{3a}) \end{cases}. \quad (\text{A61})$$

Now let us consider the case of $r_1 = r_2$. When $r_1 = r_2$, in region II the fundamental integral over r is given by equation (A13). Since the integration from $r = r_1$ to $r_a < r_1 = r_2$ is infinite, there cannot be a turning point at $r = r_2$. However, there can be a turning point at $r = r_3$. Let us define

$$\hat{\tau}_3 \equiv \frac{1}{\sqrt{(r_1 - r_3)(r_1 - r_4)}} \ln \left[\frac{r_1 + r_3}{\sqrt{(r_1 - r_3)(r_1 - r_4)}} \right], \quad (\text{A62})$$

$$\hat{\tau}_a \equiv \frac{1}{\sqrt{(r_1 - r_3)(r_1 - r_4)}} \ln \left[\frac{\sqrt{(r_a - r_3)(r_a - r_4)}}{r_1 - r_a} + \frac{r_1^2 + r_3 r_4 + 2r_1 r_a}{(r_1 - r_a)\sqrt{(r_1 - r_3)(r_1 - r_4)}} \right], \quad (\text{A63})$$

$$\hat{\tau}_e \equiv \frac{1}{\sqrt{(r_1 - r_3)(r_1 - r_4)}} \ln \left[\frac{\sqrt{(r_e - r_3)(r_e - r_4)}}{r_1 - r_e} \right]$$

$$+ \frac{r_1^2 + r_3 r_4 + 2r_1 r_e}{(r_1 - r_e) \sqrt{(r_1 - r_3)(r_1 - r_4)}} \Big]. \quad (\text{A64})$$

We have

$$\int_{r_3}^{r_a} \frac{dr}{\sqrt{R}} = \hat{\tau}_a - \hat{\tau}_3. \quad (\text{A65})$$

Then, when $k_r < 0$ at $r = r_a$, the integration over r along the path of the photon is (there is no turning point)

$$\tau_r = \int_{r_a}^{r_e} \frac{dr}{\sqrt{R}} = \hat{\tau}_e - \hat{\tau}_a. \quad (\text{A66})$$

The solution for r_e is determined by $\tau_r = \tau_\mu$. Since $\int_{r_a}^{r_1} \frac{dr}{\sqrt{R}} = \infty$, the solution for r_e always exists. It is given equation (A44) with γ_a replaced by

$$\gamma_a \equiv - \exp \left[(\hat{\tau}_a + \tau_\mu) \sqrt{(r_1 - r_3)(r_1 - r_4)} \right]. \quad (\text{A67})$$

When $k_r > 0$ at $r = r_a$, the integration over r along the path of the photon is

$$\tau_r = \begin{cases} \int_{r_e}^{r_a} \frac{dr}{\sqrt{R}} = \hat{\tau}_a - \hat{\tau}_e, & (\tau_\mu \leq \hat{\tau}_a - \hat{\tau}_3) \\ \left(\int_{r_3}^{r_a} + \int_{r_3}^{r_e} \right) \frac{dr}{\sqrt{R}} = \hat{\tau}_a + \hat{\tau}_e - 2\hat{\tau}_3, & (\tau_\mu > \hat{\tau}_a - \hat{\tau}_3) \end{cases}. \quad (\text{A68})$$

When $\tau_\mu \leq \hat{\tau}_a - \hat{\tau}_3$, there is no turning point in r ; and when $\tau_\mu > \hat{\tau}_a - \hat{\tau}_3$, there is a turning point at $r = r_3$. Since $\int_{r_3}^{r_1} \frac{dr}{\sqrt{R}} = \infty$, the solution for r_e always exists. It is given by equation (A44) with γ_a replaced by

$$\gamma_a \equiv \begin{cases} - \exp \left[(\hat{\tau}_a - \tau_\mu) \sqrt{(r_1 - r_3)(r_1 - r_4)} \right], & (\tau_\mu \leq \hat{\tau}_a - \hat{\tau}_3) \\ - \exp \left[(\tau_\mu - \hat{\tau}_a + 2\hat{\tau}_3) \sqrt{(r_1 - r_3)(r_1 - r_4)} \right], & (\tau_\mu > \hat{\tau}_a - \hat{\tau}_3) \end{cases}. \quad (\text{A69})$$

Of course, when $r_H > r_3$, there cannot be a turning point. Then, when $k_r > 0$ at $r = r_a$, the solution is given by equation (A44) and the first line of equation (A69) (i.e., for the case $\tau_\mu \leq \hat{\tau}_a - \hat{\tau}_3$ only).

As in Appendix A.1, the value of r_e obtained above for the case of $r_1 = r_2$ should be substituted back in the original equation $\tau_r = \tau_\mu$ to check if r_e is a true solution.

Case 2: $R = 0$ has two complex roots and two real roots, region $r \geq r_3$ The fundamental integral over r is given by equation (A14). Let us define

$$\tau_a \equiv \frac{1}{\sqrt{AB}} \text{cn}^{-1} \left[\frac{(A - B)r_a + r_3 B - r_4 A}{(A + B)r_a - r_3 B - r_4 A} \middle| m_2 \right]. \quad (\text{A70})$$

Other relevant integrations are τ_∞ and τ_e , defined by equations (A28) and (A29) respectively.

When $k_r < 0$ at $r = r_a$, the integral over r along the path of the photon is (there is no turning point)

$$\tau_r = \int_{r_a}^{r_e} \frac{dr}{\sqrt{R}} = \left(\int_{r_3}^{r_e} - \int_{r_3}^{r_a} \right) \frac{dr}{\sqrt{R}} = \tau_e - \tau_a. \quad (\text{A71})$$

Obviously, the solution for r_e exists only if $\tau_\mu < \tau_\infty - \tau_a$. Then, setting $\tau_r = \tau_\mu$, we get the solution for r_e

$$r_e = \frac{r_4 A - r_3 B - (r_4 A + r_3 B) \text{cn}(\xi_{2a}|m_2)}{(A - B) - (A + B) \text{cn}(\xi_{2a}|m_2)}, \quad (\text{A72})$$

where

$$\xi_{2a} \equiv (\tau_\mu + \tau_a) \sqrt{AB}. \quad (\text{A73})$$

When $k_r > 0$ at $r = r_a$, the integral over r along the path of the photon is

$$\tau_r = \begin{cases} \left(\int_{r_3}^{r_a} - \int_{r_3}^{r_e} \right) \frac{dr}{\sqrt{R}} = \tau_a - \tau_e, & (\tau_\mu \leq \tau_a) \\ \left(\int_{r_3}^{r_a} + \int_{r_3}^{r_e} \right) \frac{dr}{\sqrt{R}} = \tau_a + \tau_e, & (\tau_a < \tau_\mu < \tau_a + \tau_\infty) \end{cases}. \quad (\text{A74})$$

When $\tau_\mu \leq \tau_a$, there is no turning point in r ; when $\tau_a < \tau_\mu < \tau_\infty$, there is a turning point at $r = r_3$; and when $\tau_\mu \geq \tau_a + \tau_\infty$, a solution for r_e does not exist. Setting $\tau_r = \tau_\mu$, we get the solution for r_e . The solution is given by equation (A72) with ξ_{2a} replaced by

$$\xi_{2a} \equiv (\tau_\mu - \tau_a) \sqrt{AB}. \quad (\text{A75})$$

When $r_H < r_3$, the above solution applies if $\tau_\mu < \tau_a + \tau_\infty$, no matter whether there is a turning point in r or not. When $r_H \geq r_3$, there cannot be a turning point at $r = r_3$, then the above solution applies only if $\tau_\mu < \tau_a$.

A.3. Conditions for photons to be captured by the black hole

To derive the conditions for a photon emitted by the disk to be captured by the black hole, we make the following simplified assumption: Any radiation that returns to the equatorial plane inside the inner boundary of the disk is captured by the black hole. This radiation, if it is not swallowed by the black hole directly, will be advected or scattered inward by the infalling gas, which has a large inward radial velocity (Agol & Krolik 2000).

Following Thorne (1974), we define a photon capture function C as follow: $C = 1$ if a photon emitted at r_e in the disk is eventually captured by the black hole; $C = 0$ if the photon eventually escapes to infinity or returns to the disk. The task in this subsection is to find out under what conditions we have $C = 1$.

Obviously, a sufficient and necessary condition for $C = 1$ is that the photon neither escapes to infinity nor returns to the disk at a radius beyond the inner boundary. In the following we translate this condition to mathematical expressions for each case discussed in Appendix A.2. These results are obtained by carefully following the analysis in Appendix A.2. However, for our purpose in this subsection, we follow the orbit of a photon by starting from the radius r_e where the photon is emitted, rather than the radius at the end of the orbit as we did in Appendix A.2 when discussing the photons returning to the disk. Then, $k_r > 0$ at $r = r_e$ means that the photon moves to the side $r > r_e$, and $k_r < 0$ at $r = r_e$ means that the photon moves to the side $r < r_e$. Since the photon must be emitted by the disk, we must have $r_{\text{in}} \leq r_e \leq r_{\text{out}}$.

In the analysis presented below, in each case (Case A1, Case A2, and Case B) the symbols have the same meanings as those in the corresponding case in Appendix A.2.

Case A1: $R = 0$ has four real roots, region I ($r \geq r_1$) When $r_1 \neq r_2$ and $r_{\text{in}} > r_1$, let us define

$$\tau_{\text{in}} \equiv \int_{r_1}^{r_{\text{in}}} \frac{dr}{\sqrt{R}} = \frac{2}{\sqrt{(r_1 - r_3)(r_2 - r_4)}} \text{sn}^{-1} \left[\sqrt{\frac{(r_2 - r_4)(r_{\text{in}} - r_1)}{(r_1 - r_4)(r_{\text{in}} - r_2)}} \middle| m_4 \right]. \quad (\text{A76})$$

Then, $C = 1$ if and only if one of the following conditions is satisfied:

Condition 1: ($r_1 \leq r_{\text{H}} < r_{\text{in}}$) & ($k_r < 0$ at $r = r_e$) & ($\tau_{\mu} > \tau_e - \tau_{\text{in}}$);

Condition 2: ($r_{\text{H}} < r_1 < r_{\text{in}}$) & ($k_r < 0$ at $r = r_e$) & ($\tau_e - \tau_{\text{in}} < \tau_{\mu} < \tau_e + \tau_{\text{in}}$).

When $r_1 = r_2$ and $r_{\text{in}} > r_1$, we define

$$\hat{\tau}_{\text{in}} \equiv \frac{1}{\sqrt{(r_1 - r_3)(r_1 - r_4)}} \ln \left[\frac{\sqrt{(r_{\text{in}} - r_3)(r_{\text{in}} - r_4)}}{r_{\text{in}} - r_1} + \frac{r_1^2 + r_3 r_4 + 2r_1 r_{\text{in}}}{(r_{\text{in}} - r_1) \sqrt{(r_1 - r_3)(r_1 - r_4)}} \right]. \quad (\text{A77})$$

Then, $C = 1$ if and only if the following condition is satisfied:

Condition 3: ($r_{\text{in}} > r_1$) & ($k_r < 0$ at $r = r_e$) & ($\tau_{\mu} > \hat{\tau}_{\text{in}} - \hat{\tau}_e$).

Case A2: $R = 0$ has four real roots, region II ($r_3 \leq r \leq r_2$) When $r_1 \neq r_2$ and $r_{\text{in}} > r_3$, let us define

$$\tau_{\text{in}} = \int_{r_{\text{in}}}^{r_2} \frac{dr}{\sqrt{R}} = \frac{2}{\sqrt{(r_1 - r_3)(r_2 - r_4)}} \text{sn}^{-1} \left[\sqrt{\frac{(r_1 - r_3)(r_2 - r_{\text{in}})}{(r_2 - r_3)(r_1 - r_{\text{in}})}} \middle| m_4 \right]. \quad (\text{A78})$$

Then, $C = 1$ if and only if one of the following conditions is satisfied:

Condition 4: ($r_3 \leq r_{\text{H}} < r_{\text{in}}$) & ($k_r > 0$ at $r = r_e$) & ($\tau_\mu > \tau_{e2} + \tau_{\text{in}}$);

Condition 5: ($r_3 \leq r_{\text{H}} < r_{\text{in}}$) & ($k_r < 0$ at $r = r_e$) & ($\tau_\mu > \tau_{\text{in}} - \tau_{e2}$);

Condition 6: ($r_{\text{H}} < r_3 < r_{\text{in}}$) & ($k_r > 0$ at $r = r_e$) & ($\tau_{e2} + \tau_{\text{in}} < \tau'_\mu < \tau_{e2} + 2\tau_{32} - \tau_{\text{in}}$);

Condition 7: ($r_{\text{H}} < r_3 < r_{\text{in}}$) & ($k_r < 0$ at $r = r_e$) & ($\tau_{\text{in}} - \tau_{e2} < \tau'_\mu < 2\tau_{32} - \tau_{\text{in}} - \tau_{e2}$).

When $r_1 = r_2$ and $r_{\text{in}} > r_3$, we define

$$\hat{\tau}_{\text{in}} \equiv \frac{1}{\sqrt{(r_1 - r_3)(r_1 - r_4)}} \ln \left[\frac{\sqrt{(r_{\text{in}} - r_3)(r_{\text{in}} - r_4)}}{r_1 - r_{\text{in}}} + \frac{r_1^2 + r_3 r_4 + 2r_1 r_{\text{in}}}{(r_1 - r_{\text{in}})\sqrt{(r_1 - r_3)(r_1 - r_4)}} \right]. \quad (\text{A79})$$

Then, $C = 1$ if and only if one of the following conditions is satisfied:

Condition 8: ($r_3 \leq r_{\text{H}} < r_{\text{in}}$) & ($k_r < 0$ at $r = r_e$) & ($\tau_\mu > \hat{\tau}_e - \hat{\tau}_{\text{in}}$);

Condition 9: ($r_{\text{H}} < r_3 < r_{\text{in}}$) & ($k_r < 0$ at $r = r_e$) & ($\hat{\tau}_e - \hat{\tau}_{\text{in}} < \tau_\mu < \hat{\tau}_e + \hat{\tau}_{\text{in}} - 2\hat{\tau}_3$).

Case 2: $R = 0$ has two complex roots and two real roots, region $r \geq r_3$ When $r_{\text{in}} > r_3$, let us define

$$\tau_{\text{in}} \equiv \frac{1}{\sqrt{AB}} \text{cn}^{-1} \left[\frac{(A - B)r_{\text{in}} + r_3 B - r_4 A}{(A + B)r_{\text{in}} - r_3 B - r_4 A} \middle| m_2 \right]. \quad (\text{A80})$$

Then, $C = 1$ if and only if one of the following conditions is satisfied:

Condition 10: ($r_3 \leq r_{\text{H}} < r_{\text{in}}$) & ($k_r < 0$ at $r = r_e$) & ($\tau_\mu > \tau_e - \tau_{\text{in}}$);

Condition 11: ($r_{\text{H}} < r_3 \leq r_{\text{in}}$) & ($k_r < 0$ at $r = r_e$) & ($\tau_e - \tau_{\text{in}} < \tau_\mu < \tau_e + \tau_{\text{in}}$).

B. Integration of Photon Orbits in a Kerr Spacetime II: The $E_\infty \approx 0$ Case

A Kerr black hole has an ergosphere inside which the energy of particles and photons can be negative (Misner et al. 1973). The radius of the ergosphere is equal to $2M$ on the equatorial plane. When the black hole rotates fast enough, the inner boundary of the disk may enter the ergosphere, i.e., $r_{\text{in}} < 2M$. For instance, when $r_{\text{in}} = r_{\text{ms}}$, the inner boundary of the disk enters the ergosphere of the black hole when $a > 0.9428M$. When this happens, for some photons emitted by the inner part of the disk, E_∞ —the energy measured at infinity—might be close to zero. This needs special treatment since when $E_\infty = 0$ the approach described in Appendix A does not apply. Even when E_∞ is nonzero but the ratio $|E_\infty|/E_{l0} \ll 1$, where E_{l0} is the energy of the photon measured by a local observer at rest with respect to the gas at radius r_0 on the disk, the numerical approach based on the procedure in Appendix A cannot give solutions with sufficient precision since then $|\lambda|/r_0$ and Q/r_0^2 are large numbers. The task of this Appendix is to develop special relations for the case of $E_\infty \approx 0$.

Let us define

$$\varepsilon \equiv \frac{E_\infty}{E_{l0}}, \quad |\varepsilon| \ll 1, \quad (\text{B1})$$

and neglect all terms of order ε^2 and higher in our calculations. Then we have

$$R'(r) \equiv R(r) \frac{E_\infty^2}{\mathcal{Q} + L_z^2} = -r^2 + 2M \left(1 - \frac{2a\lambda'\varepsilon}{Q' + \lambda'^2} \right) r - \frac{a^2 Q'}{Q' + \lambda'^2}, \quad (\text{B2})$$

$$\Theta'_\mu(\mu) \equiv \Theta_\mu(\mu) \frac{E_\infty^2}{\mathcal{Q} + L_z^2} = \frac{Q'}{Q' + \lambda'^2} - \mu^2, \quad (\text{B3})$$

where $\lambda' \equiv L_z/E_{l0}$, $Q' \equiv \mathcal{Q}/E_{l0}^2$, which are geometric quantities that do not depend on the energy of photons. The motion of the photon in the $r - \vartheta$ plane is then described by

$$\int_{r_e}^r \frac{dr}{\sqrt{R'(r)}} = \pm \int_{\mu_e}^\mu \frac{d\mu}{\sqrt{\Theta'_\mu(\mu)}}. \quad (\text{B4})$$

The integral over μ can be worked out by the following indefinite integration

$$\int \frac{d\mu}{\sqrt{\Theta'_\mu(\mu)}} = \arctan \left(\frac{\mu}{\sqrt{\mu_m^2 - \mu^2}} \right), \quad \mu_m \equiv \sqrt{\frac{Q'}{Q' + \lambda'^2}}. \quad (\text{B5})$$

The two roots of $R'(r) = 0$ are $r'_1 = r_1(1 + \delta)$ and $r'_2 = r_2(1 - \delta)$, where

$$r_{1,2} \equiv M \pm \sqrt{M^2 - \frac{a^2 Q'}{Q' + \lambda'^2}}, \quad \delta \equiv \frac{-2Ma\lambda'\varepsilon}{\sqrt{(Q' + \lambda'^2) [M^2 (Q' + \lambda'^2) - a^2 Q']}}. \quad (\text{B6})$$

The physically allowed region is given by $R' \geq 0$, i.e. $r_- \leq r \leq r_+$, where $r_+ = \max(r'_1, r'_2)$, $r_- = \min(r'_1, r'_2)$. Thus, the integral over r can be worked out by

$$\int \frac{dr}{\sqrt{R'(r)}} = \int \frac{dr}{\sqrt{(r_+ - r)(r - r_-)}} = \arctan \left[\frac{2r - r'_1 - r'_2}{2\sqrt{(r'_1 - r)(r - r'_2)}} \right]. \quad (\text{B7})$$

Since the physically allowed region is bounded by r_+ and r_- , the photon must return to the disk or be captured by the black hole. It cannot escape to infinity.

First let us consider the case when the photon returns to the disk. Then, we must have $\mu = \cos(\pi/2) = 0$ as the photon approaches the disk at radius r_a . Since as it leaves the disk at radius r_e we also have $\mu = 0$, the photon must have encountered a turning point in ϑ during its trip. Thus, by equation (B5), along the photon orbit the total integral over μ is

$$\tau_\mu \equiv 2 \int_0^{\mu_m} \frac{d\mu}{\sqrt{\Theta'_\mu(\mu)}} = \pi. \quad (\text{B8})$$

The integral over r along the photon orbit depends on the sign of k_r at $r = r_a$ —i.e., it depends on the direction from which the photon approaches the disk at r_a . It can be shown that we always have $r_- < r_H$ for $a^2 < M^2$ and $Q' > 0$. Since a photon cannot get out of a black hole after it falls in, its orbit cannot have a turning point in r at $r = r_-$. However, it can have a turning point at $r = r_+$. Let us define the following integrals

$$\tau_{e+} \equiv \int_{r_e}^{r_+} \frac{dr}{\sqrt{R'}} = \frac{\pi}{2} - \arctan \left[\frac{2r_e - r'_1 - r'_2}{2\sqrt{(r'_1 - r_e)(r_e - r'_2)}} \right], \quad (\text{B9})$$

$$\tau_{a+} \equiv \int_{r_a}^{r_+} \frac{dr}{\sqrt{R'}} = \frac{\pi}{2} - \arctan \left[\frac{2r_a - r'_1 - r'_2}{2\sqrt{(r'_1 - r_a)(r_a - r'_2)}} \right], \quad (\text{B10})$$

$$\tau_{-+} \equiv \int_{r_-}^{r_+} \frac{dr}{\sqrt{R'}} = \pi. \quad (\text{B11})$$

Since $\tau_{-+} = \tau_\mu$ and $r_- < r_H < r_a < r_+$, for a photon emitted by the disk and returning to the disk, it must have $k_r < 0$ at $r = r_a$ (i.e., the photon must approach the disk at r_a from the side of $r > r_a$) and it must have encountered a turning point at $r = r_+$. Then, the total integral over r is

$$\tau_r = \left(\int_{r_a}^{r_+} + \int_{r_e}^{r_+} \right) \frac{dr}{\sqrt{R'}} = \tau_{a+} + \tau_{e+}. \quad (\text{B12})$$

Setting $\tau_r = \tau_\mu = \pi$, we can solve for r_e . The solution is given by

$$r_e + r_a = r'_1 + r'_2 = 2M \left(1 - \frac{2a\lambda'}{Q' + \lambda'^2} \varepsilon \right). \quad (\text{B13})$$

Of course, a physical solution must satisfy $r_e + r_a \geq 2r_{\text{in}}$. According to equation (B13), this condition corresponds to

$$-2a\lambda'\varepsilon \geq \left(\frac{r_{\text{in}}}{M} - 1\right) (Q' + \lambda'^2) . \quad (\text{B14})$$

Note that the solution in equation (B13) and the condition in equation (B14) do not depend on whether we choose $E_{l0} = E_{la}$ or $E_{l0} = E_{le}$.

From the above results it is easy to obtain the condition for the photon to be captured by the black hole, which is as follow: either $k_r < 0$ at $r = r_e$, or $k_r > 0$ at $r = r_e$ but the inequality (B14) is violated.

C. Calculation of the Constants of Motion

In the first part of this section we express the constants of motion of a photon (in particular, λ and Q) in terms of the direction of the velocity of the photon and the radius as the photon crosses the equatorial plane. In the second part, we express the constants of motion in terms of the impact parameters of the photon at infinity. The former is useful for calculating the orbits of the photons that return to the disk or are captured by the black hole, while the latter is useful for calculating the orbits of photons that escape to infinity. We will also calculate the redshift factor of the photon in each case.

1. Evaluation of the constants of motion in terms of quantities on the equatorial plane

We need to relate the local rest frame attached to the disk fluid to the locally nonrotating frame. The relation is given by the Lorentz transformation

$$e_t^a = \Gamma [e_{(t)}^a - v_\varphi e_{(\varphi)}^a] , \quad (\text{C1})$$

$$e_\varphi^a = \Gamma [-v_\varphi e_{(t)}^a + e_{(\varphi)}^a] , \quad (\text{C2})$$

$$e_r^a = e_{(r)}^a , \quad (\text{C3})$$

$$e_z^a = e_{(z)}^a , \quad (\text{C4})$$

where $\{e_t^a, e_r^a, e_\varphi^a, e_z^a\}$ are the locally nonrotating frame (see, e.g., Bardeen, Press, & Teukolsky 1972), $\{e_{(t)}^a, e_{(r)}^a, e_{(\varphi)}^a, e_{(z)}^a\}$ are the local rest frame of the disk [$e_{(t)}^a = u^a$ is the four-velocity of a disk particle], v_φ is the azimuthal velocity of a disk particle relative to the locally nonrotating frame, and $\Gamma = (1 - v_\varphi^2)^{-1/2}$ is the corresponding Lorentz factor.

In the coordinates (t, r, φ, z) , the locally nonrotating frame are defined by

$$e_t^a = \frac{1}{\chi} \left[\left(\frac{\partial}{\partial t} \right)^a + \omega \left(\frac{\partial}{\partial \varphi} \right)^a \right] , \quad (\text{C5})$$

$$e_\varphi^a = \left(\frac{r^2}{A}\right)^{1/2} \left(\frac{\partial}{\partial\varphi}\right)^a, \quad (\text{C6})$$

$$e_r^a = \left(\frac{\Delta}{r^2}\right)^{1/2} \left(\frac{\partial}{\partial r}\right)^a, \quad (\text{C7})$$

$$e_z^a = \left(\frac{\partial}{\partial z}\right)^a = -\frac{1}{r} \left(\frac{\partial}{\partial\vartheta}\right)^a, \quad (\text{C8})$$

where $\Delta = r^2 - 2Mr + a^2$, $A = r^4 + a^2r(r + 2M)$, $\chi = (r^2\Delta/A)^{1/2}$ (the lapse function in the equatorial plane), and $\omega = 2Mar/A$ (the frame dragging angular velocity in the equatorial plane).

The direction of the velocity of a photon as it crosses the disk plane is specified by the normalized four-wavevector of the photon, $n^a \equiv k^a/k^{(t)} = k^a/E_l$, where k^a is the four-wavevector of the photon, $E_l = k^{(t)} = -k_a e_{(t)}^a = -k_a u^a$ is the energy (frequency) of the photon measured in the local rest frame. The components of n^a in the local rest frame of the disk are

$$n^{(t)} = 1, \quad n^{(z)} = \cos\theta, \quad n^{(r)} = \sin\theta \cos\phi, \quad n^{(\phi)} = \sin\theta \sin\phi, \quad (\text{C9})$$

where (θ, ϕ) are spherical coordinates in the local rest frame, with the polar angle θ measured from the normal of the disk, and the azimuthal angle ϕ measured from $e_{(r)}^a$ along the disk radial direction.

By equations (C2) and (C9), we have

$$k_a e_\varphi^a = \Gamma [-v_\varphi k_a e_{(t)}^a + k_a e_{(\varphi)}^a] = \Gamma E_l (v_\varphi + \sin\theta \sin\phi). \quad (\text{C10})$$

By equation (C6) and $L_z = k_a (\partial/\partial\phi)^a$, we have

$$k_a e_\varphi^a = \left(\frac{r^2}{A}\right)^{1/2} k_a \left(\frac{\partial}{\partial\varphi}\right)^a = \left(\frac{r^2}{A}\right)^{1/2} L_z. \quad (\text{C11})$$

Equations (C10) and (C11) lead to

$$L_z = \left(\frac{A}{r^2}\right)^{1/2} \Gamma (v_\varphi + \sin\theta \sin\phi) E_l. \quad (\text{C12})$$

Similarly, equations (C1), (C5), (C9), and $E_\infty = -k_a (\partial/\partial t)^a$ lead to

$$\begin{aligned} E_\infty &= \Gamma \chi (1 + v_\varphi \sin\theta \sin\phi) E_l + \omega L_z \\ &= \Gamma \chi \left\{ 1 + \frac{\omega}{\chi} \left(\frac{A}{r^2}\right)^{1/2} v_\varphi + \left[v_\varphi + \frac{\omega}{\chi} \left(\frac{A}{r^2}\right)^{1/2} \right] \sin\theta \sin\phi \right\} E_l, \end{aligned} \quad (\text{C13})$$

where in the last step equation (C12) has been used.

Equations (C12) and (C13) can be simplified by introducing $L^\dagger = \Gamma(A/r^2)^{1/2}v_\varphi$, $E^\dagger = \Gamma\chi + \omega L^\dagger$, and $\Omega = \omega + \chi(r^2/A)^{1/2}v_\varphi$, which are respectively the specific angular momentum, the specific energy-at-infinity, and the angular velocity of disk particles. The results are

$$L_z = \left[L^\dagger + \left(\frac{A}{r^2} \right)^{1/2} \Gamma \sin \theta \sin \phi \right] E_l . \quad (\text{C14})$$

$$E_\infty = \left[E^\dagger + \left(\frac{A}{r^2} \right)^{1/2} \Gamma \Omega \sin \theta \sin \phi \right] E_l . \quad (\text{C15})$$

Note that, although E_l is always positive, E_∞ can be negative when the black hole rotates so fast that the radius where the photon is emitted is inside the ergosphere of the black hole (see Appendix B). Let ψ denote the angle between the photon wavevector and the direction of $e_{(\phi)}^a$ in the local rest frame. Then $\cos \psi = \sin \theta \sin \phi$, and equation (C15) implies that $E_\infty < 0$ if and only if $\psi_0 < \psi \leq \pi$, where

$$\psi_0 = \arccos \left(-\frac{rE^\dagger}{A^{1/2}\Gamma\Omega} \right) . \quad (\text{C16})$$

The solution for ψ_0 exists for $r < 2M$, i.e. inside the ergosphere of the black hole. At $r = 2M$ (the boundary of the ergosphere), we have $\psi_0 = \pi$ for a Keplerian disk.

Equations (C4), (C8), and (C9) lead to

$$\mathcal{Q} = \left[k_a \left(\frac{\partial}{\partial \vartheta} \right)^a \right]_{\vartheta=\pi/2}^2 = r^2 (k_a e_z^a)^2 = r^2 E_l^2 \cos^2 \theta , \quad (\text{C17})$$

where the first identity comes from the definition of \mathcal{Q} (Bardeen et al. 1972).

From equations (C14), (C15), and (C17) we have

$$\lambda = \frac{L_z}{E_\infty} = \frac{L^\dagger + (A/r^2)^{1/2}\Gamma \sin \theta \sin \phi}{E^\dagger + (A/r^2)^{1/2}\Gamma\Omega \sin \theta \sin \phi} , \quad (\text{C18})$$

$$Q = \frac{\mathcal{Q}}{E_\infty^2} = \frac{r^2 \cos^2 \theta}{[E^\dagger + (A/r^2)^{1/2}\Gamma\Omega \sin \theta \sin \phi]^2} . \quad (\text{C19})$$

These two equations relate λ and Q to the direction of the photon wavevector (θ, ϕ) , the radius (r) , as well as the quantities specifying the disk motion (L^\dagger , E^\dagger , Ω , and Γ —of course they are not independent) at the point where the orbit of the photon crosses the disk plane. For the formulae for calculating L^\dagger , E^\dagger , Ω ... in the case of a Keplerian disk, see Page &

Thorne (1974). The parameters λ and Q do not depend on the energy of the photon E_l , which is expected under the geometric optics approximation.

Equation (C18) can be rewritten as

$$\Omega\lambda = 1 - \frac{E^\dagger - \Omega L^\dagger}{E^\dagger + (A/r^2)^{1/2}\Gamma\Omega \sin\theta \sin\phi}, \quad (\text{C20})$$

which by equation (C15) leads to

$$\frac{E_\infty}{E_l} = \frac{E^\dagger - \Omega L^\dagger}{1 - \Omega\lambda}. \quad (\text{C21})$$

Equation (C21) is useful for calculating the redshift factor of a photon. For example, if a photon is emitted from the disk at $r = r_e$ and then absorbed by the disk at $r = r_a$, the ratio of locally measured energy (frequency) of the photon at r_e and r_a is simply

$$\frac{E_{la}}{E_{le}} = \frac{E_e^\dagger - \Omega_e L_e^\dagger}{E_a^\dagger - \Omega_a L_a^\dagger} \frac{1 - \Omega_a \lambda}{1 - \Omega_e \lambda}, \quad (\text{C22})$$

where label “ e ” means evaluation at $r = r_e$, and label “ a ” means evaluation at $r = r_a$. Equation (C22) implies that if a photon is emitted and returns to the disk at the same radius, then the locally measured energy of the photon does not change.

Given λ and Q , we can also calculate the value of $\cos\theta$. From equations (C19) and (C20), we have

$$\cos\theta = \pm \frac{\sqrt{Q}}{r} \frac{E^\dagger - \Omega L^\dagger}{|1 - \Omega\lambda|}, \quad (\text{C23})$$

where the sign of $\cos\theta$ should be chosen according to the problem at hand. If the photon is leaving the disk, then $0 \leq \theta < \pi/2$, and $\cos\theta$ is positive. If the photon is approaching the disk, then $\pi/2 < \theta \leq \pi$, and $\cos\theta$ is negative. Note, according to equation (C21), $1 - \Omega\lambda$ has the same sign as E_∞ since both E_l and $E^\dagger - \Omega L^\dagger$ are positive.⁶ Since E_∞ can be negative, $1 - \Omega\lambda$ can also be negative. This is the reason for the absolute value signs in equation (C23).

2. Evaluation of the constants of motion in terms of photon impact parameters at infinity The apparent position of the disk image as seen by an observer is conveniently represented by two impact parameters α and β , measured relative to the direction to the center of the black hole. The impact parameters α and β are, respectively, the displacement of the image perpendicular to the projection of the rotation axis of the black hole on the sky

⁶ $E^\dagger - \Omega L^\dagger = \chi/\Gamma$ for any particle whose velocity has only an azimuthal component.

and the displacement parallel to the projection of the axis. They are related to the conserved parameters λ and Q by (Cunningham & Bardeen 1973; Cunningham 1975)

$$\alpha = -\lambda \csc \vartheta_{\text{obs}} , \quad \beta = \pm (Q + a^2 \cos^2 \vartheta_{\text{obs}} - \lambda^2 \cot^2 \vartheta_{\text{obs}})^{1/2} , \quad (\text{C24})$$

where ϑ_{obs} is the polar angle of the observer with respect to the rotation axis of the black hole (i.e., the inclination angle). From equation (C24) we can solve for λ and Q . The solutions are

$$\lambda = -\alpha \sin \vartheta_{\text{obs}} , \quad Q = \beta^2 + (\alpha^2 - a^2) \cos^2 \vartheta_{\text{obs}} . \quad (\text{C25})$$

For ray-tracing, it is more convenient to use polar coordinates in the plane of the disk since disk particles are on circular orbits. Figure 13 shows the relation between the impact parameters in the observer’s sky (the plane S , the image plane) and the polar coordinates in the plane of the disk (the plane S'). For a point P on S , labeled by a pair of impact parameters (α, β) , there is a corresponding point P' on S' . P' is obtained from P by drawing a straight line from P parallel to the line of sight. The polar coordinates (r', φ') of P' are related to the impact parameters (α, β) by

$$\alpha = r' \cos \varphi' , \quad \beta = r' \sin \varphi' \cos \vartheta_{\text{obs}} . \quad (\text{C26})$$

Therefore, the image of a circular orbit in the disk plane is a circle in S' , but an ellipse in S .

From equations (C25) and (C26) we obtain

$$\lambda = -r' \cos \varphi' \sin \vartheta_{\text{obs}} , \quad Q = (r'^2 - a^2) \cos^2 \vartheta_{\text{obs}} . \quad (\text{C27})$$

These two equations relate the conserved quantities λ and Q to the polar coordinates on the S' plane which is gridded into many surface elements to make the ray-tracing computation.⁷ The element of solid angle seen by the observer is then

$$d\Omega_{\text{obs}} = \frac{d\alpha d\beta}{D^2} = \frac{\cos \vartheta_{\text{obs}} r' dr' d\varphi'}{D^2} , \quad (\text{C28})$$

where D is the distance from the observer to the black hole.

⁷The fictitious image plane is gridded as follow: Using the polar coordinates r' and φ' in S' , with the origin at the intersection of the line of sight with S' , we divide $\log r'$ uniformly from $\log r' = \log r_{\text{in}}$ to $\log r' = \log r_{\text{out}}$, and divide φ uniformly from $\varphi = 0$ to $\varphi = 2\pi$. Because of the light focusing effect of the black hole, the image of the inner boundary of the disk on S' has a somewhat larger radius than r_{in} . So, starting the computation from $r' = r_{\text{in}}$ does not miss points in the inner region of the disk. Since $r_{\text{out}} \gg r_{\text{g}}$, the image of the outer boundary of the disk on S' has a radius that is almost equal to r_{out} .

D. The Radiation Flux of the Disk and the Balance of Energy

The conservation of angular momentum in a geometrically thin accretion disk rotating around a Kerr black hole in the equatorial plane is described by (Novikov & Thorne 1973; Page & Thorne 1974)

$$\frac{d}{dr} \left(\dot{M} L^\dagger - g \right) = 4\pi r T_\varphi^z|_{z=H} . \quad (\text{D1})$$

Here, as usual, \dot{M} is the mass accretion rate, L^\dagger is the specific angular momentum of disk particles, g is the internal torque of the disk which transports angular momentum outward in the radial direction, T_φ^z is the φ - z component of the stress-energy tensor of the radiation produced by the disk, which describes the flow and transport of angular momentum in the vertical direction, and H is the half-thickness of the disk.

Similarly, the conservation of energy in the disk is described by

$$\frac{d}{dr} \left(\dot{M} E^\dagger - g\Omega \right) = -4\pi r T_t^z|_{z=H} , \quad (\text{D2})$$

where E^\dagger is the specific energy of disk particles, Ω is the angular velocity of the disk, and T_t^z is the t - z component of the stress-energy tensor of the radiation, which describes the flow and transport of energy in the vertical direction.

In a local Lorentz frame, the stress-energy tensor of photons can be expressed as an integral (Misner et al. 1973; Thorne 1974)

$$T^{ab} = \int n^a n^b I d\Omega , \quad (\text{D3})$$

where $n^a = k^a/E_l$, k^a is the four-wavevector of the photon, E_l is the energy of the photon measured in the local Lorentz frame (n^a does not depend on the energy of the photon), I is the intensity of photons which is a function of direction, and $d\Omega$ is the element of solid angle defined by the direction of the three-wavevector of the photon.

The evaluation of T^{ab} on the surface of the disk can be written in spherical coordinates (θ, ϕ) in the local rest frame of the disk particles, where θ is measured from the normal of the disk surface (see Appendix C). Then we have

$$T_t^z|_{z=H} = \int n_t \cos \theta I(\theta, \phi) d\Omega , \quad T_\varphi^z|_{z=H} = \int n_\varphi \cos \theta I(\theta, \phi) d\Omega , \quad (\text{D4})$$

where $d\Omega = \sin \theta d\theta d\phi$, and we have used $n^z = n^{(z)} = \cos \theta$ (see eq. [C9]).

From the definition of n^a , we have $n_t = k_t/E_l = -E_\infty/E_l$, $n_\varphi = k_\varphi/E_l = L_z/E_l$, where E_∞ is the energy-at-infinity of the photon, and $L_z = \lambda E_\infty$ is the angular momentum of the photon about the axis of the black hole. Then, by equations (C14) and (C15) we have

$$n_t = -E^\dagger - \left(\frac{A}{r^2}\right)^{1/2} \Gamma \Omega \cos \psi, \quad n_\varphi = L^\dagger + \left(\frac{A}{r^2}\right)^{1/2} \Gamma \cos \psi, \quad (\text{D5})$$

where $\cos \psi = \sin \theta \sin \phi$, ψ is the angle between the wavevector of the photon and the direction of $e_{(\phi)}^a$ in the local rest frame.

Substituting equations (D4) and (D5) into equations (D1) and (D2), we get

$$\frac{d}{dr} \left(\dot{M} L^\dagger - g \right) = 4\pi r (L^\dagger F + S), \quad (\text{D6})$$

$$\frac{d}{dr} \left(\dot{M} E^\dagger - g \Omega \right) = 4\pi r (E^\dagger F + S \Omega), \quad (\text{D7})$$

where

$$F \equiv \int \cos \theta I d\Omega \quad (\text{D8})$$

is the local energy flux density of the radiation,

$$S \equiv \left(\frac{A}{r^2}\right)^{1/2} \Gamma \int \cos \psi \cos \theta I d\Omega \quad (\text{D9})$$

is the stress density of the radiation which represents the transport of angular momentum in the vertical direction. When $S > 0$, the angular momentum is transported along the $+z$ direction, which means that the radiation exerts a negative torque on the disk.

Equations (D6) and (D7) have the formal solution (Cunningham 1976; Li 2002a)

$$F = F_0 + F_S, \quad (\text{D10})$$

where

$$F_0 \equiv \frac{\dot{M}}{4\pi r} f + \frac{g_{\text{in}}}{4\pi} \left(E_{\text{in}}^\dagger - \Omega_{\text{in}} L_{\text{in}}^\dagger \right) \frac{1}{r} \left(-\frac{d\Omega}{dr} \right) (E^\dagger - \Omega L^\dagger)^{-2}, \quad (\text{D11})$$

$$F_S \equiv -\frac{1}{r} \left(-\frac{d\Omega}{dr} \right) (E^\dagger - \Omega L^\dagger)^{-2} \int_{r_{\text{in}}}^r (E^\dagger - \Omega L^\dagger) S r dr, \quad (\text{D12})$$

the subscript “in” denotes evaluation at the inner boundary of the disk, and

$$f \equiv \left(-\frac{d\Omega}{dr} \right) (E^\dagger - \Omega L^\dagger)^{-2} \int_{r_{\text{in}}}^r (E^\dagger - \Omega L^\dagger) \frac{dL^\dagger}{dr} dr. \quad (\text{D13})$$

The quantity g_{in} denotes the value of the internal torque of the disk at the inner boundary. The function f has been worked out by Page & Thorne (1974) and is given by their equation (15n). Note, F_0 is just the solution for the radiation flux density of the disk when the effect of returning radiation is ignored.

We call the solution given by equation (D10) a “formal solution” since the stress density S is a functional of the flux density of the returning radiation in general.

The flux density F defined by equation (D8) is the “net” flux of energy, which usually contains two components: an outgoing component, corresponding to the radiation leaving the disk surface; and an ingoing component, corresponding to the radiation approaching the disk surface. To decompose the net flux density into an outgoing component and an ingoing component, let us write

$$I(\theta, \phi) = \begin{cases} I_{\text{out}}(\theta, \phi), & 0 \leq \theta < \pi/2 \\ I_{\text{in}}(\theta, \phi), & \pi/2 < \theta \leq \pi \end{cases}. \quad (\text{D14})$$

That is, we use I_{out} to denote the radiation intensity for the outgoing photons, and I_{in} to denote the radiation intensity for the ingoing photons. Then, the outgoing flux density F_{out} defined earlier, is given by

$$F_{\text{out}} \equiv \int_{\Omega_+} \cos \theta I_{\text{out}} d\Omega = \int_0^{2\pi} \int_0^{\pi/2} I_{\text{out}}(\theta, \phi) \cos \theta \sin \theta d\theta d\phi, \quad (\text{D15})$$

where Ω_+ denotes the whole solid angle above the disk surface, i.e. the solid angle defined by $0 \leq \theta < \pi/2$ and $0 \leq \phi < 2\pi$. The ingoing flux density F_{in} is similarly given by

$$\begin{aligned} F_{\text{in}} &\equiv - \int_{\Omega_-} \cos \theta I_{\text{in}} d\Omega = - \int_0^{2\pi} \int_{\pi/2}^{\pi} I_{\text{in}}(\theta, \phi) \cos \theta \sin \theta d\theta d\phi \\ &= \int_0^{2\pi} \int_0^{\pi/2} I_{\text{in}}(\pi - \theta, \pi + \phi) \cos \theta \sin \theta d\theta d\phi, \end{aligned} \quad (\text{D16})$$

where Ω_- denotes the whole solid angle below the disk surface, i.e. the solid angle defined by $\pi/2 < \theta \leq \pi$ and $0 \leq \phi < 2\pi$.

In the last line of equation (D16), we have expressed F_{in} as an integral over the reverse direction of the wavevector of the incoming photons, i.e. an integral over Ω_+ , which in practice is easier to handle. With the above definitions, we have $F_{\text{out}} \geq 0$, $F_{\text{in}} \geq 0$, and $F = F_{\text{out}} - F_{\text{in}}$. Then, by equation (D10), we have

$$F_{\text{out}} = F_0 + F_{\text{in}} + F_S. \quad (\text{D17})$$

Equation (D17) shows that the returning radiation makes two distinct contributions to the outgoing flux density, F_{in} and F_S . F_{in} comes directly from the energy carried by the returning

radiation, while F_S represents the work done by the returning radiation on the disk arising from the fact that the returning radiation is nonaxisymmetric about the normal of the disk surface at the point where the photon crosses the disk (see below).

The outgoing radiation, which is emitted by the disk locally, is symmetric around the normal of the disk surface. However the ingoing radiation, emitted by the disk remotely and focused by the gravity of the black hole, must be highly nonsymmetric. Thus we have in the frame moving with the disk fluid

$$\partial I_{\text{out}}/\partial\phi = 0, \quad \partial I_{\text{in}}/\partial\phi \neq 0. \quad (\text{D18})$$

Because of the presence of $\cos\psi \equiv \sin\theta \sin\phi$ in equation (D9) that defines S , only the part of I that is nonsymmetric around the disk normal contributes to S . By equation (D18), this means that only the ingoing component of the radiation contributes to S . Thus we have

$$\begin{aligned} S &= \left(\frac{A}{r^2}\right)^{1/2} \Gamma \int_{\Omega_-} I_{\text{in}}(\theta, \phi) \cos\psi \cos\theta d\Omega \\ &= \left(\frac{A}{r^2}\right)^{1/2} \Gamma \int_{\Omega_+} I_{\text{in}}(\pi - \theta, \pi + \phi) \cos\theta \sin\theta \sin\phi d\Omega. \end{aligned} \quad (\text{D19})$$

We assume that the radiation emitted by the disk is either isotropic, i.e., I_{out} is independent of θ and ϕ , or limb-darkened which corresponds to $I_{\text{out}} \propto 2 + 3 \cos\theta$ (see Chandrasekhar 1950; Cunningham 1976). Then, by equation (D15), the outgoing intensity is related to the outgoing flux by

$$I_{\text{out}} = \frac{1}{\pi} F_{\text{out}} \Upsilon, \quad \Upsilon \equiv \begin{cases} 1, & \text{for isotropic radiation} \\ \frac{1}{2} + \frac{3}{4} \cos\theta, & \text{for limb-darkened radiation} \end{cases}. \quad (\text{D20})$$

The evaluation of I_{in} in a given direction at radius $r = r_a$ in the disk can be calculated from the outgoing intensity at radius $r = r_e$ at the point where the photon comes from. Since I_{E_l}/E_l^3 is invariant along the orbit of the photon (Misner et al. 1973), where I_{E_l} is the specific intensity that is related to the intensity I by $I = \int_0^\infty I_{E_l} dE_l$, we have

$$I_{\text{in}}(r = r_a) = \hat{g}^4 I_{\text{out}}(r = r_e), \quad (\text{D21})$$

where $\hat{g} \equiv E_l(r = r_a)/E_l(r = r_e)$ is the redshift factor of the returning photon, given in equation (C22).

Since F_{in} and F_S themselves are determined by F_{out} at the radii where the photons contributing to F_{in} and F_S come from—as equation (D21) shows—equation (D17) must be

solved iteratively. First, we ignore the effect of returning radiation and take $F_{\text{out}} = F_0$. With this outgoing flux as an input, we calculate I_{in} by equations (D20) and (D21), then F_{in} and S by equations (D16) and (D19), and F_S by equation (D12). Next, we add F_{in} and F_S to F_0 to obtain a new outgoing flux density F_{out} , and repeat the calculations to obtain a new F_{in} and a new F_S . This process is repeated until the solution converges. In practice, five iterations are sufficient for convergence.

The integrals in equations (D16) and (D19) can be computed with the ray-tracing technique. We divide the solid angle Ω_+ at radius r_a into a number of small elements, and for each element in a direction defined by (θ, ϕ) we trace the orbit of the photon—by using the formulae provided in Appendixes A.2 and C—until the orbit crosses the disk at radius r_e . Then, we calculate I_{out} at r_e through equation (D20), the redshift factor \hat{g} through equation (C22), and the corresponding I_{in} at r_a through equation (D21). Thus we obtain the integrand in equations (D16) and (D19) for each element of solid angle. Summing the contributions gives rise to F_{in} and S at r_a . We remark that since most of the returning radiation comes from the general direction of the black hole, to obtain results with high precision it is necessary to divide the solid angle Ω_+ nonuniformly, with many more resolution elements in the direction of the black hole. This is most critical when $r_a \gg M$.

The radiation returning to the disk is, as we have assumed in this paper, absorbed and reprocessed by the disk, and then reradiated away. Then, the radiation that permanently leaves the disk consists of only two parts: one part escapes to infinity, the other is captured by the black hole. The total power of the disk, i.e. the total energy carried by the radiation that permanently leaves the disk per unit time as measured by an observer at infinity, is (Thorne 1974)

$$\mathcal{L}_{\text{total}} = -4\pi \int_{r_{\text{in}}}^{r_{\text{out}}} T_t^z|_{z=H} r dr . \quad (\text{D22})$$

Substituting equation (D2) into equation (D22), and using suitable boundary conditions at r_{out} (i.e., $E^{\dagger} \approx 1$ and $g\Omega \approx 0$ at $r_{\text{out}} \gg r_{\text{in}}$), we obtain $\mathcal{L}_{\text{total}}$ in terms of \dot{M} and g_{in} , which is just equation (1) in §2. Equation (1) clearly shows that the power of the disk comes from the gravitational binding energy of disk particles and a contribution from a torque at the inner boundary of the disk whenever the torque is nonzero.

E. The Disk Spectrum as Observed by a Distant Observer

The specific flux density of the disk radiation as observed by a remote observer, whose distance to the black hole is much larger than the size of the disk, is given by

$$F_{E_{\text{obs}}} = \int I_{E_{\text{obs}}} d\Omega_{\text{obs}} , \quad (\text{E1})$$

where $I_{E_{\text{obs}}}$ is the specific intensity of the radiation, E_{obs} is the photon energy, both measured by the remote observer, and $d\Omega_{\text{obs}}$ is the element of the solid angle subtended by the image of the disk on the observer's sky.

Using the fact that I_{E_l}/E_l^3 is invariant along the path of a photon, where E_l is the energy measured by any local observer on the path (Misner et al. 1973), equation (E1) can be rewritten as

$$F_{E_{\text{obs}}} = \int g^3 I_{E_{\text{em}}} d\Omega_{\text{obs}} . \quad (\text{E2})$$

E_{em} is the energy of the photon at its point of emission on the disk as measured by an observer located at that point who is corotating with the disk. $I_{E_{\text{em}}}$ is the specific intensity measured by that observer, and

$$g \equiv \frac{E_{\text{obs}}}{E_{\text{em}}} \quad (\text{E3})$$

is the redshift of the photon (see eq. [C21], where $E_{\infty} = E_{\text{obs}}$, $E_l = E_{\text{em}}$).

Suppose the disk radiates like a blackbody. Then the effective temperature of the disk measured by a locally corotating observer is simply

$$T_{\text{eff}}(r) = \left[\frac{F_{\text{out}}(r)}{\sigma_{\text{SB}}} \right]^{1/4} , \quad (\text{E4})$$

where σ_{SB} is the Stefan-Boltzmann constant, and F_{out} is the outgoing energy flux of the disk measured by the locally corotating observer (Appendix D). Suppose the color temperature T_{col} is related to the effective temperature by

$$T_{\text{col}}(r) = f_{\text{col}} T_{\text{eff}}(r) , \quad (\text{E5})$$

where f_{col} is a constant. Then, the local specific intensity of the radiation emitted by the disk is

$$I_{E_{\text{em}}} = \frac{2f_{\text{col}}^{-4} E_{\text{em}}^3}{\exp(E_{\text{em}}/k_{\text{B}}T_{\text{col}}) - 1} \Upsilon , \quad (\text{E6})$$

where k_B is the Boltzmann constant, Υ is a function of θ (the angle between the wavevector of the photon emitted by the disk and the normal of the disk surface) and is given by equation (D20) when the disk emission is isotropic or limb-darkened.

Substituting equations (E3), (E5), and (E6) into equation (E2), we have

$$F_{E_{\text{obs}}} = 2f_{\text{col}}^{-4} E_{\text{obs}}^3 \int \frac{\Upsilon d\Omega_{\text{obs}}}{\exp[E_{\text{obs}}/(gf_{\text{col}}k_B T_{\text{eff}})] - 1}. \quad (\text{E7})$$

The integral in equation (E7) has a form that is suitable for computations with the ray-tracing technique (see the second part in App. C).

F. Comparison of KERRBB with GRAD

We have compared KERRBB with the model GRAD in XSPEC, which considers a relativistic disk around a Schwarzschild black hole (Hanawa 1989; Ebisawa et al. 1991, 2003). For this comparison, we set $a = 0$ in KERRBB and ignored the returning radiation and limb-darkening since these are the assumptions made by GRAD. (Note that, for the case of a Schwarzschild black hole, the effect of returning radiation is not important, see §3.1.) We find that, at low inclination angles KERRBB gives results that are consistent with those of GRAD. However, at high inclination angles, the results differ.

We find that the inconsistency between KERRBB and GRAD is caused by the following two problems in GRAD: (1) GRAD uses an incorrect formula to calculate the redshift factor of a photon approaching the observer (see below). (2) GRAD takes the resolution in the azimuthal direction to be independent of the inclination angle. This leads to large errors for high inclination angles. Our ray-tracing code uses a resolution proportional to $1/\cos\vartheta_{\text{obs}}$, which gives better numerical accuracy.

The correct formula for calculating the redshift factor of a photon emitted by a Keplerian disk around a Schwarzschild black hole, adapted to the form used in GRAD, is

$$g = \sqrt{1 - \frac{3M}{r}} \left[1 - \left(1 - \frac{2M}{r}\right)^{-1} \sqrt{Mr} \left(\frac{d\varphi}{dt}\right)_{\text{ph}} \right]^{-1}, \quad (\text{F1})$$

where $(d\varphi/dt)_{\text{ph}}$ is the angular velocity of the photon evaluated at the point on the disk where it is emitted. Equation (F1) can easily be obtained from equation (C21) by using $(d\varphi/dt)_{\text{ph}} = \lambda\Delta/r^4$ when $a = 0$ (Bardeen et al. 1972; Chandrasekhar 1983).

Equation (F1) differs from equation (B2) in Ebisawa et al. (2003)—which is used in GRAD—in the following respects: the power index of $(1 - 2M/r)$ in equation (F1) is -1 ,

whereas in equation (B2) in Ebisawa et al. (2003) it is taken to be -0.5 . [Note that equation (F1) agrees with equation (A15) in Ebisawa et al. (1991), except that $d\varphi_{\text{ph}}/dt_{\text{ph}}$ in their (A15) should be $d\varphi'_{\text{ph}}/dt_{\text{ph}}$ according to their notation.]

Equation (B2) in Ebisawa et al. (2003) was derived from equations (A6)–(A14) in Ebisawa et al. (1991). However, equation (A7) in Ebisawa et al. (1991) is wrong; it should be

$$\begin{pmatrix} \epsilon \\ p_r \\ p_{\theta'} \\ p_{\varphi'} \end{pmatrix}_{\text{LNRO}} = \epsilon_{\text{LNRO}} \begin{bmatrix} 1 \\ (1 - 2M/r)^{-1}(dr_{\text{ph}}/d\theta_{\text{ph}})/(dt_{\text{ph}}/d\theta_{\text{ph}}) \\ (1 - 2M/r)^{-1/2}r(d\theta'_{\text{ph}}/d\theta_{\text{ph}})/(dt_{\text{ph}}/d\theta_{\text{ph}}) \\ (1 - 2M/r)^{-1/2}r(d\varphi'_{\text{ph}}/d\theta_{\text{ph}})/(dt_{\text{ph}}/d\theta_{\text{ph}}) \end{bmatrix}, \quad (\text{F2})$$

where we have used the same notation as in Ebisawa et al. (1991) and we have set $G = c = 1$. Since on a photon orbit in the Schwarzschild spacetime we have $ds^2 = 0 = -(1 - 2M/r)dt^2 + (1 - 2M/r)^{-1}dr^2 + r^2d\theta'^2 + r^2\sin^2\theta'd\varphi'^2$, it is easy to check that equation (F2) satisfies the null condition $\epsilon^2 - p_r^2 - p_{\theta'}^2 - p_{\varphi'}^2 = 0$ (note, $\vartheta' = \pi/2$ on the equatorial plane), but equation (A7) in Ebisawa et al. (1991) does not. In addition, there are a few other errors and typos in the Appendix of Ebisawa et al. (1991): their equation (A8) is incorrect (subsequently corrected in Ebisawa et al. 2003), and in the 4×4 matrix in their equation (A11), the element on the top-right corner should be $-\beta\gamma$, not $\beta\gamma$ (this is obvious since the Lorentz transformation matrix should be symmetric).

If the above correct equations are used, then one can derive a redshift factor that is exactly the same as our equation (F1).

Unfortunately, equation (B2) of Ebisawa et al. (2003) has been used in the current version of GRAD in XSPEC (both XSPEC11 and XSPEC12) at the time the present paper was written. In addition, as Ebisawa et al. applied their equation in GRAD, they replaced the “ $-$ ” sign in front of $(1 - 2M/r)$ by a “ $+$ ” sign. Although the correct formula was shown in Ebisawa et al. (1991)—i.e., their equation (A15), except that $d\varphi_{\text{ph}}/dt_{\text{ph}}$ should be $d\varphi'_{\text{ph}}/dt_{\text{ph}}$ —lately it was replaced by an incorrect equation—equation (B2) in Ebisawa et al. (2003).

In Figure 14 we show some examples that compare the results given by KERRBB, those given by GRAD, and those given by a modified GRAD where we replaced the following statement in GRAD,

$$\text{Red} = 1.0\text{D}0/(1.0\text{D}0+\text{SQRT}(\text{R}0/2.0\text{D}0))/(1.0\text{D}0-1.0\text{D}0/\text{R}0)**0.5\text{D}0*\text{dphdx}/\text{dtdx},$$

by

$$\text{Red} = 1.0\text{D}0/(1.0\text{D}0-\text{SQRT}(\text{R}0/2.0\text{D}0))/(1.0\text{D}0-1.0\text{D}0/\text{R}0)*\text{dphdx}/\text{dtdx},$$

(i.e., changing the “+” in front of “SQRT” to a “–”, and deleting “**0.5”). The parameters for the calculated models are: $M = 10M_{\odot}$, $D = 10\text{kpc}$, $\dot{M} = 10^{19}\text{g sec}^{-1}$, $f_{\text{col}} = 1$, and $\vartheta_{\text{obs}} = 20^{\circ}$, 60° , and 85° in each panel. (As already mentioned, for KERRBB we set $a = 0$, $\eta = 0$, and turned off returning radiation and limb-darkening.) The horizontal axis shows the observed photon energy in units of keV. The vertical axis shows the specific photon number density calculated by KERRBB (solid lines), GRAD (dashed lines), and the modified GRAD (dashed lines), in units of photons $\text{keV}^{-1} \text{cm}^{-2} \text{sec}^{-1}$.

Figure 14 shows that, after the incorrect formula in GRAD is replaced with the correct one, GRAD agrees quite well with KERRBB. However, for the case of $\vartheta_{\text{obs}} = 85^{\circ}$, even the modified GRAD differs from KERRBB significantly. This is caused by insufficient azimuthal resolution in GRAD when the disk is highly inclined.

REFERENCES

- Abramowicz, M. A., & Kato, S. 1989, *ApJ*, 336, 304
- Abramowitz, M., & Stegun, I. A. 1972, *Handbook of Mathematical Functions* (New York: Dover Publications, Inc.)
- Afshordi, N., & Paczyński, B. 2003, *ApJ*, 592, 354
- Agol, E., & Krolik, J. H. 2000, *ApJ*, 528, 161
- Armitage, P. J., Reynolds, C. S., & Chiang, J. 2001, *ApJ*, 548, 868
- Arnaud, K. A., 1996, *Astronomical Data Analysis Software and Systems V*, ed. G. H. Jacoby & J. Barnes (San Francisco: ASP), 17
- Bardeen, J. M., Press, W. H., & Teukolsky, S. A. 1972, *ApJ*, 178, 347
- Birkhoff, G., & Mac Lane, S. A. 1965, *A Survey of Modern Algebra* (New York: Macmillan)
- Byrd, P. F., & Friedman, M. D. 1954, *Handbook of Elliptic Integrals for Engineers and Physicists* (Berlin: Springer-Verlag)
- Čadež, A., Fanton, C., & Calvani, M. 1998, *New Astronomy*, 3, 647
- Carter, B. 1968, *Phys. Rev.*, 174, 1559
- Chandrasekhar, S. 1950, *Radiative Transfer* (Oxford: Oxford University Press)

- Chandrasekhar, S. 1983, *The Mathematical Theory of Black Holes* (Oxford: Oxford University Press)
- Cunningham, C. T. 1975, *ApJ*, 202, 788
- Cunningham, C. T. 1976, *ApJ*, 208, 534
- Cunningham, C. T., & Bardeen, J. M. 1973, *ApJ*, 183, 237
- Davis, S. W., Blaes, O. M., Hubeny, I., & Turner, N. J. 2004, *ApJ*, submitted; astro-ph/0408590
- Dovčiak, M., Karas, V., Martocchia, A., Matt, G., & Yaqoob, T. 2004, in *Proceedings of the Workshop 'Processes in the Vicinity of Black Holes and Neutron Stars'* (Silesian University, Opava), in press; preprint astro-ph/0407330
- Ebisawa, K., Mitsuda, K., & Hanawa, T. 1991, *ApJ*, 367, 213
- Ebisawa, K., Życki, P., Kubota, A., Mizuno, T., & Watarai, K. 2003, *ApJ*, 597, 780
- Fabian, A. C., Rees, M., Stella, L., & White, N. E. 1989, *MNRAS*, 238, 729
- Fanton, C., Calvani, M., de Felice, F., & Čadež, A. 1997, *PASJ*, 49, 159
- Gammie, C. F. 1999, *ApJ*, 522, L57
- Gierliński, M., & Done, C. 2004, *MNRAS*, 347, 885
- Gierliński, M., Maciolek-Niedzwiecki, A., & Ebisawa, K. 2001, *MNRAS*, 325, 1253
- Gierliński, M., Zdziarski, A. A., Poutanen, J., et al. 1999, *MNRAS*, 309, 496
- Hanawa, T. 1989, *ApJ*, 341, 948
- Hawley, J. F., & Krolik, J. H. 2002, *ApJ*, 566, 164
- Hjellming, R. M., & Rupen, M. P. 1995, *Nature*, 375, 464
- Krolik, J. K. 1999, *ApJ*, 515, L73
- Kubota, A., Tanaka, Y., Makishima, K., et al. 1998, *PASJ*, 50, 667
- Laor, A. 1991, *ApJ*, 376, 90
- Li, L. -X. 2000, *ApJ*, 533, L115

- Li, L. -X. 2002a, *ApJ*, 567, 463
- Li, L. -X. 2002b, *A&A*, 392, 469
- Li, L. -X. 2003a, *Phys. Rev. D*, 67, 044007
- Li, L. -X. 2003b, *Phys. Rev. D*, 68, 024022
- Li, L. -X. 2004, *PASJ*, 56, 685
- Lynden-Bell, D., & Pringle, J. E. 1974, *MNRAS*, 168, 603
- Makishima, K., Maejima, Y., Mitsuda, K., et al. 1986, *ApJ*, 308, 635
- McClintock, J. E., & Remillard, R. A. 2004, *astro-ph/0306213*
- Misner, C. W., Thorne, K. S., & Wheeler, J. A. 1973, *Gravitation* (San Francisco: Freeman)
- Mitsuda, K., Inoue, H., Koyama, K., et al. 1984, *PASJ*, 36, 741
- Muchotrzeb, B., & Paczyński, B. 1982, *Acta Astr.*, 32, 1
- Müller, A., & Camenzind, M. 2004, *A&A*, 413, 861
- Novikov, I. D., & Thorne, K. S. 1973, in *Black Holes*, ed. C. DeWitt & B. S. DeWitt (New York: Gordon and Breach), 343
- Orosz, J. A., & Bailyn, C. D. 1997, *ApJ*, 477, 876
- Orosz, J. A., Jain, R. K., Bailyn, C. D., McClintock, J. E., & Remillard, R. A. 1998, *ApJ*, 499, 375
- Orosz, J. A., Groot, P. J., van der Klis, M., et al. 2002, *ApJ*, 568, 845
- Orosz, J. A. 2004, in preparation
- Paczyński, B. 2000, *astro-ph/0004129*
- Paczyński, B., & Wiita, P. J. 1980, *A&A*, 88, 23
- Page, D., & Thorne, K. S. 1974, *ApJ*, 191, 499
- Park, S. Q., Miller, J. M., McClintock, J. E., et al. 2004, *ApJ*, 610, 378
- Pringle, J. E., & Rees, M. J. 1972, *A&A*, 21, 1
- Rauch, K. P., & Blandford, R. D. 1994, *ApJ*, 421, 46

- Ross, R. R., Fabian, A. C., & Mineshige, S. 1992, *MNRAS*, 258, 189
- Schnittman, J. D., & Bertschinger, E. 2003, *ApJ*, 606, 1098
- Shakura, N. I., & Sunyayev, R. A. 1973, *A&A*, 24, 337
- Shimura, T., & Takahara, F. 1993, *ApJ*, 419, 78
- Shimura, T., & Takahara, R. 1995, *ApJ*, 445, 780
- Sobczak, G. J., McClintock, J. E., Remillard, R. A., Bailyn, C. D., & Orosz, J. A. 1999, *ApJ*, 520, 776
- Sobczak, G. J., McClintock, J. E., Remillard, R. A., et al. 2000, *ApJ*, 544, 993
- Speith, R., Riffert, H., & Ruder, H. 1995, *Comp. Phys. Comm.*, 88, 109
- Stella, L. 1990, *Nature*, 344, 747
- Syunyaev, R. A., & Shakura, N. I. 1977, *Sov. Astron. Lett.*, 3, 138
- Tanaka, Y., & Lewin, W. H. G. 1995, in *X-ray Binaries*, eds. W. H. G. Lewin, J. van Paradijs, and E. P. J. van den Heuvel (Cambridge Univ. Press: Cambridge), 126
- Thorne, K. S. 1974, *ApJ*, 191, 507
- Uzdensky, D. A. 2004a, *ApJ*, 603, 652
- Uzdensky, D. A. 2004b, *ApJ*, accepted; astro-ph/0410715
- Wang, D. X., Xiao, K., & Lei, W. H. 2002, *MNRAS*, 335, 655
- Wang, D. -X., Ma, R. -Y., Lei, W. -H., & Yao, G. -Z. 2003, *ApJ*, 595, 109
- Zhang, S. N., Cui, W., & Chen, W. 1997, *ApJ*, 482, L155
- Zimmerman, E. R., Narayan, R., McClintock, J. E., & Miller, J. M. 2004, *ApJ*, submitted (astro-ph/0408209) (Z04)
- Zwillinger, D. 2002, *CRC Standard Mathematical Tables and Formulae* (Coca Raton, Florida: Chapman & Hall/CRC)

Table 1. Average Ratios of Fitted Parameters for U1543

Parameter	KERRBB	GRAD	DISKPN	EZDISKBB	DISKBB
\dot{M}	1	1.03	0.61	0.25	0.017
D	1	1.01	0.82	0.67	0.31

Table 2. Average Ratios of Fitted Parameters for J1550

Parameter	KERRBB	GRAD	DISKPN	EZDISKBB	DISKBB
\dot{M}	1	1.25	1.54	0.76	0.052
D	1	1.11	1.47	1.21	0.55

Table 3. Sensitivity of Results on U1543 to Input Parameters^a

Adjusted Parameter and Value	\dot{M} (10^{18} g/s)	a_*	χ^2 per dof
$\vartheta_{\text{obs}} = 22.2^\circ$	2.27	0.58	0.87
$\vartheta_{\text{obs}} = 19.2^\circ$	2.14	0.63	0.88
$M = 10.4M_\odot$	2.00	0.71	0.87
$M = 8.4M_\odot$	2.43	0.48	0.89
$D = 8.0$ kpc	2.65	0.54	0.88
$D = 7.0$ kpc	1.81	0.68	0.88
$f_{\text{col}} = 1.9$	2.66	0.32	0.90
$f_{\text{col}} = 1.5$	1.76	0.83	0.87
Nominal values ^b	2.18	0.61	0.88

^aThe fits were done with KERRBB using the spectral data obtained on MJD 52,467.20 (see Figs. 10 and 12). For each fit, one of the following four parameters was varied from its “correct” value by either adding or subtracting 1σ : inclination (20.7 ± 1.5 degrees), mass ($9.4 \pm 1.0 M_\odot$), distance (7.5 ± 0.5 kpc), and spectral hardening factor (1.7 ± 0.2). The resulting \dot{M} , a_* and χ^2 for the fit are listed.

^bValues obtained by fixing the parameters at their central values: $\vartheta_{\text{obs}} = 20.7^\circ$, $M = 9.4M_\odot$, $D = 7.5$ kpc, $f_{\text{col}} = 1.7$.

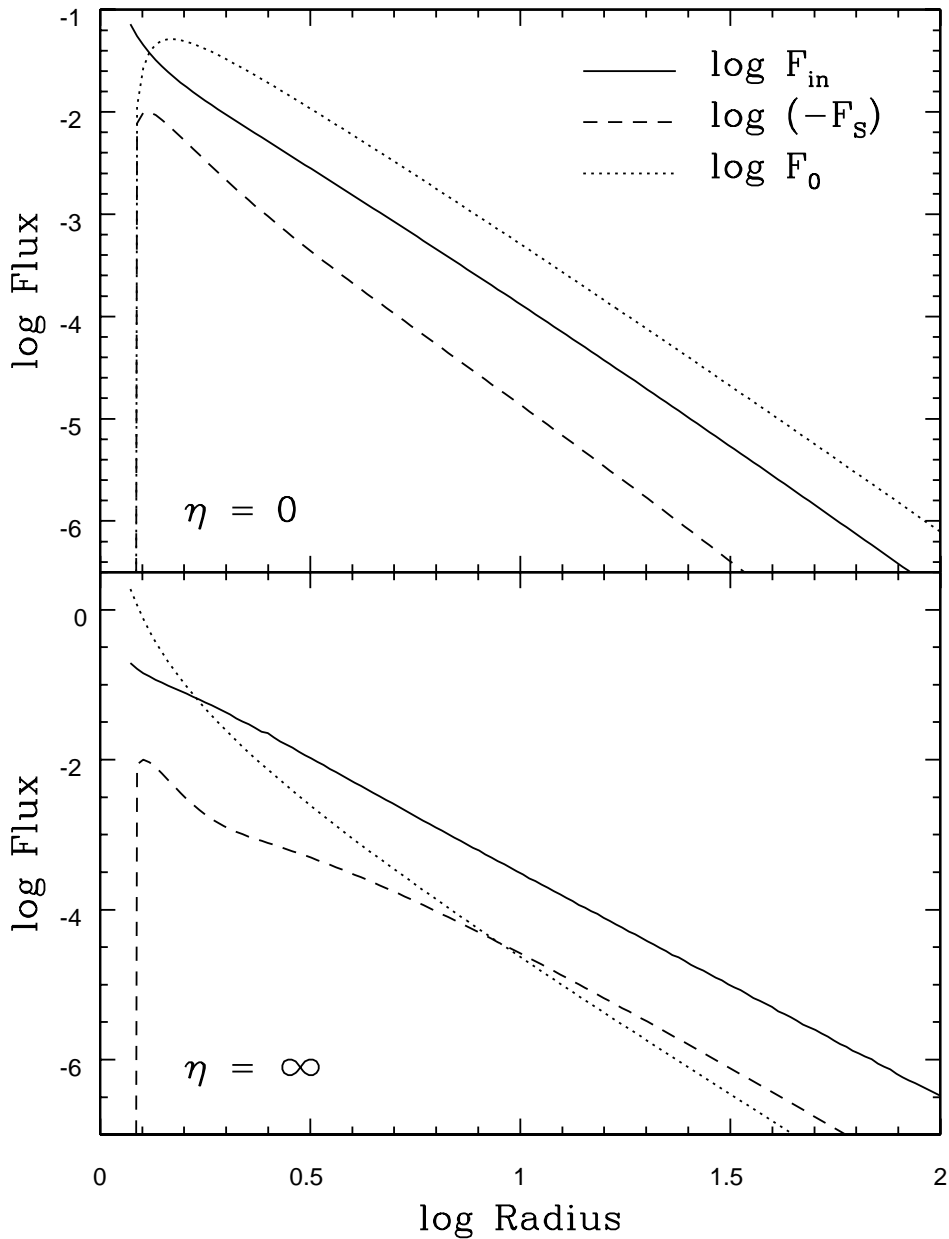


Fig. 1.— The flux density of the radiation returning to the disk for $\eta = 0$ (upper panel) and $\eta = \infty$ (lower panel) for a black hole with $a = 0.999M$. F_{in} is the flux density of the returning (ingoing) radiation (eq. [D16]), and F_S is the flux density arising from the angular momentum of the returning radiation (eq. [D12]). For comparison, the outgoing flux density when the returning radiation is ignored (F_0 , eq. [D11]) is also shown. The disk radius is in units of $r_g = M$ and the fluxes are in units of $3\dot{M}_{\text{eff}}/8\pi r_g^2$. Note that F_S is negative.

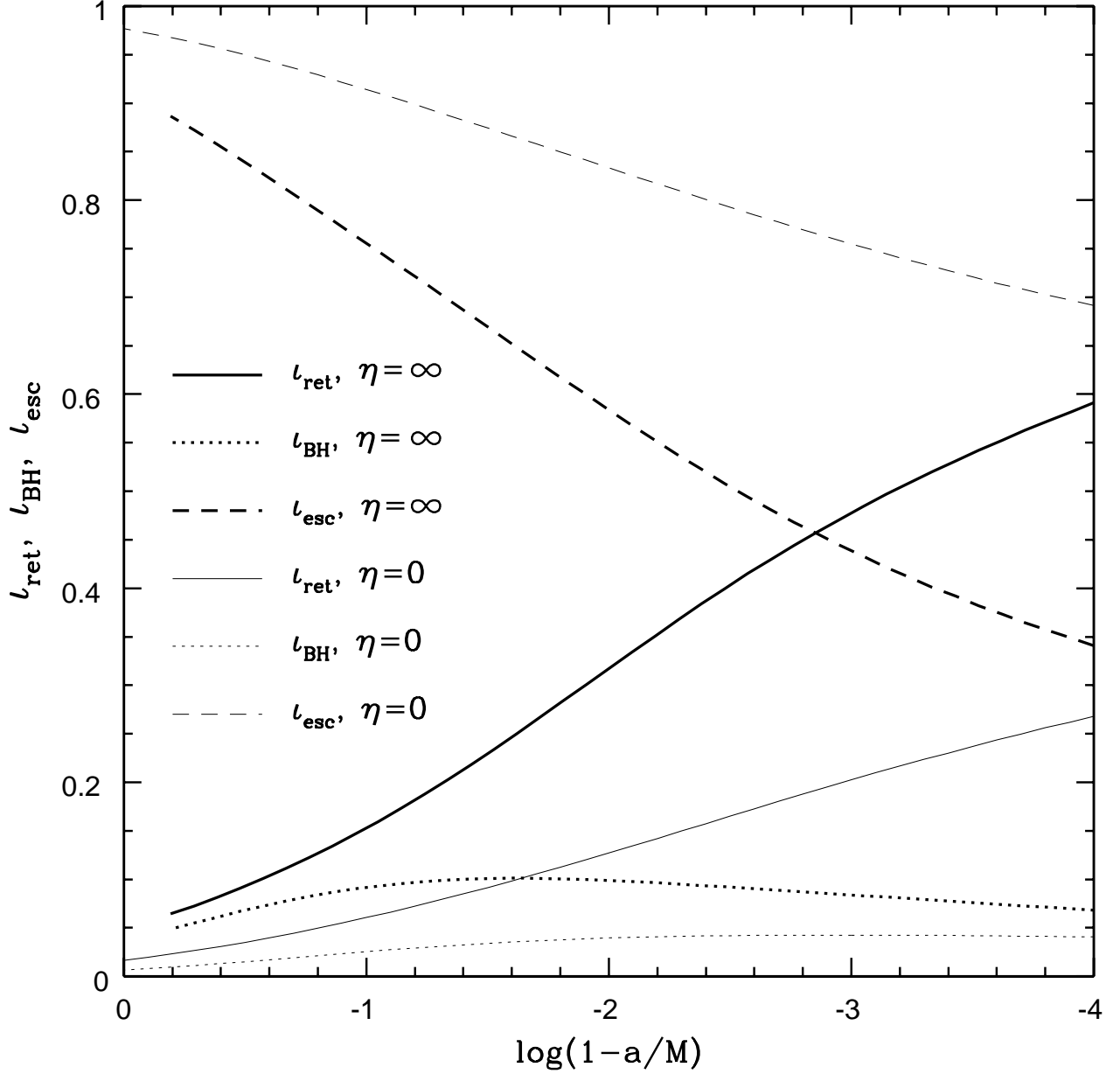


Fig. 2.— Photons emitted by the disk consist of three components: some photons return to the disk, some go into the black hole, and the rest escape to infinity. The fraction of each component in the “total” energy radiated by the disk is shown as a function of the spin of the black hole. The definitions of these fractions, which satisfy $\iota_{\text{ret}} + \iota_{\text{BH}} + \iota_{\text{esc}} = 1$, are given in eq. (7). Thin lines correspond to the case of a standard Keplerian disk ($\eta = 0$, $g_{\text{in}} = 0$) and thick lines correspond to the case of a nonaccreting disk ($\eta = \infty$, $\dot{M} = 0$, but $g_{\text{in}} \neq 0$).

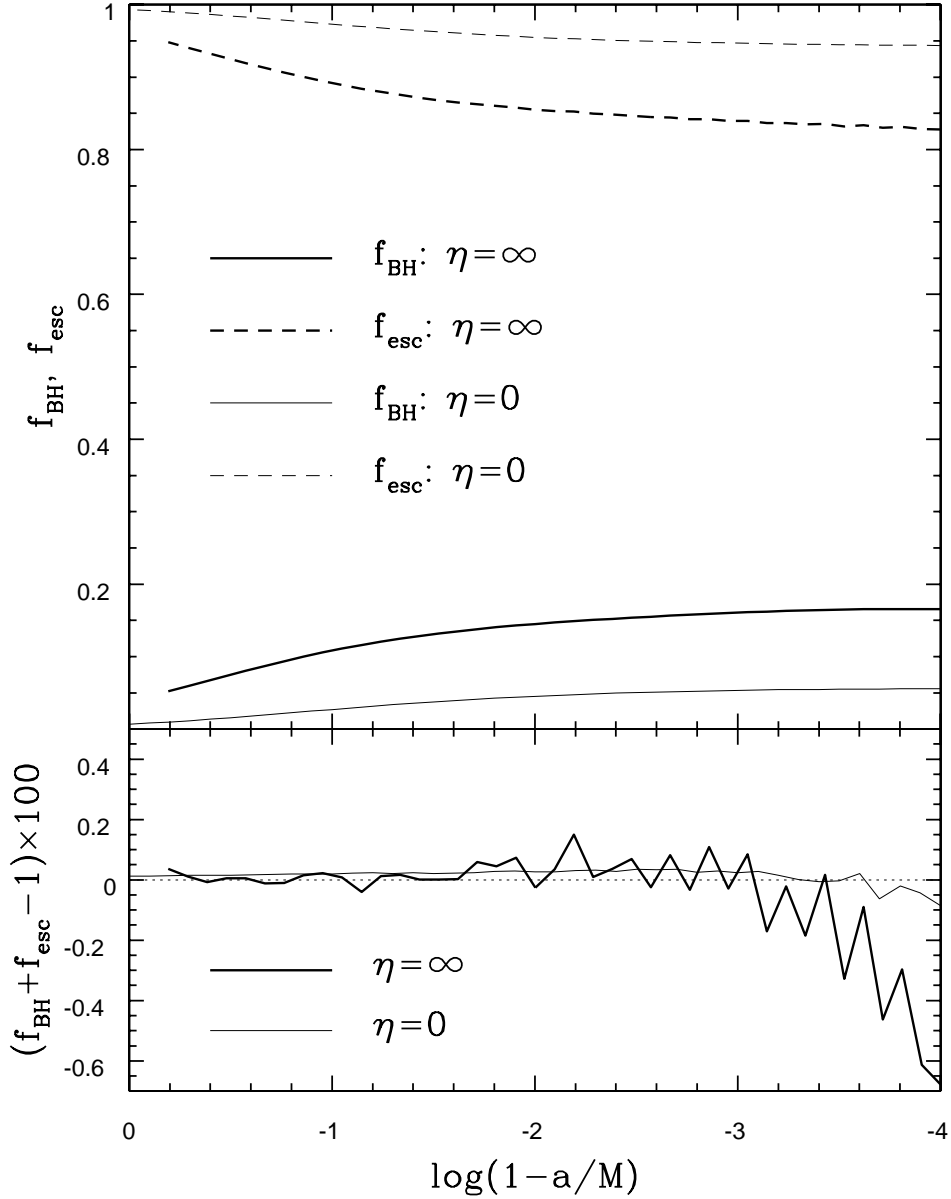


Fig. 3.— The “net” radiation from the disk—i.e., the radiation that permanently leaves the disk—consists of two parts: one falls into the black hole, the other escapes to infinity. The upper panel shows the fractions of each as a function of the spin of the black hole. The definitions of the fractions are given in eq. (9). The lower panel tests the conservation of energy, $f_{\text{BH}} + f_{\text{esc}} = 1$, in the calculations. It is seen to be satisfied within the errors of the code. Thin lines correspond to the case of a standard Keplerian disk ($\eta = 0$) and thick lines correspond to the case of a nonaccreting disk ($\eta = \infty$).

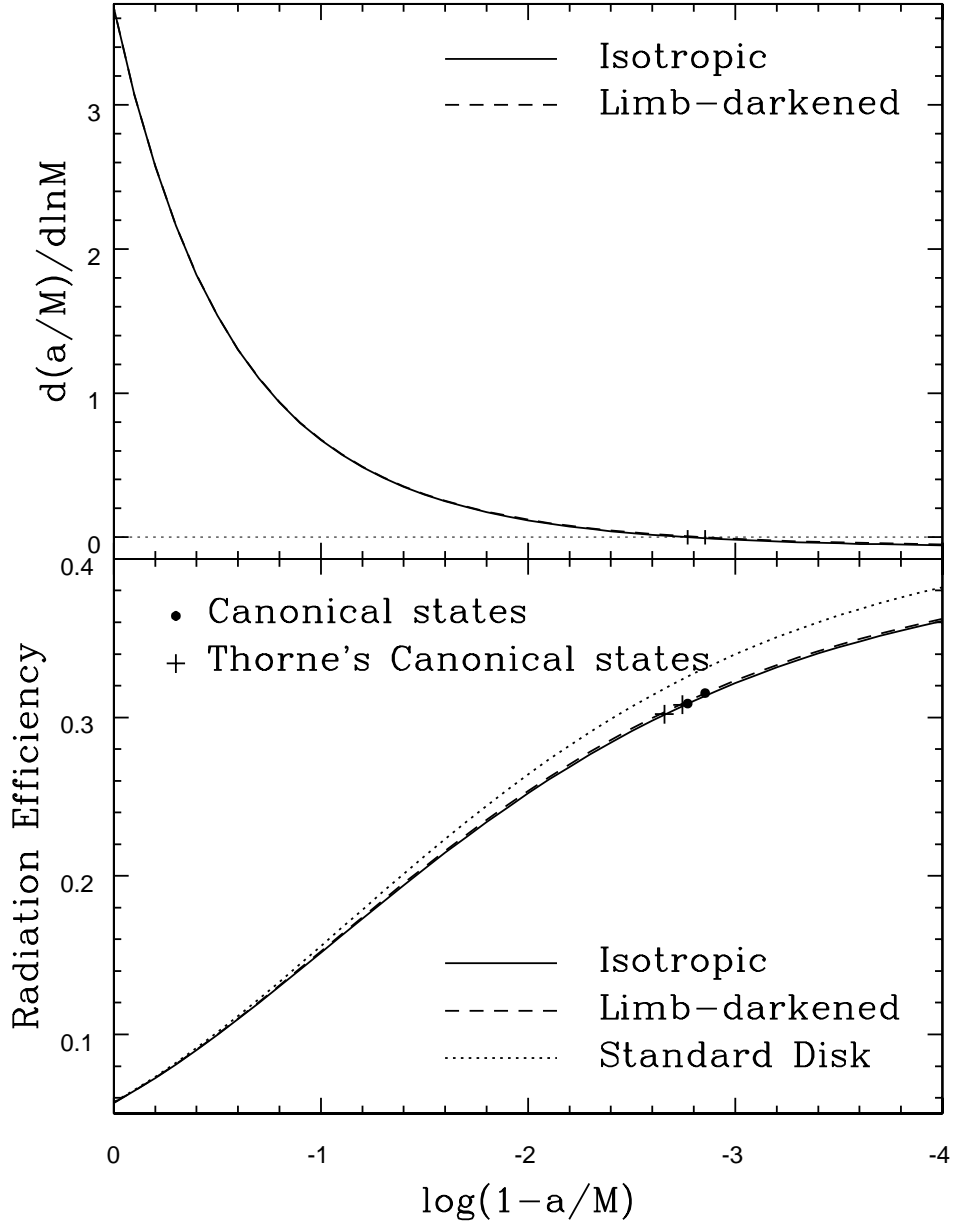


Fig. 4.— Upper panel: The spin-up function defined in equation (10). The equilibrium spin of the black hole [or, the “canonical” state, Thorne (1974)] corresponds to the condition $d(a/M)/d\ln M = 0$, which gives $a = 0.9983M$ when the disk radiation is isotropic, and $a = 0.9986M$ when the disk radiation is limb-darkened (indicated by the two vertical lines). Lower panel: The efficiency of a standard Keplerian disk in converting rest mass into outgoing radiation (see the text for definition) as a function of the spin of the black hole. The corresponding efficiency when the effect of returning radiation is ignored is shown by the dotted line.

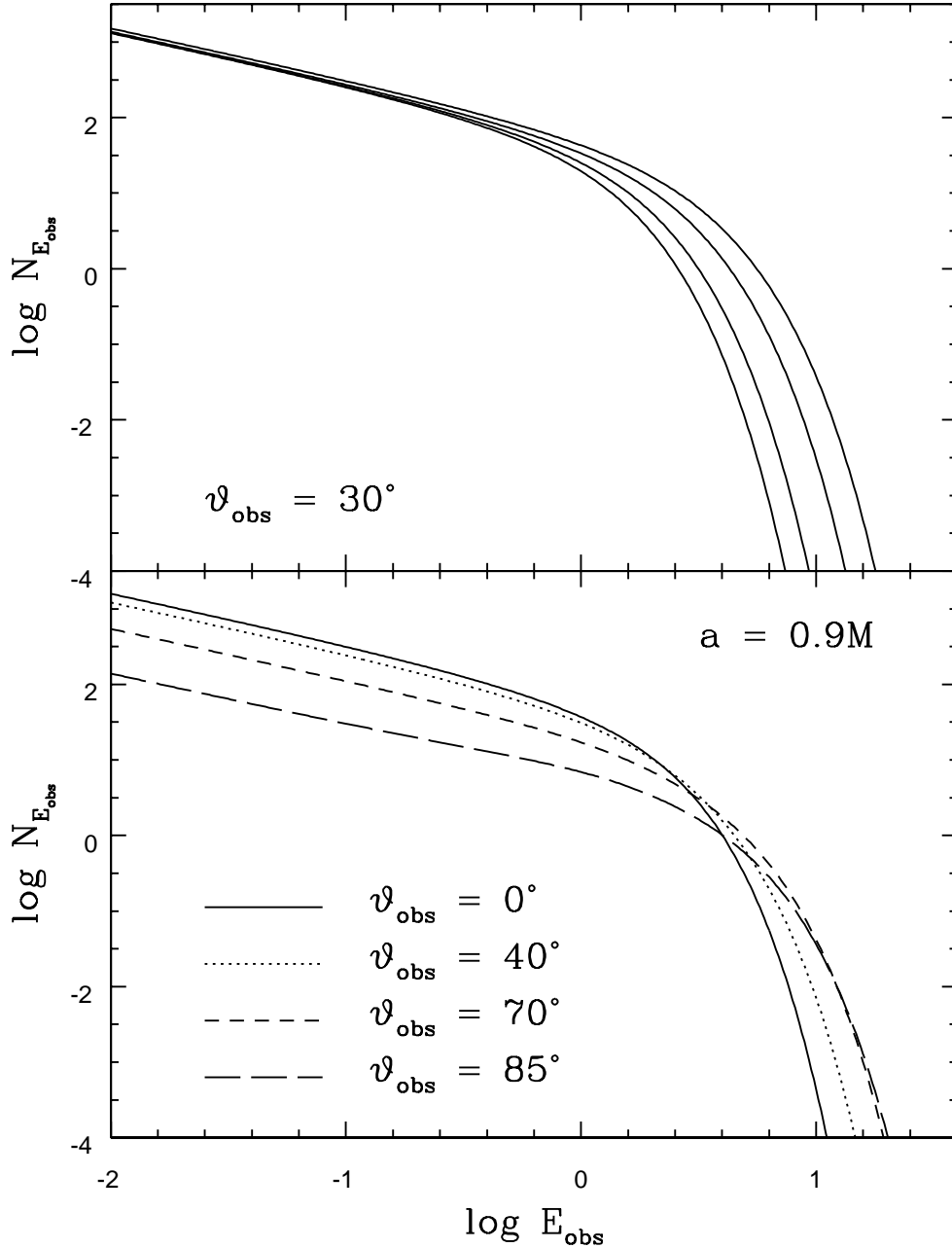


Fig. 5.— Upper panel: Effect of the spin of the black hole on the observed spectrum of the disk. From left to right: $a/M = 0, 0.5, 0.9$, and 0.999 . Other parameters are: $\eta = 0$, $\vartheta_{\text{obs}} = 30^\circ$, $M = 10M_\odot$, $D = 10\text{kpc}$, $\dot{M} = 10^{19}\text{g sec}^{-1}$, and $f_{\text{col}} = 1$. Lower panel: Effect of the inclination angle of the disk on the observed spectrum. The inclination angles are: $\vartheta_{\text{obs}} = 0^\circ, 40^\circ, 70^\circ$, and 85° , as indicated. Other parameters are: $\eta = 0$, $a = 0.9M$, $M = 10M_\odot$, $D = 10\text{kpc}$, $\dot{M} = 10^{19}\text{g sec}^{-1}$, and $f_{\text{col}} = 1$. The energy E_{obs} is in keV, and the flux density $N_{E_{\text{obs}}}$ is in units of photons $\text{keV}^{-1} \text{cm}^{-2} \text{sec}^{-1}$.

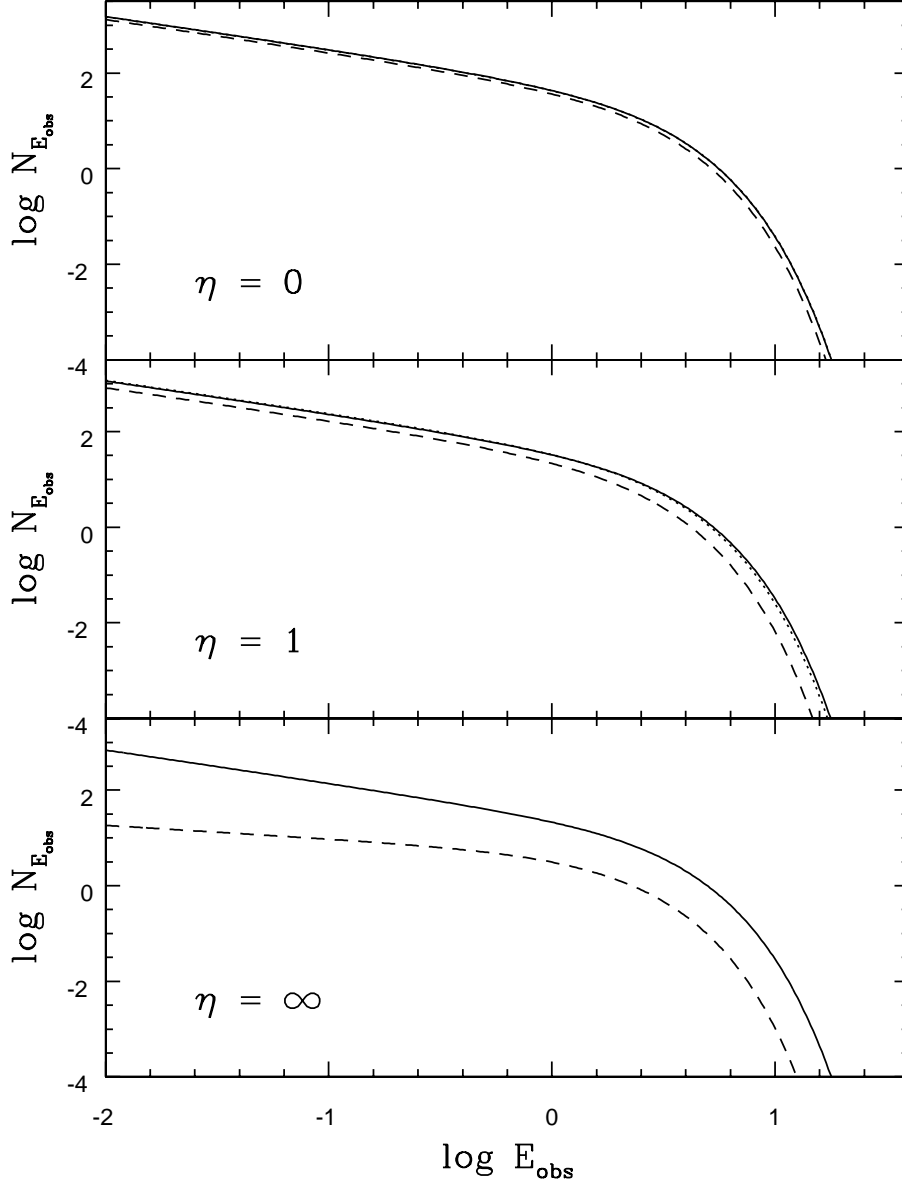


Fig. 6.— Effect of the returning radiation on the observed spectrum of an accretion disk. The three cases correspond to $\eta = 0$ (upper panel), $\eta = 1$ (middle panel), and $\eta = \infty$ (lower panel). The solid line is the spectrum when the returning radiation is included, and the dashed line is the spectrum when the returning radiation is ignored. Parameters are: $a = 0.999M$, $\vartheta_{\text{obs}} = 30^\circ$, $M = 10M_\odot$, $D = 10\text{kpc}$, $\dot{M}_{\text{eff}} = 10^{19}\text{g sec}^{-1}$, and $f_{\text{col}} = 1$. The dotted line in the upper panel (almost coincident with the solid line) is the spectrum when the returning radiation is ignored, but \dot{M} is increased to $1.23 \times 10^{19}\text{g sec}^{-1}$. The dotted line in the middle panel is the spectrum when the returning radiation is ignored, and \dot{M}_{eff} is increased to $1.7 \times 10^{19}\text{g sec}^{-1}$.

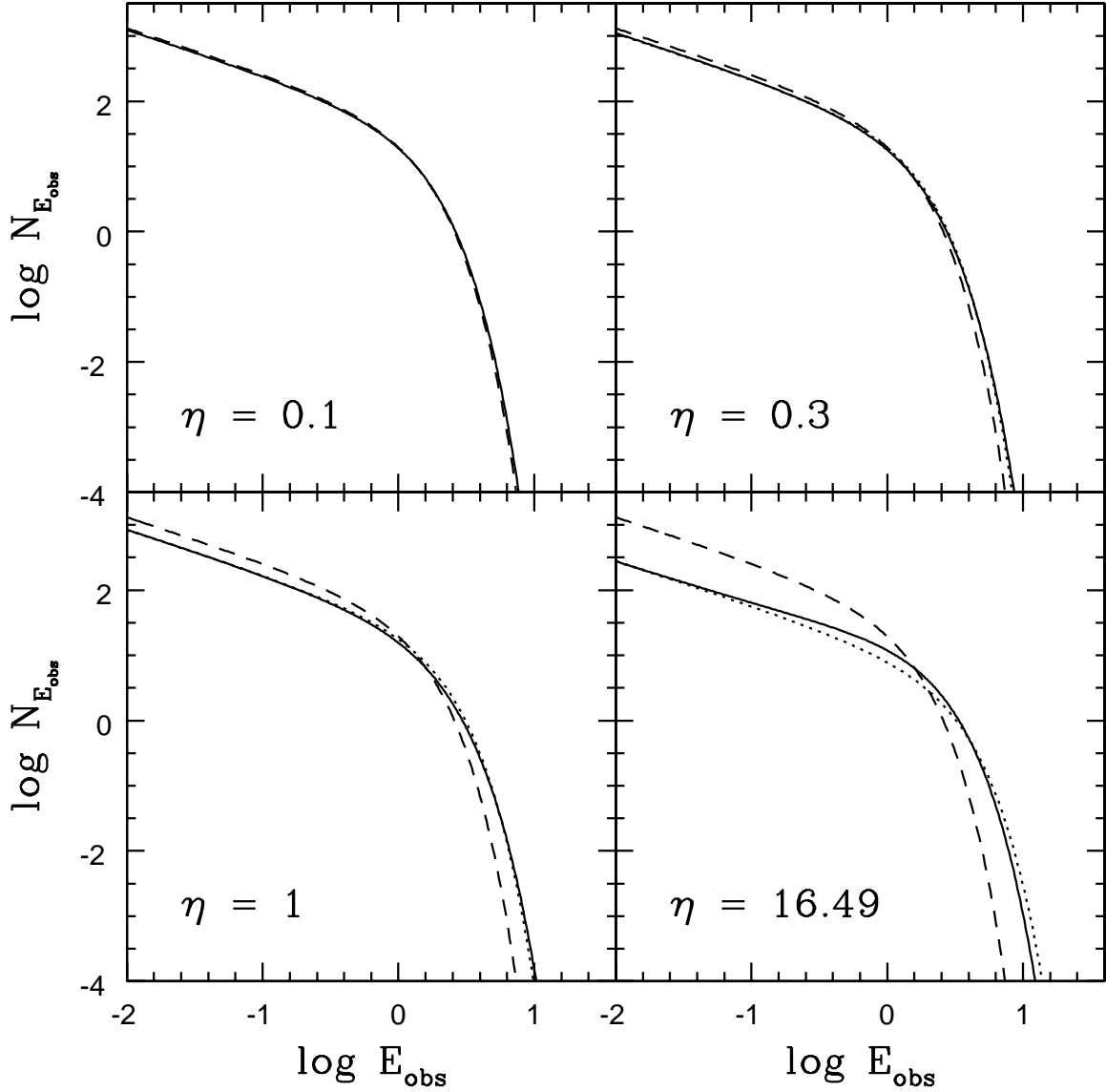


Fig. 7.— Effect of the torque at the inner boundary of the disk. In each panel, the solid line is the spectrum of the disk with a torque corresponding to the indicated value of η (see eq. [2]) and the dashed line is the spectrum of a disk with the same value of \dot{M}_{eff} but with the torque at the inner boundary set to zero. Parameters are: $a = 0$ (Schwarzschild black hole), $\vartheta_{\text{obs}} = 30^\circ$, $M = 10M_\odot$, $D = 10\text{kpc}$, $\dot{M}_{\text{eff}} = 10^{19}\text{g sec}^{-1}$, and $f_{\text{col}} = 1$. The dotted lines in the last three panels represent the spectra of zero-torque models in which the values of \dot{M}_{eff} and f_{col} have been adjusted for the best fit of the corresponding solid lines. The parameters of the dotted line models are: $\dot{M}_{\text{eff}} = 10^{19}\text{g sec}^{-1}$ and $f_{\text{col}} = 1.15$ for $\eta = 0.3$; $\dot{M}_{\text{eff}} = 10^{19}\text{g sec}^{-1}$ and $f_{\text{col}} = 1.4$ for $\eta = 1$; $\dot{M}_{\text{eff}} = 6 \times 10^{18}\text{g sec}^{-1}$ and $f_{\text{col}} = 2.5$ for $\eta = 16.49$.

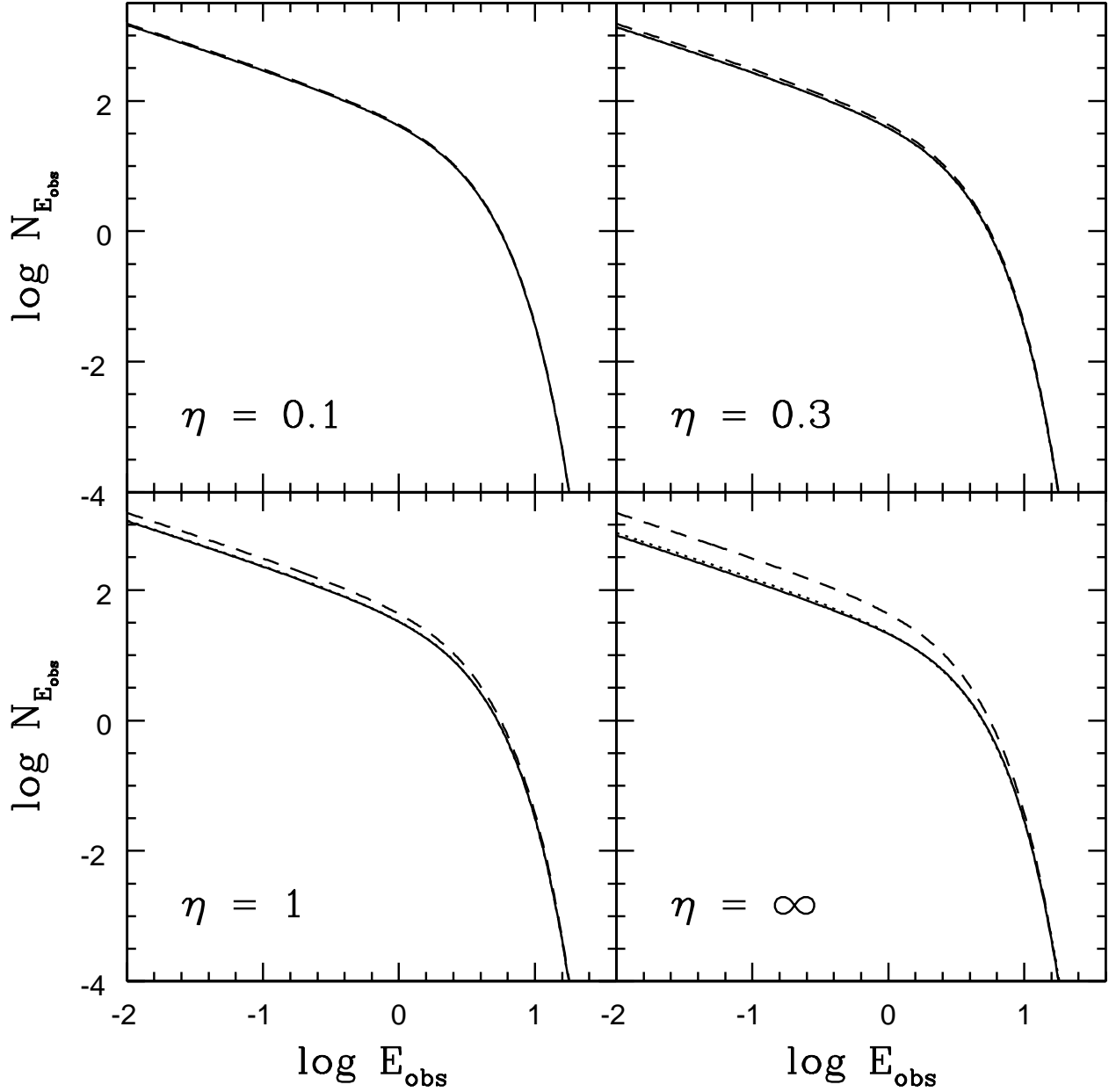


Fig. 8.— Similar to Fig. 7 except that $a/M = 0.999$. The parameters of the dotted line models are: $\dot{M}_{\text{eff}} = 8.9 \times 10^{18} \text{g sec}^{-1}$ and $f_{\text{col}} = 1.03$ for $\eta = 0.3$; $\dot{M}_{\text{eff}} = 7.8 \times 10^{18} \text{g sec}^{-1}$ and $f_{\text{col}} = 1.08$ for $\eta = 1$; $\dot{M}_{\text{eff}} = 5.4 \times 10^{18} \text{g sec}^{-1}$ and $f_{\text{col}} = 1.25$ for $\eta = \infty$.

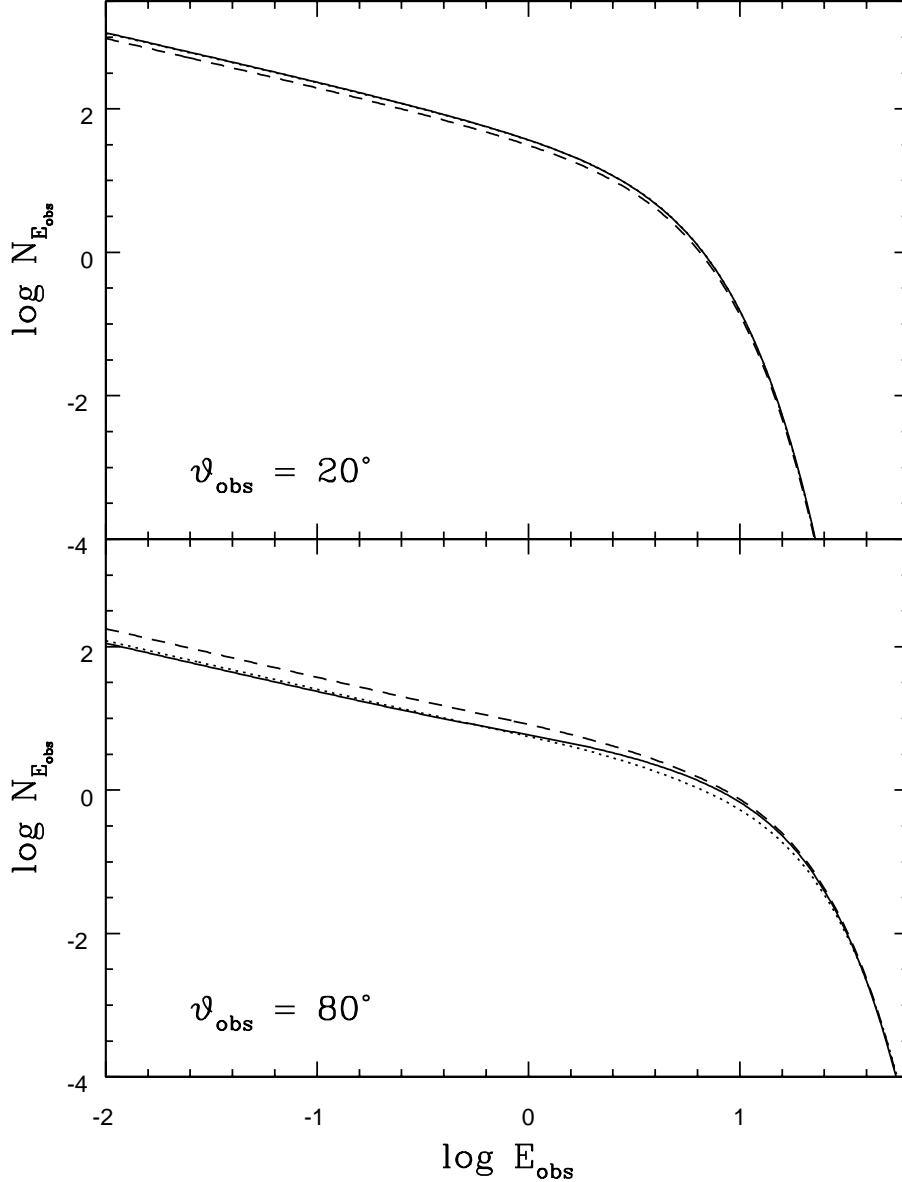


Fig. 9.— Effect of limb-darkening on the observed spectrum. The two cases correspond to two different disk inclination angles: $\vartheta_{\text{obs}} = 20^\circ$ (upper panel) and $\vartheta_{\text{obs}} = 80^\circ$ (lower panel). The solid line is the spectrum when the disk emission is limb-darkened, and the dashed line is the spectrum when the disk emission is isotropic. Other model parameters are: $\eta = 0$, $a = 0.999M$, $M = 10M_\odot$, $D = 10\text{kpc}$, $\dot{M} = 10^{19}\text{g sec}^{-1}$, and $f_{\text{col}} = 1.5$. The dotted line in each panel (hardly visible in the upper panel) represents the best fit of the solid line with a disk with isotropic emission by adjusting the values of \dot{M} and f_{col} . The parameters of the dotted lines are: $\dot{M} = 1.17 \times 10^{19}\text{g sec}^{-1}$ and $f_{\text{col}} = 1.43$ in the upper panel, $\dot{M} = 0.72 \times 10^{19}\text{g sec}^{-1}$ and $f_{\text{col}} = 1.7$ in the lower panel.

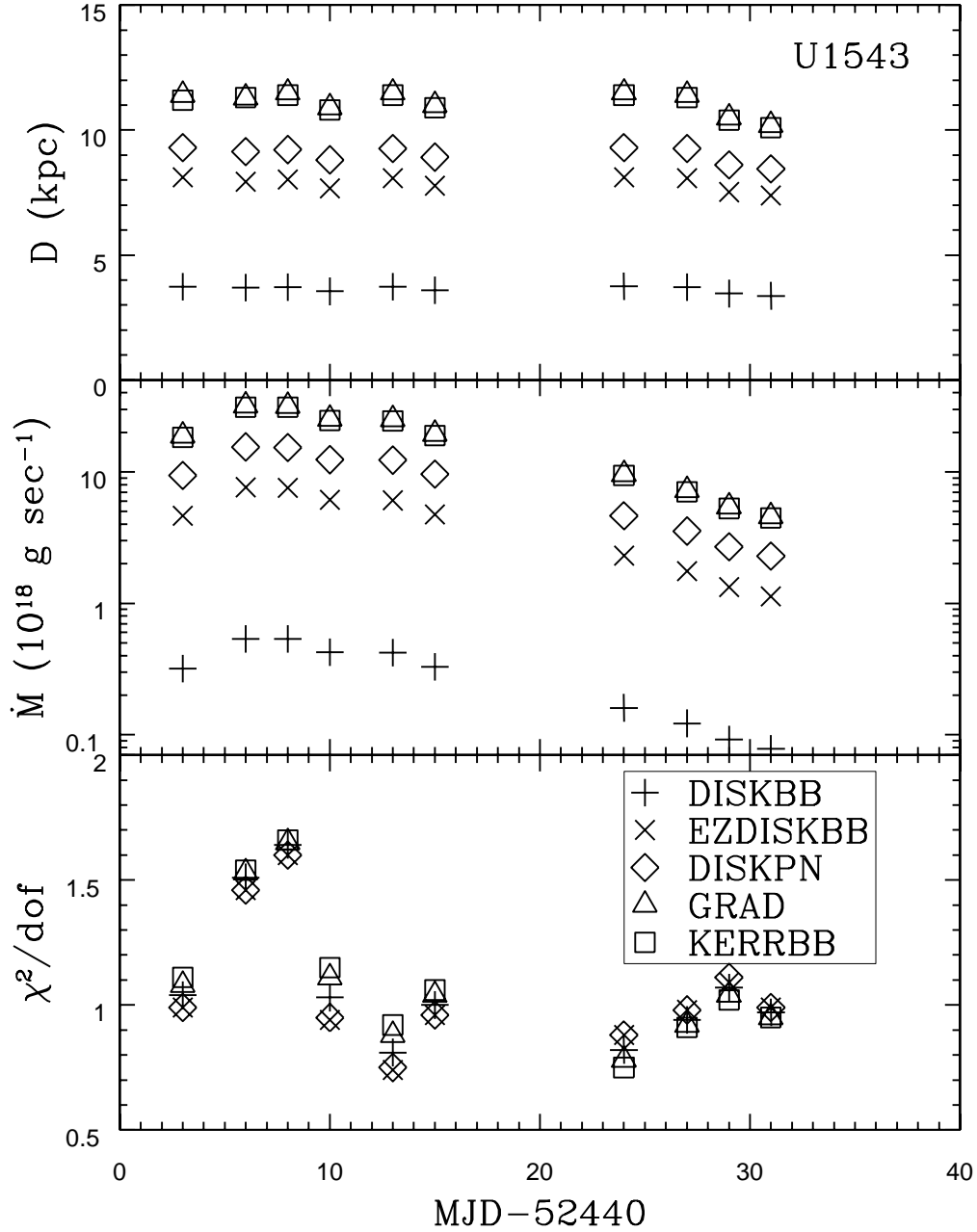


Fig. 10.— Fits of 10 observations of the source U1543 during the high/soft state. The data are from Park et al. (2004). Each observation was fitted separately using KERRBB, GRAD, DISKPN, EZDISKBB and DISKBB with $f_{\text{col}} = 1.7$. The resulting estimates of the distance D and the mass accretion rate \dot{M} , and the χ^2 of the fit, are shown in the three panels.

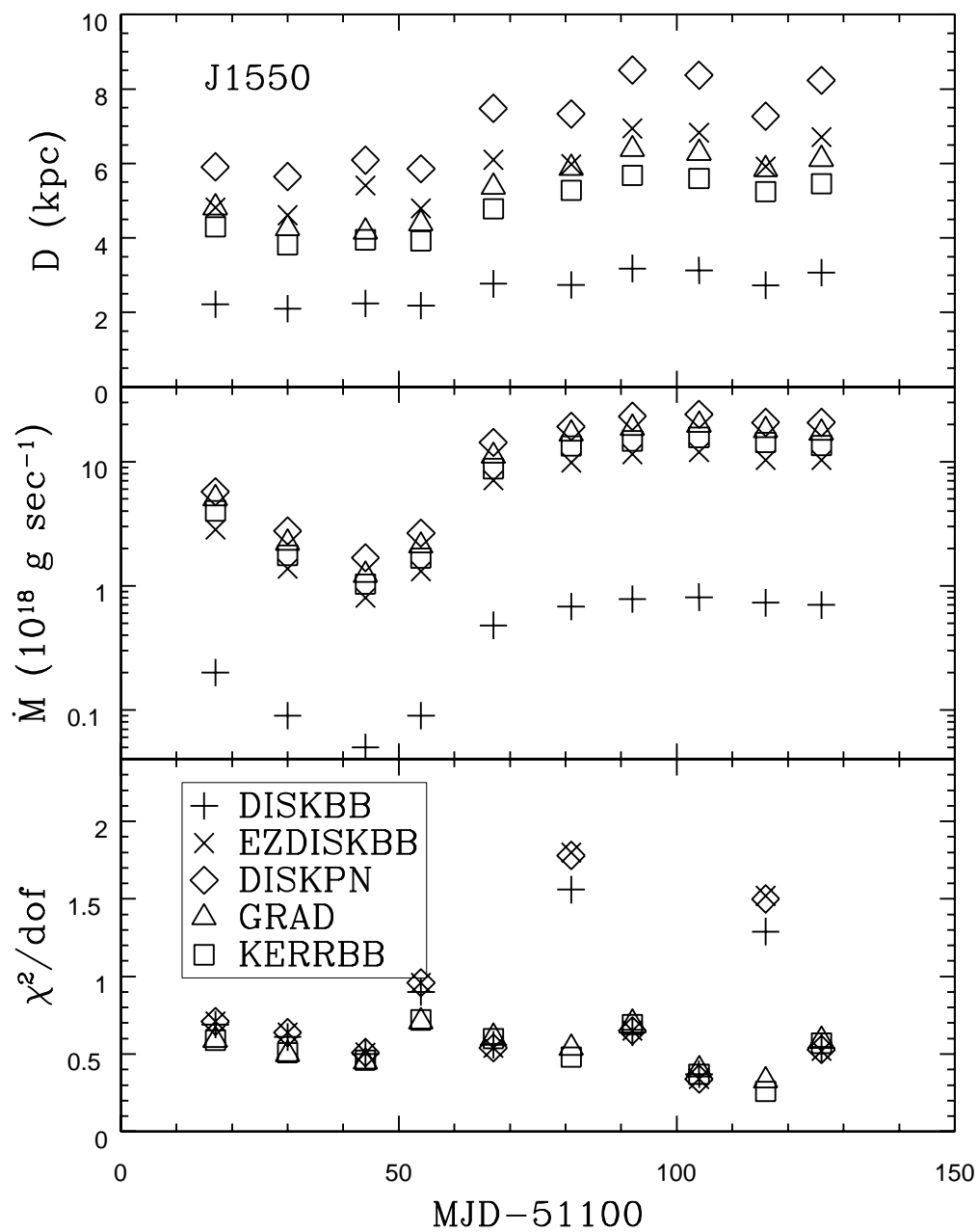


Fig. 11.— Fits of 10 observations of the source J1550 during the high/soft state. The data are from Sobczak et al. (2000). Each observation was fitted separately using KERRBB, GRAD, DISKPN, EZDISKBB and DISKBB with $f_{\text{col}} = 1.7$. The resulting estimates of the distance D and the mass accretion rate \dot{M} , and the χ^2 of the fit, are shown in the three panels.

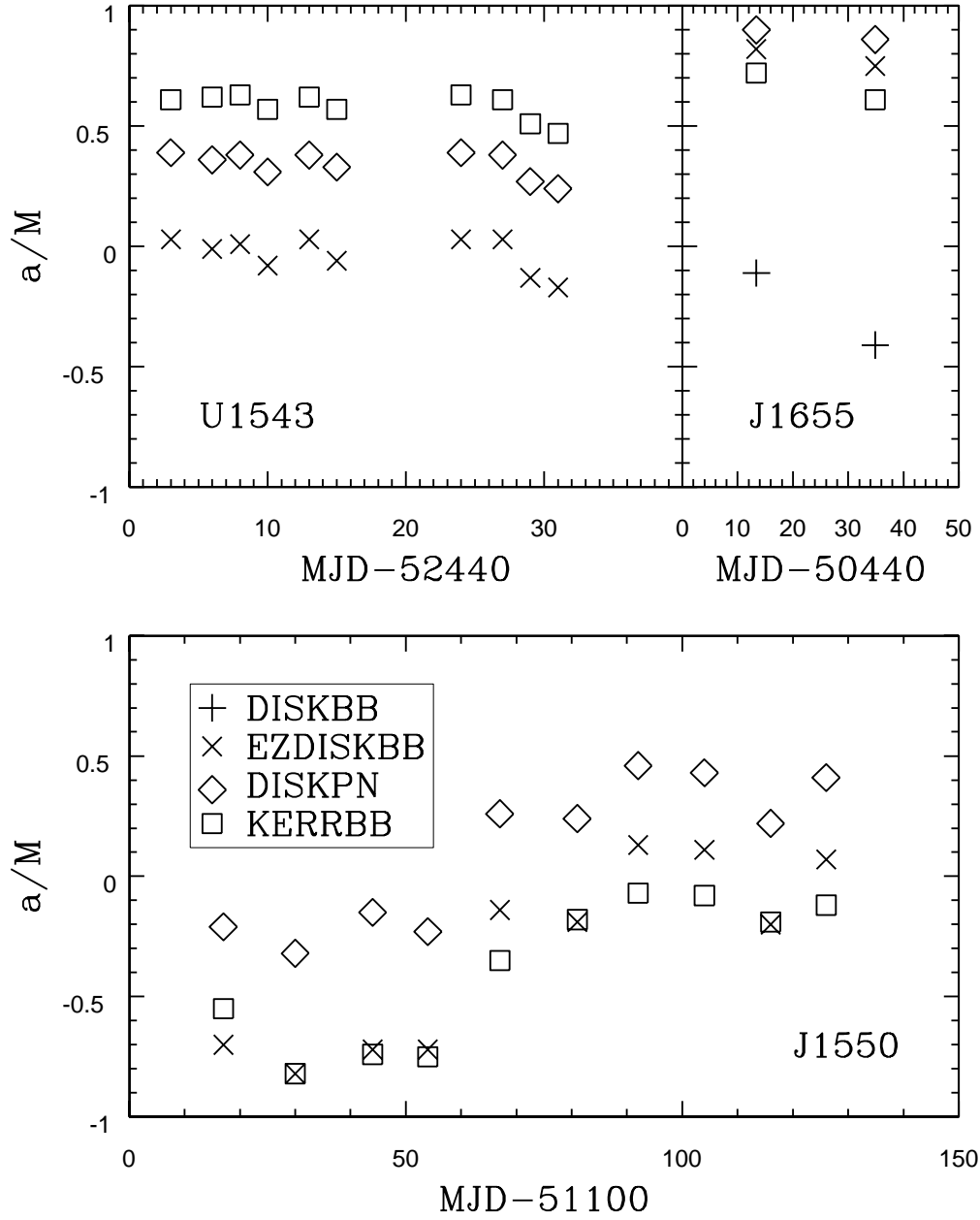


Fig. 12.— Estimates of the black hole spin parameter a/M in U1543, J1550 and J1655. The same 10 observations shown in Figs. 10 and 11 were used for the first two sources, and two observations from Sobczak et al. (1999) were used for J1655. For each observation, the black hole spin was estimated separately using KERRBB, DISKPN, EZDISKBB, and DISKBB with $f_{\text{col}} = 1.7$. No consistent solution was obtained with DISKBB for any of the observations of U1543 and J1550.

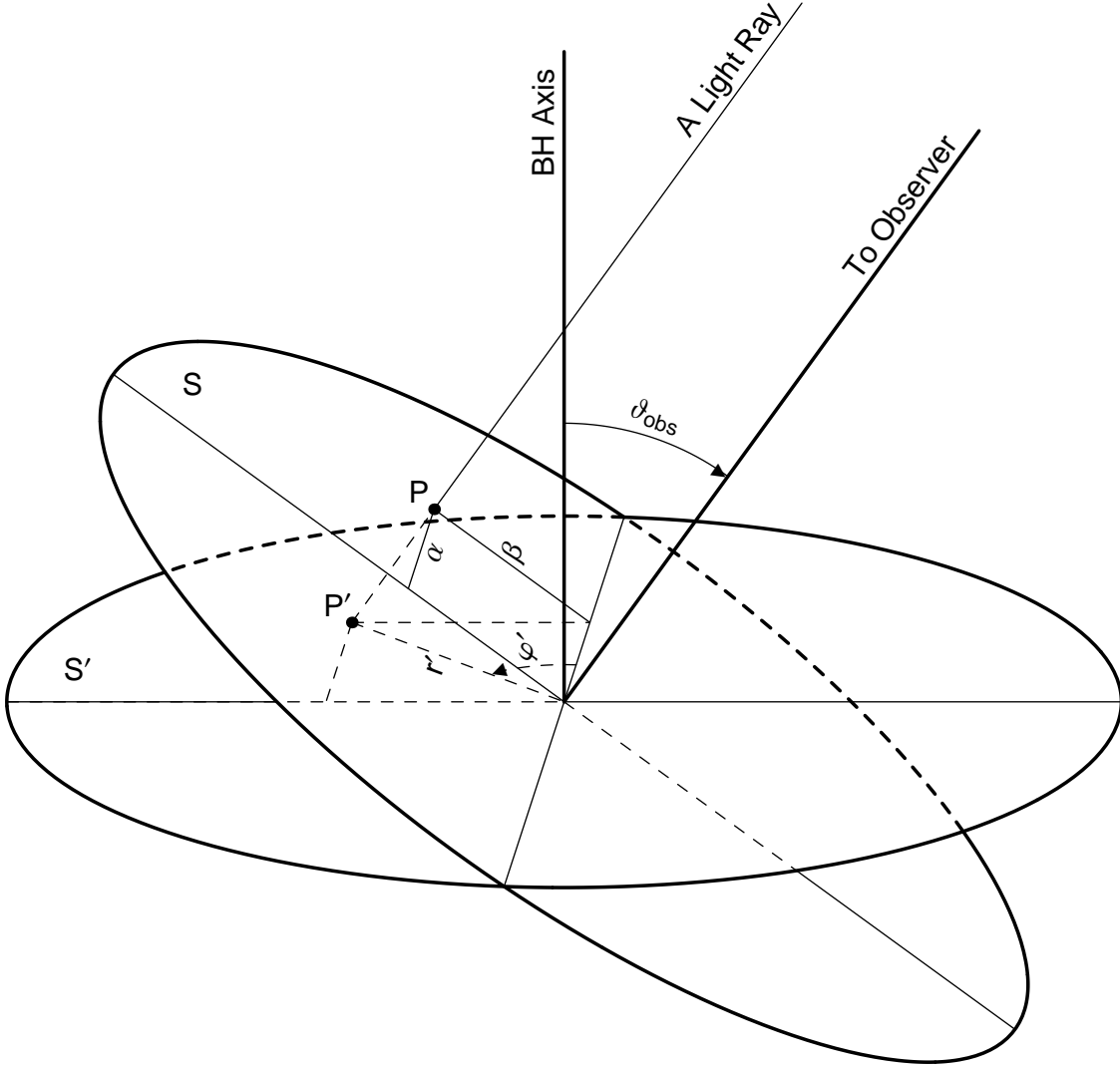


Fig. 13.— Relation between the impact parameters of a photon in the image plane S of an observer and polar coordinates in the equatorial plane S' of the black hole. On the image plane S , which is perpendicular to the line of sight, each point P is specified by a pair of impact parameters (α, β) . In the equatorial plane S' , which is perpendicular to the rotation axis of the black hole, each point P' is specified by a pair of polar coordinates (r', φ') . P and P' are connected by a straight line drawn parallel to the direction of the line-of-sight. The coordinates (α, β) of P are related to the coordinates (r', φ') of P' by equation (C26). The polar angle of the observer, or equivalently the inclination angle of the disk, is ϑ_{obs} .

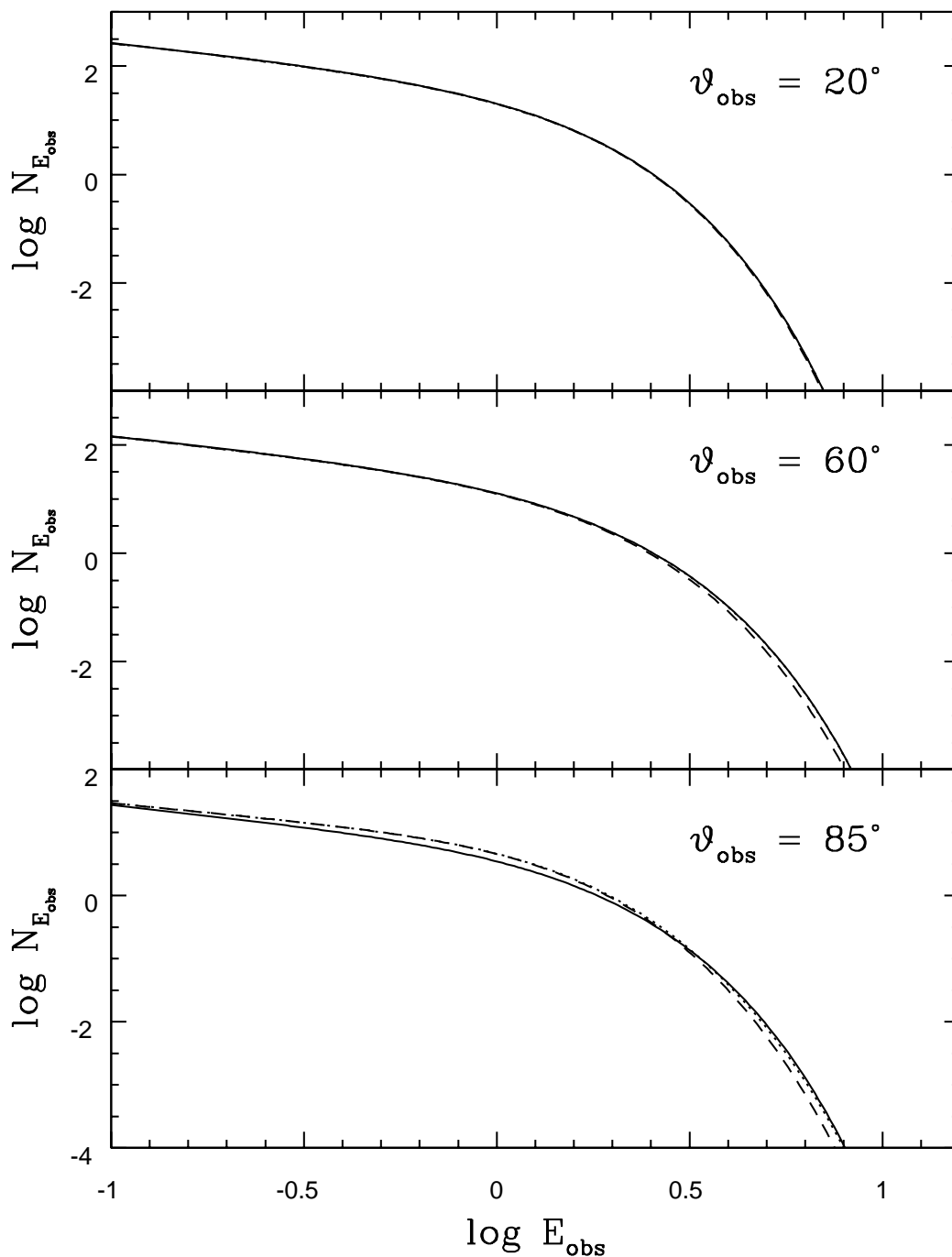


Fig. 14.— Comparison of KERRBB with GRAD. The specific photon number density calculated by KERRBB is shown with solid lines, calculated with GRAD is shown with dashed lines, and that calculated with modified GRAD is shown with dotted lines. Three panels correspond to three different disk inclination angles as labeled. In the upper and middle panels, the dashed lines are almost coincident with the solid lines.